NEURAL NETWORK BASED ADAPTIVE OUTPUT FEEDBACK CONTROL: APPLICATIONS AND IMPROVEMENTS

A Dissertation
Presented to
The Academic Faculty

by

Ali Turker Kutay

In Partial Fulfillment
of the Requirements for the Degree
Doctor of Philosophy in the
School of Aerospace Engineering

Georgia Institute of Technology
December 2005

NEURAL NETWORK BASED ADAPTIVE OUTPUT FEEDBACK CONTROL: APPLICATIONS AND IMPROVEMENTS

Approved by:

Dr. Anthony J. Calise, Advisor
School of Aerospace Engineering
Georgia Institute of Technology

Dr. Nader Sadegh
School of Mechanical Engineering
Georgia Institute of Technology

Dr. Panagiotis Tsiotras
School of Aerospace Engineering
Georgia Institute of Technology

Dr. J. Eric Corban
Guided Systems Technologies, Inc.

Dr. Eric N. Johnson
School of Aerospace Engineering
Georgia Institute of Technology

Date Approved: November 23, 2005

To my family, present and future

ACKNOWLEDGEMENTS

My foremost thank goes to my advisor Dr. Anthony Calise. I am greatly indebted to him for his patience and encouragement that carried me on through difficult times, and for his insights and suggestions that helped to shape my research skills. His wisdom and guidance that extend far beyond the contents of this dissertation made it possible for me to arrive at this point. I am also very thankful to the members of my doctoral committee, Drs. Anthony Calise, Panagiotis Tsiotras, Eric Johnson, Nader Sadegh, and Eric Corban for taking their time to read and evaluate this thesis.

I am grateful to Drs. Flavio Nardi, Moshe Idan, Naira Hovakimyan, and Ilkay Yavrucuk for their invaluable assistance in my early years at Georgia Tech. Their experience and enthusiasm have helped me produce this work. I extend my thanks to my former and current lab mates Seungjae "Franz" Lee, Hesham El-Shirbiny, Suresh Kannan, Nakwan Kim, Bong-Jun Yang, Suraj Unnikrishnan, Ramachandra Sattigeri, Matt Johnson, Venky Madyastha, Yoonghyun "John" Shin, Gerhard Heynen, Choong-Yil Kim, Konstantin Volyanskyy, Nimrod Rooz, Jonathan Muse, and Nathan Graybeal. Their generosity and brilliance made our lab a warm and creative place to work.

I would like to thank Dr. Raffaello D'Andrea of Cornell University for providing me an opportunity to work on the Cornell formation flight wind tunnel test bed and Dr. Jeff Fowler for his assistance in conducting the experiments presented in Chapter 5. I would also like to thank Dr. Mark Costello for providing the nonlinear six degrees-of-freedom spinning projectile simulation code "BOOM" for the simulations in Chapter 2.

Finally I would like to express my deepest gratitude to my family; my parents Melike and Irfan, my brothers Alper and Halil and their families, and my wife Nilgun for their never ending love and support. My wife Nilgun, in particular, has been with me in every moment of my life during my studies. Without her, this work would have been impossible.

TABLE OF CONTENTS

ACKNOWLEDGEMENTS vi

LIST OF TABLES xi

LIST OF FIGURES xii

SUMMARY xiv

CHAPTER

1 INTRODUCTION 1

1.1 Adaptive Output Feedback Augmentation of Existing Controllers 3

1.2 Sensitivity to Sensor Noise 7

1.3 Distributed Control of Interconnected Systems 8

1.4 Micro-Adaptive Flow Control (MAFC) Actuators 10

1.5 Contributions of this Thesis 13

1.6 Outline of the Thesis 15

2 ADAPTIVE AUGMENTATION OF NONLINEAR CONTROLLERS 16

2.1 Overview 16

2.2 Stability with Nonlinear Existing Controllers 18

2.2.1 Open Loop Reference Model-Following Approach [16] 20

2.2.2 Arbitrary Reference Model-Following Approach [23] 22

2.3 Simulation Example 23

2.3.1 Guidance Law Overview 25

2.3.2 Actuation via Flow Control 27

2.3.2.1 Actuator modeling 27

2.3.2.2 Jet firing law 29

2.3.3 Adaptive controller augmentation 30

2.3.4 Simulation Results 30

2.4 Conclusions 34

3 ARBITRARY REFERENCE MODEL-FOLLOWING ADAPTIVE AUGMENTING CONTROL FOR NON-MINIMUM PHASE SYSTEMS 35

3.1 Background 36

3.2 Problem Formulation 37

3.3 Controller Architecture 38

3.3.1 Reference Model 39

3.3.2 Modeling Uncertainties 40

3.3.3 Error Dynamics 42

3.3.4 Adaptive Controller Design 43

3.3.5 Error Observer 45

3.3.6 NN Adaptation Laws 46

3.4 Stability Analysis 46

3.5 Performance Improvement 50

3.6 Simulation Example 51

3.7 Conclusions 53

4 ARBITRARY REFERENCE MODEL-FOLLOWING ADAPTIVE AUGMENTING CONTROL FOR SYSTEMS WITH INPUT NONLINEARITIES 55

4.1 Background 55

4.2 Command Hedging Formulation 60

4.3 Stability with Command Hedging 62

4.4 Simulation Example 64

4.5 Conclusions 68

5 DISTRIBUTED CONTROL OF STRUCTURED INTERCONNECTED SYSTEMS 69

5.1 Background 69

5.2 System Description and Problem Formulation 70
5.3 Controller Architecture 73
5.3.1 Reference Model 74
5.3.2 Modeling Uncertainties 74
5.3.3 Error Dynamics 75
5.3.4 Adaptive Controller Design 75
5.3.5 Error Observer 77
5.3.6 NN Adaptation Laws 78
5.4 Stability Analysis 78
5.5 Description of the Wind Tunnel Experiment 81
5.5.1 Configuration design 81
5.5.2 Specifications 82
5.6 Experiment Results 83
5.7 Conclusions 86
6 FLIGHT CONTROL USING MAFC ACTUATORS 88
6.1 Nomenclature 89
6.2 Equations of Motion 90
6.2.1 Aerodynamic Forces 91
6.2.2 Linearization 93
6.3 Controller Design 95
6.3.1 Trim Controller Design 96
6.3.2 Inner Loop Controller Design 97
6.3.3 Outer Loop Controller Design 97
6.3.3.1 Linear compensator design for the outer loop 98
6.3.3.2 Adaptive NN design for the outer loop 98
6.4 Actuator and Sensor Modeling 99
6.4.1 Elevator model 99

6.4.2 MAFC Actuator Model 100
6.4.3 Sensor Model.....101
6.5 Simulation Results.....101
6.5.1 High Damping Inner Loop Design.....102
6.5.2 Low Damping Inner Loop Design 103
7 ADAPTIVE OUTPUT FEEDBACK CONTROL WITH REDUCED SENSITIVITY TO SENSOR NOISE 106
7.1 Problem Formulation.....106
7.2 Controller Architecture.....107
7.3 Reduced Order Observer Design.....111
7.4 Numerical Noise Sensitivity Analysis.....112
7.5 Adaptive Control Design.....115
7.6 Stability Analysis.....117
7.7 Experimental Application.....119
7.8 Summary.....122
8 CONCLUDING REMARKS 123
8.1 Conclusions 123
8.2 Recommendations for Future Research.....125
APPENDIX
A CHAPTER 3 PROOF 126
B CHAPTER 5 PROOF 130
C CHAPTER 7 PROOF 133
REFERENCES 135

LIST OF TABLES

Table 6-1. Aerodynamic parameters. 102
Table 6-2. Inner loop and outer loop linear controller designs. 103

LIST OF FIGURES

Figure 1-1. The open loop reference model-following adaptive augmenting architecture [16]. 4

Figure 1-2. The closed loop reference model-following adaptive augmenting architecture [19]. 5

Figure 1-3. The arbitrary reference model-following adaptive augmenting architecture [23]. 7

Figure 1-4. Three-DOF model helicopter. 8

Figure 1-5. Formation flight apparatus. 10

Figure 1-6. Spinning projectile. 12

Figure 1-7. Two-DOF wind tunnel model with passive traverse..... 13

Figure 2-1. Adaptive augmenting architectures: (a) open-loop reference model-following approach [16], (b) arbitrary reference model-following approach [23]. 17

Figure 2-2. Equivalent representations of the open loop and arbitrary reference model adaptive augmenting architectures. 18

Figure 2-3. Transient control with an active flow actuator: a) Time history of the circulation when control is activated, b) Flow visualization images during flow reattachment: i. separated flow, ii. collapse of the separation domain, iii. beginning of full reattachment, and iv. full reattachment [48]. 28

Figure 2-4. Modeling of Jet force Profile. 28

Figure 2-5. Schematic of the jet firing process. 29

Figure 2-6. Simulation results without adaptation. 31

Figure 2-7. Simulation results with adaptation without hedging. 33

Figure 2-8. Simulation results with adaptation with hedging. 33

Figure 2-9. Precession motion for three controlled cases. 34

Figure 3-1. Arbitrary reference model-following control architecture for non-minimum phase systems. 39

Figure 3-2. Comparison of step responses with the closed-loop reference model approach, [17]. 52

Figure 3-3. Comparison of step responses with the arbitrary reference model approach. 53

Figure 3-4. Matched and unmatched modeling errors and adaptive signal. 54

Figure 4-1. Arbitrary reference model-following adaptive augmenting control architecture. 56

Figure 4-2. Implementation of control hedging in the arbitrary reference model-following adaptive augmenting control architecture. 62

Figure 4-3. Nonlinear actuator model. 65

Figure 4-4. Simulation results without adaptive augmentation. 66

Figure 4-5. Simulation results with adaptive augmentation without control hedging. 67

Figure 4-6. Simulation results with adaptive augmentation with control hedging. 68

Figure 5-1. Augmenting adaptive controller architecture for the ith subsystem. 73

Figure 5-2. Disturbance rejection with adaptive and non-adaptive controllers. 84

Figure 5-3. Command tracking with existing non-adaptive controllers. 85

Figure 5-4. Command tracking with the augmenting adaptive controllers. 86

Figure 6-1. Free-body diagram of the 2-DOF wind tunnel model. 91

Figure 6-2. Controller architecture for closed loop flight control using MAFC actuators 99

Figure 6-3. Step response of $G_f(s)$. 100

Figure 6-4. Simulation results with high damping model. 104

Figure 6-5. Simulation results with low damping model. 105

Figure 7-1. Error observer based adaptive output feedback controller with reduced order observer. 112

Figure 7-2. Bode diagrams of the transfer functions from sensor noise to learning signal for the full and reduced order observers. 114

Figure 7-3. Output tracking and control histories with NN adaptation with full order observer (0 – 30 secs), reduced order observer (30 – 60 secs), and without adaptation (60 – 90 secs). 121

SUMMARY

Application of recently developed neural network based adaptive output feedback controllers to a diverse range of problems both in simulations and experiments is investigated in this thesis. The purpose is to evaluate the theory behind the development of these controllers numerically and experimentally, identify the needs for further development in practical applications, and to conduct further research in directions that are identified to ultimately enhance applicability of adaptive controllers to real world problems.

We mainly focus our attention on adaptive controllers that augment existing fixed gain controllers. A recently developed approach holds great potential for successful implementations on real world applications due to its applicability to systems with minimal information concerning the plant model and the existing controller. In this thesis the formulation is extended to the multi-input multi-output case for distributed control of interconnected systems and successfully tested on a formation flight wind tunnel experiment. The command hedging method is formulated for the approach to further broaden the class of systems it can address by including systems with input nonlinearities. Also a formulation is adopted that allows the approach to be applied to non-minimum phase systems for which non-minimum phase characteristics are modeled with sufficient accuracy and treated properly in the design of the existing controller. It is shown that the approach can also be applied to augment nonlinear controllers under certain conditions and an example is presented where the nonlinear guidance law of a spinning projectile is augmented. Simulation results on a high fidelity 6 degrees-of-freedom nonlinear simulation code are presented.

The thesis also presents a preliminary adaptive controller design for closed loop flight control with active flow actuators. Behavior of such actuators in dynamic flight

conditions is not known. To test the adaptive controller design in simulation, a fictitious actuator model is developed that fits experimentally observed characteristics of flow control actuators in static flight conditions as well as possible coupling effects between actuation, the dynamics of flow field, and the rigid body dynamics of the vehicle.

CHAPTER 1

INTRODUCTION

Automatic control plays a vital role in modern life from space-vehicle systems to industrial processes. Starting from James Watt's centrifugal governor for the speed control of a steam engine in the eighteenth century, automatic control has evolved a long way to today's adaptive controllers that can perform sufficiently well in vastly diverse operating conditions with little information about the system.

Advances in control theory have been motivated by the requirements imposed by real world applications. Until the late 1950s, the frequency response and root locus methods, the core tools of the classical control theory, have been mainly used to design control systems that satisfy performance and robustness requirements [1], [2]. Emerging complex systems with many inputs and outputs led researchers to focus on alternative approaches to deal with such systems. Development of digital computers made time-domain analysis of complex systems possible and led to development of modern control theory, emphasizing time-domain analysis and synthesis methods in the state space [3], [4]. Optimal and robust control of linear deterministic and stochastic systems were fully investigated from 1960s to 1980s [5], [6].

Development of advanced nonlinear systems, such as those in aerospace applications, forced researchers to investigate nonlinear control, as the assumption of linearity no longer held. Research in nonlinear control theory yielded several analysis and synthesis tools including feedback linearization and recursive backstepping methods [7], [8].

Systems for which no reasonably accurate low order models exist, such as flow and combustion processes, as well as systems where dynamic characteristics change

rapidly in time (perhaps due to failures or environmental changes), have motivated research in adaptive control. In the early 1980s, significant advances in adaptive control started to appear, albeit under restrictive assumptions such as known system structure, affinity in the control and/or unknown parameters [9], [10]. More recently, research has focused on relaxing these assumptions by incorporating neural networks (NNs) to model complex nonlinear physical phenomena. A detailed survey of NNs and fuzzy logic systems in feedback control can be found in [11].

One major limitation that prevents direct use of a majority of control methods on real systems stems from the fact that for many systems it is not possible, or practical to measure all the state variables. This motivated researchers to develop output feedback control methods that utilize available measurements only. The traditional approach to output feedback has been to make use of state estimation, which implies that the dimension of the plant is known. Recently, an inverting adaptive direct output feedback controller has been developed that is applicable to non-affine in control systems having unknown dimension with the assumption that the relative degree of the regulated output is known [12]. The linear-in-parameters NN used in this approach to approximate the modeling error has been replaced with a single hidden layer (SHL) NN to accommodate a larger class of nonlinearities by introducing a linear observer for the tracking error dynamics [13]. This formulation has been extended to multi-input multi-output (MIMO) systems in [14]

Although novel adaptive control methods have shown excellent performance on several challenging numerical and experimental problems, it appears that for such controllers to be broadly used in military and commercial applications, a higher level of maturity has to be reached in the theory. Boundedness of error signals can be guaranteed for a wide class of problems, however, direct control of the error bounds and transient performance remain open issues. Under these circumstances, it is hard to expect industry to be willing to abandon well established approaches to control design. Inspired by this

perception, an adaptive augmenting controller was developed in [15] in full state feedback setting. Adaptive output feedback controllers that augment general linear controllers following the ideas of [12] and [13] have followed in [16]–[23]. These approaches keep all the benefits of the years of experience gained on designing the existing controllers, and add the advantages of adaptive control.

Physical limitations of actuation devices, such as position and rate limits, or other nonlinearities introduced at the input level such as quantized [24] or discrete actuation [25] that adaptive controllers cannot adapt to, has stimulated research in this area. A novel approach called pseudo-control hedging (PCH) for treating nonlinearities at the input level in a dynamic inversion based controller has been proposed in [26]–[28]. Later it has been integrated in an output feedback setting [23] and in an augmenting approach [17]–[18].

In this thesis, we implement state-of-the-art adaptive control methodologies on various challenging problems both in simulations and experiments. Our goal is to evaluate the theoretical results of the adaptive output feedback controllers developed in [12]–[23] numerically and experimentally, identify the need for further development in practical applications, and to conduct further research in directions that are identified. The following sections describe the areas we focus on.

1.1 Adaptive Output Feedback Augmentation of Existing Controllers

NN based adaptive controllers have attracted great attention in control of nonlinear systems with unknown structure. Universal approximation capabilities of NNs [29], [30] have been employed to parameterize uncertainties in the system with unknown structure. The NN approximation approach of [31] allowed use of a finite number of delayed values of available input/output data to approximate observable uncertainties. Further improved in [32], the NN approximation scheme led to a major progress in adaptive output feedback control. The adaptive output feedback controllers of [12] and

[13] utilized the NN approximation approach of [31] and [32] to stabilize nonlinear non-affine in control systems having unknown dimensions in a dynamic inversion setting. One drawback of these controllers that limits their usage on practical problems is that unless the existing control architecture is already based on inversion, it must be replaced with one that is. The adaptive algorithms of [12] and [13] have later been implemented in a model-following context to augment more general fixed gain linear controllers [16]–[23]. A common requirement in [16]–[22] is that a linear model of the plant be available. It is further assumed that the closed-loop system consisting of the plant model regulated by the existing controller meets the performance specifications. This is often not the case, particularly when the existing controller gains are tuned in an operational environment.

In [16]–[18], the reference model is defined as the linear plant model controlled by the existing controller as illustrated in Figure 1-1. Since the input to the reference model is the linear control signal driven by the error signal based on the true system output y rather than the reference output y_m, this architecture is referred to as the open

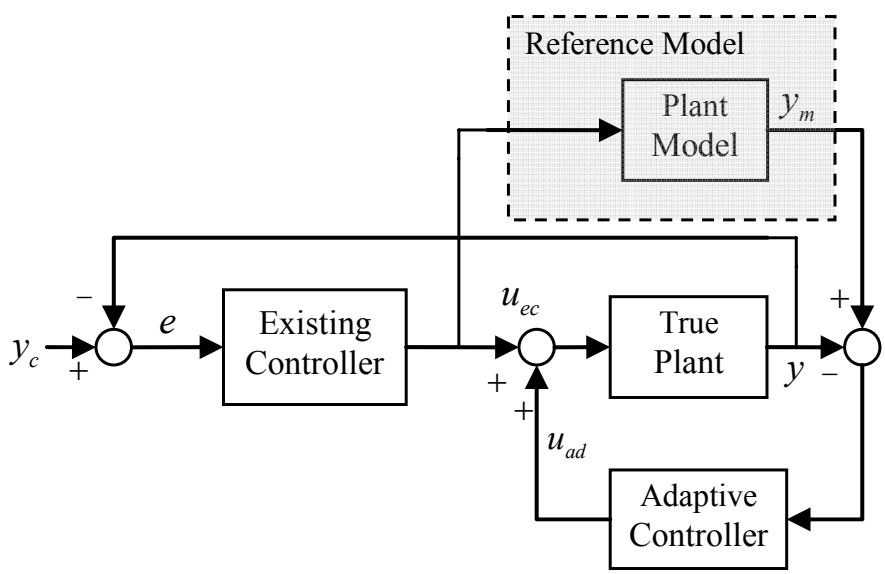

Figure 1-1. The open loop reference model-following adaptive augmenting architecture [16].

loop reference model-following adaptive augmenting architecture. The PCH technique for treating actuator nonlinearities in a dynamic inversion based controller was modified for the open loop reference model adaptive augmenting approach in [17], [18] and simply called control hedging.

In [19]–[21] the reference model is formed by closing the loop around the linear system model with the existing linear controller as shown in Figure 1-2. We refer to this architecture as the closed loop reference model-following adaptive augmenting architecture. An important feature of this architecture is that it does not rely on feedback linearization, and thus it can be applied to non-minimum phase systems. It is assumed that the linear model of the system represents the non-minimum zeros of the true plant to a sufficient accuracy, and that the linear controller takes into account the presence of these zeros. The approach has also been extended to MIMO systems in [20], [21].

The open loop and closed loop augmenting approaches assume that the existing controllers have been designed for the linear model of the system to achieve satisfactory

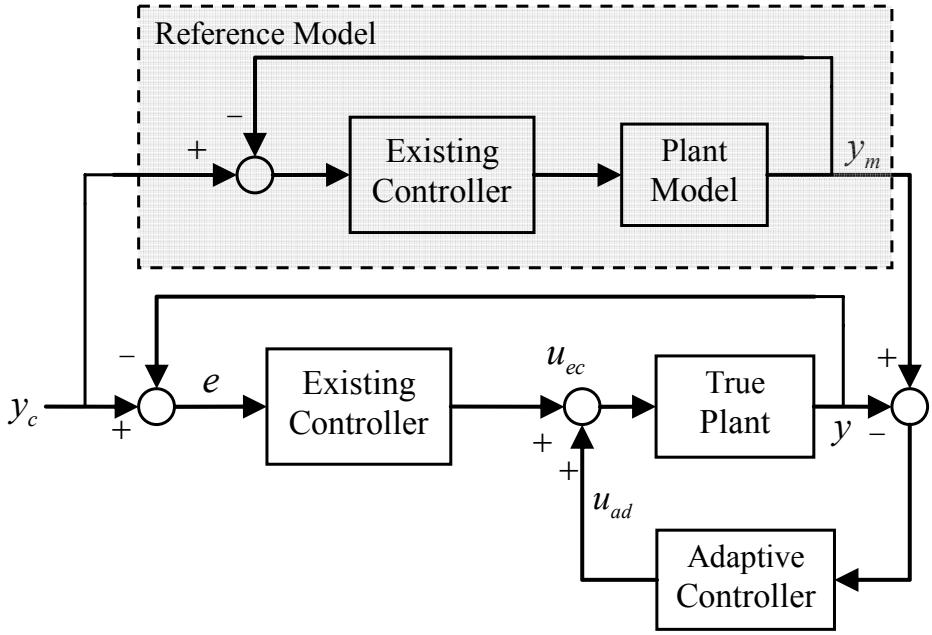

Figure 1-2. The closed loop reference model-following adaptive augmenting architecture [19].

dynamics. For systems where the controller has been designed by other means, for example by a tuning process while in operation with the true plant, and not by a model based design approach, these two approaches cannot be applied. No matter how accurate the available model is, when a model based controller is implemented in a real world application, it almost always requires further tuning on the system. If the linear model does not represent the true dynamics with sufficient accuracy, the model based controller tuned on the true system may no longer yield satisfactory dynamics when applied to the model. The formation flight experiment test bed presented in Chapter 5 is an example where hand tuned controllers cannot adequately control the experimentally identified model.

An adaptive augmenting approach that addresses the limitations of the open loop and closed augmenting approaches mentioned above has been proposed in [23] where a simple stable linear model is introduced as the reference model as depicted in Figure 1-3. Since selection of the reference model is not restricted by the dynamics of the true system, except that its relative degree has to match that of the regulated output, we refer to this architecture as the arbitrary reference model-following adaptive augmenting architecture.

The arbitrary reference model architecture has a greater potential for successful implementations on real applications compared to the other two augmenting approaches. In this thesis we further enhance its capabilities. We start with an analysis to show that the open loop and arbitrary reference model approaches can be applied to augment nonlinear controllers subject to certain conditions. As an example we augment the nonlinear guidance law of a spinning projectile with an adaptive element following the open loop reference model approach in Chapter 2. Then we adopt the formulation of the closed loop reference model approach to make the arbitrary reference model approach applicable to non-minimum phase systems as long as the non-minimum phase dynamics are modeled with sufficient accuracy and the existing controller design takes into account the existence of these dynamics. We test this formulation on a numerical simulation in

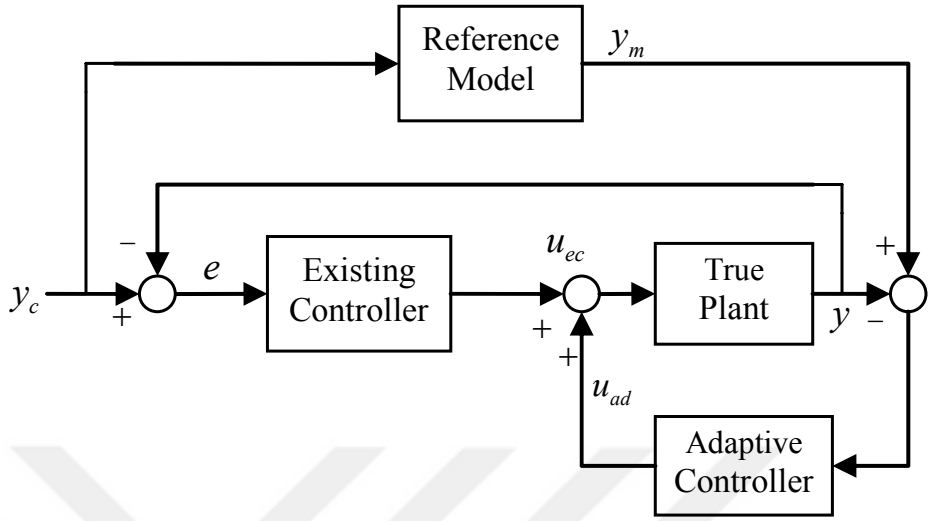

Figure 1-3. The arbitrary reference model-following adaptive augmenting architecture [23].

Chapter 3. We also implement command hedging to make it applicable to systems with input nonlinearities and test it on a numerical simulation in Chapter 4. Finally we extend the formulation to the MIMO case for distributed control of structured interconnected systems, further discussed in Section 1.3.

1.2 Sensitivity to Sensor Noise

The inverting adaptive direct output feedback controller of Ref. [12] resulted in a highly noisy control signal when applied to a 3-DOF model helicopter laboratory experiment shown in Figure 1-4 [33], [34]. The error observer based controller with SHL NN of Ref. [13] also produced similar results. Investigation of the problem revealed that the source of the noise is the low resolution optical sensor used to measure the angular position. It is shown in simulation that higher resolution sensors reduce the noise in control, and noise is totally eliminated with perfect sensors. Considering the fact that using high quality expensive measuring equipment is not always an option, especially for consumer level products and for expendable military systems, reducing the sensitivity of

the adaptive controllers to measurement noise is necessary for their broader use in industry.

Amplification of sensor noise in adaptive controllers has been reported in several previous applications before [35], [36]. In [37], a time varying Kalman filter is used in an adaptive position control problem to suppress the control signal noise due to a low-resolution encoder. However, requirement of the knowledge of system dynamics to design a Kalman filter makes it inapplicable to systems with unmodeled dynamics. We propose replacing the linear observer in [13], for the error and dynamic compensator states, with a reduced order one that only estimates the unknown error dynamics. Numerical analysis on a sample problem and experiment results on the 3-DOF model helicopter show that sensitivity to sensor noise is significantly reduced, while the stability properties are still maintained [38].

1.3 Distributed Control of Interconnected Systems

Many control problems involve interaction and cooperation of a number of similar units. Examples of such systems include automated highway systems [39], communication networks, or formations of aerial vehicles [40]-[42]. Lumped approximations of partial differential equations can also be considered in this class of systems, such as deflection of beams and plates, and active flow control [43]. Even when individual units have simple realistic models and interactions occur in a simple and

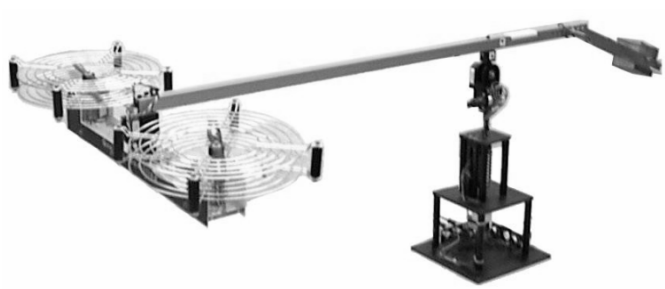

Figure 1-4. Three-DOF model helicopter.

predictable manner, the resulting large scale system usually exhibits rich and complex behavior. One way to control these systems is to design a centralized controller treating the whole system as a multi variable large scale system. However, these controllers require high levels of communication, impose a substantial computational burden, and are configuration dependent and hence sensitive to modifications and failures. There is an extensive body of literature devoted to addressing these issues in the form of a fully decentralized controller architecture, where a controller is designed for each subsystem to perform the given task, while no communication is allowed between the controllers. A detailed review of the literature regarding decentralized controllers can be found in [44].

For closely interconnected systems, utilizing available information about the structure of the system may substantially increase performance compared to a fully decentralized controller, while still avoiding the disadvantages of a centralized controller. In [45], model based distributed controllers are proposed that interact in the same way as the plant for spatially invariant interconnected systems. Stability and performance of the full distributed closed loop system is guaranteed for linear time invariant subsystems and interconnections captured by integral quadratic constraints. This result is extended to heterogeneous systems with arbitrary interconnections in [46].

When a number of systems with existing controllers that satisfy performance requirements for individual isolated systems are interconnected to form a large-scale system, augmentation of these controllers to compensate for the interconnection effects may be much preferred to replacing them with a totally new architecture. Formation flight of aerial vehicles provides a good example where a legacy of experience with designing controllers for individual vehicles exists.

Extension of the closed loop reference model-following adaptive augmenting controller to a decentralized setup has been developed in [20], [21]. It is assumed that the desired trajectories of the subsystems are known to all the controllers. In this thesis we extend the formulation of the arbitrary reference model-following adaptive augmenting

architecture to the MIMO case for distributed control of interconnected systems. We show boundedness of the overall large scale system using Lyapunov's direct method in a way similar to [20]. We test the controller on the formation flight wind tunnel test bed at Cornell University shown in Figure 1-5. This provides an illustration of the role that adaptation can play in designing distributed controllers for structured interconnected systems.

1.4 Micro-Adaptive Flow Control (MAFC) Actuators

Active flow control is a multi-disciplined approach to modifying flow field characteristics to achieve a desired aerodynamic performance. It combines sensing, actuation, and flow physics. In contrast to passive techniques, such as wall shaping or coatings, active control involves introducing a time dependent forcing of the system. By imposing this type of control one is able to achieve a state of the flow that would not naturally occur. The term "micro-adaptive" is often used to refer to the leveraging of natural flow instabilities to amplify the control authority of micro actuators in combination with adaptive feedback control.

A classic example, for which many feedback control approaches have been considered, is the distributed and direct manipulation of turbulent structures in a wall-

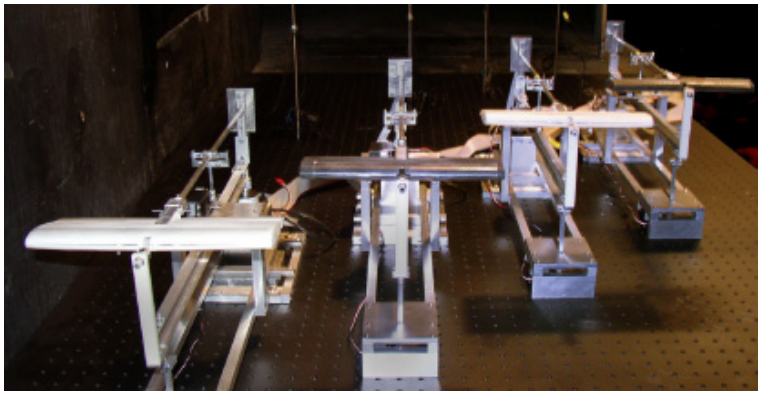

Figure 1-5. Formation flight apparatus.

bounded flow to achieve significant viscous drag reduction. In other cases, one can concentrate actuation to a compact region where the flow is highly receptive to properly configured actuation. Examples of this include keeping wings from stalling at high angles of attack, dramatic increases in mixing rates in plumes, and direct control of vortex formation and asymmetry on forebodies and highly swept wings.

Open-loop approaches are more than adequate when the state of the flow can be adequately measured, the flow phenomenon is sufficiently deterministic, and the actuation approach is fully robust. However, in many cases some form of feedback control is required to achieve the desired performance gains, such as turbulent viscous drag reduction. Closed-loop approaches can enable greater performance, compensate for limited information about the flow state, provide robustness in the presence of noise, and adapt to dramatic changes in the behavior of the system or to failures in the actuators/sensors.

Responses of MAFC actuators in static flow conditions have been studied extensively in static wind tunnel experiments [47]-[49]. In [49], closed loop hingeless control of a wing using synthetic jet actuators has been studied. A radial basis function (RBF) NN has been trained off-line with the wind tunnel experiment data to model the actuators. Authors praise the ability of the RBF NN to model actuator characteristics, but do not use it in closed loop control. Instead, they derive a linear model from the trained NN and use it in a PID controller. They also use a polynomial fit to model the synthetic jet and use the model in a sliding mode controller. Considering the difficulties of generating the data to create an actuator model off-line, it would be very useful to use a NN in a closed loop control system and train it online to model the actuator using available measurements. The fact that available wind tunnel data in the literature only covers static flight conditions further increases the value of using an online trained NN in a dynamic control problem.

We applied the open loop reference model augmenting controller to two applications where MAFC actuators are employed. Simulation models of these applications contain actuator characteristics observed in wind tunnel experiments.

In the first application a spinning projectile depicted in Figure 1-6 is controlled by placing a control mechanism on board that employs synthetic jets to generate the required forces [25]. In this application, the nonlinear guidance law designed for the horizontal and vertical plane motion of a spinning projectile is augmented with an adaptive controller following the arbitrary reference model approach. The guidance law aims to find the constant force commands to steer the projectile to the target using a simple point mass model. Actuation is provided by discrete firing of a synthetic jet with rise and decay profiles modeled to match wind tunnel experiment results. Simulation results obtained using a nonlinear 6-DOF simulation code in Fortran showed that adaptation successfully cancels the effects of the modeling errors and nonlinear actuation. The projectile follows the reference model, i.e, the point mass trajectory, very closely.

In a second application we implemented active flow control actuators for 2-DOF pitching and plunging control of a model composed of a wing and a tail depicted in Figure 1-7. To simulate the MAFC actuators in dynamic flight conditions, we created a nonlinear dynamic model that represents experimentally observed behavior in static flight conditions as well as possible coupling effects between actuation, the dynamics of flow field, and the rigid body dynamics of the model. A linear LQR controller is designed

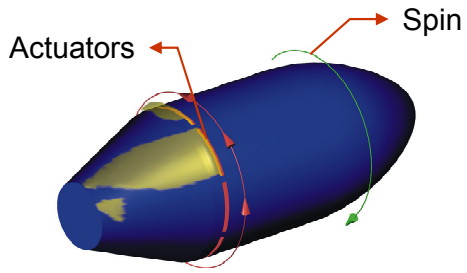

Figure 1-6. Spinning projectile.

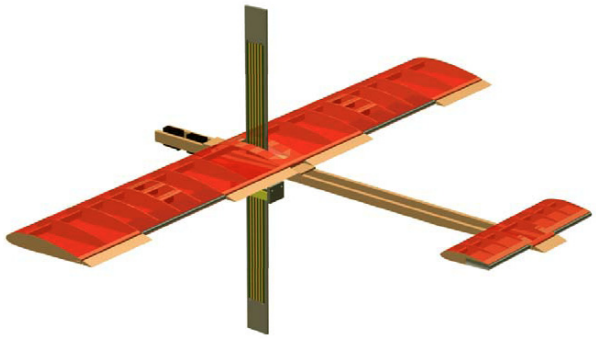

Figure 1-7. Two-DOF wind tunnel model with passive traverse.

using full state feedback and then augmented by an adaptive controller following the open loop reference model approach. To test the robustness of the controller to changes in vehicle dynamics, an inner loop controller is designed to change the stability properties of the model using rate feedbacks with a conventional elevator. Simulation results show successful adaptation to varying stability characteristics and unmodeled nonlinear dynamic actuation of the jets.

1.5 Contributions of this Thesis

The purpose of this thesis has been to improve applicability of novel NN based adaptive output feedback controllers to real world problems. The field of adaptive control is still in rapid development. Although an impressive amount of work has been reported in the adaptive control literature, universally accepted techniques for analysis and synthesis of adaptive systems do not exist. The current level of adaptive control theory leads us to believe that a beneficial use of existing adaptive control technology in control engineering would be in assisting well established non-adaptive controllers to improve their performance. With this motivation we have focused our attention on adaptive augmentation of existing controllers. Among the three recently developed adaptive augmenting controllers, the arbitrary reference model approach of [23] has a greater potential because of its less restrictive requirements.

This thesis formulates the command hedging technique for the arbitrary reference model-following adaptive augmenting controller to address systems with input nonlinearities. The arbitrary reference model-following adaptive augmenting controller formulation is extended to non-minimum phase systems. Following the idea of [19] we prove that existing controllers for non-minimum phase systems can be augmented provided that the existence of non-minimum phase zeros is recognized in the linear controller design.

The arbitrary reference model-following adaptive augmenting controller formulation is extended to MIMO systems for distributed control of structured interconnected systems. We demonstrate the effectiveness of the approach on a wind tunnel experiment.

We show that the open loop and arbitrary reference model augmenting controllers can be used to augment nonlinear controllers subject to certain conditions. We successfully apply the open loop reference model augmenting controller with control hedging to augment the nonlinear guidance law of a spinning projectile.

We have observed on a laboratory experiment that the adaptive output feedback controllers of [12] and [13] are highly sensitive to sensor noise. In an effort to reduce noise sensitivity of the error observer based approach of [13], we propose a reduced order observer that eliminates the redundancy in estimating the already available compensator states. The proposed modification shows significant improvements in simulation and on the experiment.

We demonstrate the effectiveness of the open loop reference model-following adaptive augmenting control in dynamic flight control using MAFC actuators. In the absence of a reliable model for MAFC actuators in dynamic flight conditions, we test the approach in simulation by using a fictitious nonlinear model that captures possible coupling effects.

1.6 Outline of the Thesis

Chapter 2 presents an analysis for augmenting nonlinear controllers with the open loop and arbitrary reference model-following adaptive augmenting controllers. A simulation example is provided where the nonlinear guidance law of a spinning projectile is augmented with an adaptive controller following the open loop reference model approach with control hedging.

Chapter 3 formulates the arbitrary reference model-following adaptive augmenting controller design for non-minimum phase systems. Stability analysis is provided together with a simulation example.

Chapter 4 formulates the command hedging implementation for the arbitrary reference model-following adaptive augmenting controller. Stability of the closed loop system with command hedging is shown and a simulation example is presented.

Chapter 5 extends the formulation of the arbitrary reference model-following adaptive augmenting controller to MIMO systems for distributed control of structured interconnected systems. A stability analysis is provided. Experiment results on the Cornell University formation flight test bed are presented.

Chapter 6 presents an adaptive approach for closed loop flight control using MAFC actuators. Simulation results of a 2-DOF wind tunnel model are presented.

Chapter 7 presents the design of a reduced order observer for the error observer based adaptive output feedback control method of [13]. Numerical analysis of the noise sensitivities of the full and reduced order observers on a sample design is shown. Experiment results on the 3-DOF model helicopter experiment setup are presented.

Chapter 8 concludes the thesis with recommended future research directions.

CHAPTER 2

ADAPTIVE AUGMENTATION OF NONLINEAR CONTROLLERS

Augmentation of fixed gain linear controllers with NN based adaptive elements has recently been addressed in [16]–[23]. While linearity of the controller is explicitly assumed in the development of the adaptive controller in the closed loop reference model approach [19]–[21], it is only assumed for proving stability of the closed loop system in the open loop and arbitrary reference model approaches [16]–[18], [23]. An augmentation architecture that can be applied to systems with nonlinear controllers would be very useful for many practical applications, particularly guidance applications. In this chapter we show that the open loop and arbitrary reference model approaches can indeed be applied to systems with nonlinear controllers provided that certain stability conditions regarding these controllers are satisfied. We present a simulation example on a 6-DOF spinning projectile simulation code where a nonlinear guidance law is augmented by an adaptive controller to partially cancel the uncertainties in the system, which include unmodeled rigid body dynamics of the projectile, parameter uncertainties, and nonlinear effects due to discrete actuation.

2.1 Overview

The open loop and arbitrary reference model-following control architectures are depicted in Figure 2-1. In both approaches, tracking error and states of the adaptive controller are guaranteed to be bounded through Lyapunov like stability analysis. Notice in Figure 2-1 (a) that boundedness of tracking error e does not necessarily imply boundedness of both y_m and y. In order to ensure both y_m and y, and the existing control signal u_{ec} will remain bounded when e is bounded, it is assumed in [16] that the

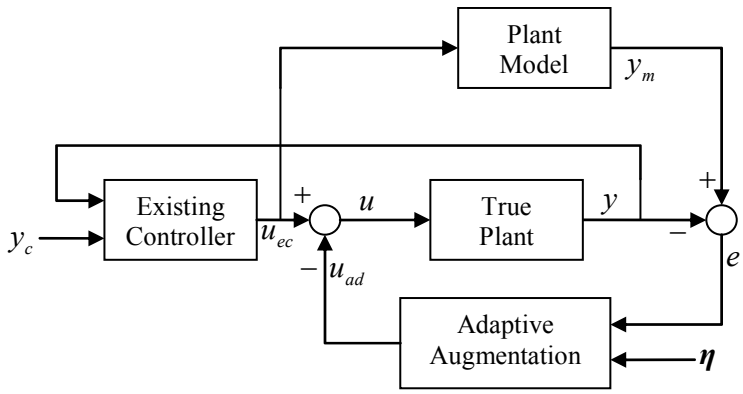

(a) Open loop reference model-following

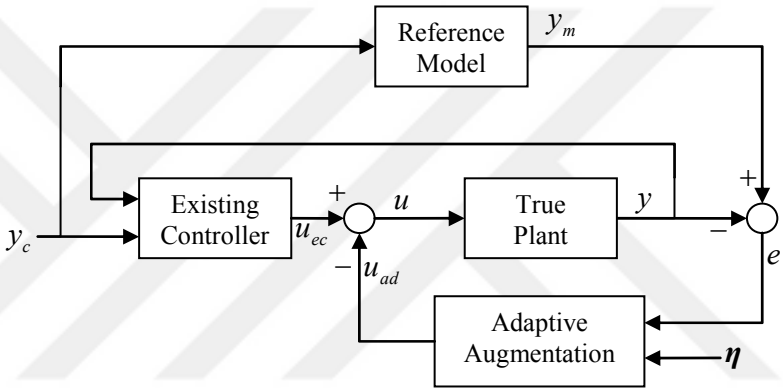

(b) Arbitrary reference model-following

Figure 2-1. Adaptive augmenting architectures: (a) open-loop reference model-following approach [16], (b) arbitrary reference model-following approach [23].

existing controller is linear and is designed to control the linear plant model. In the arbitrary reference model-following control approach in Figure 2-1 (b), y_m is always bounded for bounded y_c since the reference model is designed as a stable linear system. The only signal that is left out in the stability proof in [23] is the existing control signal u_{ec}, which is guaranteed to remain bounded by assuming that the existing controller is a linear stable dynamic system.

The assumptions regarding the existing controller in [16] and [23] are sufficient to prove boundedness of all the signals in the closed loop system. Consider the equivalent block diagram representations in Figure 2-2 with tracking error e viewed as an external

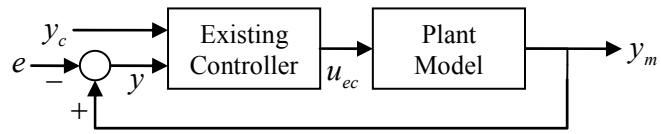

(a) Open loop reference model-following [16]

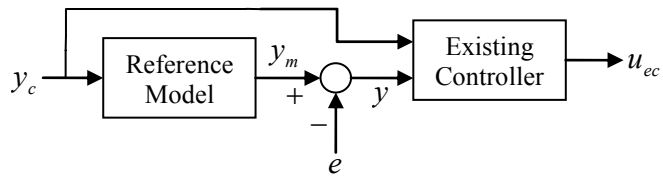

(b) Arbitrary reference model-following [23]

Figure 2-2. Equivalent representations of the open loop and arbitrary reference model adaptive augmenting architectures.

signal that is known to be bounded. It is clear from Figure 2-2 (a) that if the existing controller is linear and is designed to stabilize the linear plant model, for bounded y_c and e, u_{ec} and y_m remain bounded. Similarly we see in Figure 2-2 (b) that if the existing controller is a linear stable system, then u_{ec} remains bounded for bounded y_c and e.

2.2 Stability with Nonlinear Existing Controllers

Let the existing controller in both augmenting approaches in Figure 2-2 be represented by

$$\begin{aligned} \dot{\boldsymbol{x}}_c &= \boldsymbol{f}_c\left(\boldsymbol{x}_c, y, y_c\right) \\ u_{ec} &= h_c\left(\boldsymbol{x}_c, y, y_c\right) \end{aligned} \tag{2.1}$$

The input-output relation of (2.1) can be represented by

$$u_{ec} = H\overline{y} \tag{2.2}$$

where H is a mapping or an operator that assigns to each input $\overline{y} = \begin{bmatrix} y & y_c \end{bmatrix}^T \in \mathbb{R}^m$ the corresponding signal $u_{ec} \in \mathbb{R}^n$. In order to make the analysis applicable to finite time

horizon problems, such as the one in Section 2.3, we consider extended $\mathcal{L}_\infty$ spaces defined by

$$\mathcal{L}_{\infty_e} = \left\{ u \middle| u_\tau \in \mathcal{L}_\infty \, \forall \, \tau \geq 0 \right\}$$

where u_τ is a truncation of u defined by

$$u_\tau(t) = \begin{cases} u(t), & 0 \leq t \leq \tau \\ 0, & t > \tau \end{cases}$$

We have the following standard definition for bounded input-bounded output stability [7].

Definition 2.1. A mapping $H : \mathcal{L}_{\infty_e}^m \to \mathcal{L}_{\infty_e}^n$ is bounded-input bounded-output stable if there exist a class $\mathcal{K}$ function α, defined on $[0, \infty)$, and a nonnegative constant β such that

$$\left\| (Hu)_\tau \right\|_{\mathcal{L}_\infty} \leq \alpha \left(\left\| u_\tau \right\|_{\mathcal{L}_\infty} \right) + \beta$$

for all $u \in \mathcal{L}_{\infty_e}$ and $\tau \in [0, \infty)$.

For completeness of the analysis of stability of the aforementioned augmenting approaches with nonlinear existing controllers, we will provide brief descriptions of the architectures. Consider the following *observable* and *stabilizable* nonlinear single-input single-output (SISO) system in normal form [8]

$$\begin{aligned} \dot{\boldsymbol{z}} &= \boldsymbol{f}(\boldsymbol{z}, \boldsymbol{x}) \\ \dot{x}_1 &= x_2 \\ &\vdots \\ \dot{x}_{r-1} &= x_r \\ \dot{x}_r &= h_r(\boldsymbol{z}, \boldsymbol{x}, u) \\ y &= x_1 \end{aligned} \tag{2.3}$$

where $\boldsymbol{z} \in \mathbb{R}^{n-r}$ and $\boldsymbol{x} = \begin{bmatrix} x_1 & \cdots & x_r \end{bmatrix}^T \in \mathbb{R}^r$ are the states of the internal and output dynamics respectively, $u, y \in \mathbb{R}$ are control and measurement variables, $\boldsymbol{f}$ and h are sufficiently smooth partially known functions, and r is the relative degree of the system. Let the existing controller be given in (2.1).

Assumption 2.1. The true plant given in (2.3) is minimum phase, i.e., the internal dynamics $\dot{\boldsymbol{z}} = \boldsymbol{f}(z, \boldsymbol{x})$ with $\boldsymbol{x} = 0$ are asymptotically stable.

2.2.1 Open Loop Reference Model-Following Approach [16]

The controller architecture is depicted in Figure 2-1 (a). Let the linearized plant model be described by

$$\begin{aligned} \dot{x}_{m_1} &= x_{m_2} \\ &\vdots \\ \dot{x}_{m_{r-1}} &= x_{m_r} \\ \dot{x}_{m_r} &= C_r \boldsymbol{x}_m + D_r u \\ y_m &= x_{m_1} \end{aligned} \tag{2.4}$$

where $\boldsymbol{x}_m = \begin{bmatrix} x_{m_1} & \cdots & x_{m_r} \end{bmatrix}^T \in \mathbb{R}^r$. The existing controller is augmented with an adaptive element as

$$u = u_{ec} - u_{ad} \tag{2.5}$$

Assumption 2.2. The linear plant model given in (2.4) is observable.

Defining tracking error as $e = y_m - y$, the error dynamics can be expressed using (2.3) and (2.4) as

$$\begin{aligned} \dot{e}_i &= e_{i+1} \\ \dot{e}_r &= -D_r \left(u - u_{ec}\right) - \Delta\left(\boldsymbol{x}, \boldsymbol{x}_m, u\right) \\ &= -D_r u_{ad} - \Delta\left(\boldsymbol{x}, \boldsymbol{x}_m, u\right) \end{aligned} \tag{2.6}$$

where

$$\Delta\left(\boldsymbol{x},\boldsymbol{x}_m,u\right)=h_r\left(z,x_1,\ldots,x_r,u\right)-C_r\boldsymbol{x}_m-D_r u\,. \tag{2.7}$$

Assumption 2.3. The closed loop system formed by the linear plant model (2.4) and the controller (2.1) as depicted in Figure 2-2 (a) is bounded input-bounded output stable.

The adaptive signal u_{ad} in (2.5) is designed as

$$u_{ad}=D_r^{-1}\left(\nu_{dc}-\nu_{ad}\right) \tag{2.8}$$

where ν_{dc} is a linear dynamic compensator signal introduced to stabilize the linear dynamics in (2.6) and ν_{ad} is an adaptive element designed as a linearly parameterized NN as

$$\nu_{ad}=\hat{\boldsymbol{W}}^T\boldsymbol{\varphi}\left(\boldsymbol{\eta}\right) \tag{2.9}$$

where $\boldsymbol{\eta}$ is the input signal comprised of system input and output and a number of their delayed values. The NN weight vector is adjusted online using

$$\dot{\hat{\boldsymbol{W}}}=-F\left(\tilde{y}_{ad}\boldsymbol{\varphi}_f+\sigma\hat{\boldsymbol{W}}\right) \tag{2.10}$$

where $F>0$ is a gain matrix, $\tilde{y}_{ad}$ is a filtered tracking error signal and $\boldsymbol{\varphi}_f$ is a filtered NN basis function output. The filters introduced in (2.10) are required for stability of the closed loop system as explained in [12].

Theorem 2.1. Consider system (2.3) under control of (2.8) with (2.1), (2.9), and (2.10). Let Assumptions 2.1–2.3 hold. Then all the signals in the system including the tracking error vector $\boldsymbol{E}\triangleq\begin{bmatrix}e & \dot{e} & \cdots & e^{(r-1)}\end{bmatrix}^T$, $\boldsymbol{x}$, $\boldsymbol{x}_m$, u_{ec}, u_{ad}, and $\hat{\boldsymbol{W}}$ are uniformly ultimately bounded.

Proof. Theorem 4.1 in [16], based on the theorems in [12], guarantees uniform ultimate boundedness of $\boldsymbol{E}=\boldsymbol{x}_m-\boldsymbol{x}$, $\hat{\boldsymbol{W}}$ and u_{ad}. Given bounded e and y_c, Assumption 2.3

ensures boundedness of $\boldsymbol{x}_m$. Bounded $\boldsymbol{E}$ and $\boldsymbol{x}_m$ imply bounded $\boldsymbol{x}$. Then given bounded $\boldsymbol{x}_m$, Assumption 2.2 guarantees that u_{ec} is bounded. ■

2.2.2 Arbitrary Reference Model-Following Approach [23]

The controller architecture is depicted in Figure 2-1 (b). A linear stable system of order r with full relative degree is selected as the reference model:

$$\begin{aligned} \dot{\boldsymbol{x}}_m &= A_m \boldsymbol{x}_m + \boldsymbol{b}_m y_c \\ y_m &= x_{m_1} = \boldsymbol{c}_m^T \boldsymbol{x}_m \end{aligned} \tag{2.11}$$

Notice that the linear model in (2.4) in Section 2.2.1 approximates the open loop plant from control u to output y, whereas the reference model in (2.11) specifies the *desired* closed loop behavior from tracking command y_c to output y.

Defining tracking error as $e = y_m - y$, the error dynamics can be expressed from (2.3) and (2.11) as

$$\begin{aligned} \dot{\boldsymbol{E}} &= A_m \boldsymbol{E} + \boldsymbol{b}_m \left(u_{ad} - \Delta\left(\boldsymbol{x}, y_c, u_{ad} \right) \right) \\ y &= e = \boldsymbol{c}_m^T \boldsymbol{E} \end{aligned} \tag{2.12}$$

Where $\boldsymbol{E} \triangleq \begin{bmatrix} e & \dot{e} & \cdots & e^{(r-1)} \end{bmatrix}^T$ and

$$\Delta\left(\boldsymbol{x}, y_c, u_{ad} \right) = D_r^{-1} \left(h_r \left(\boldsymbol{z}, x_1, \ldots, x_r, u \right) - C_r \boldsymbol{x}_m \right) - y_c + u_{ad} \,. \tag{2.13}$$

Assumption 2.4. The existing controller (2.1) is bounded input-bounded output stable.

The existing controller (2.1) is augmented with an adaptive element as

$$u = u_{ec} - u_{ad} \tag{2.14}$$

where

$$u_{ad} = \hat{M}^T \boldsymbol{\sigma} \left(\hat{N}^T \boldsymbol{\eta} \right) \tag{2.15}$$

and $\boldsymbol{\eta}$ is the input signal comprised of system input and output and a number of their delayed values. The NN weight matrices are adjusted online using

$$\begin{aligned} \dot{\hat{M}} &= -\Gamma_M \left[2\left(\hat{\boldsymbol{\sigma}} - \hat{\sigma}'\hat{N}^T\boldsymbol{\eta}\right)\hat{\boldsymbol{E}}^T\bar{P}B_1 + k\hat{M} \right] \\ \dot{\hat{N}} &= -\Gamma_N \left[2\boldsymbol{\eta}\hat{\boldsymbol{E}}^T\bar{P}B_1\hat{M}^T\hat{\sigma}' + k\hat{N} \right], \end{aligned} \tag{2.16}$$

where Γ_M, Γ_N are positive definite adaptation gain matrices, $k > 0$ is a $\sigma-$ modification gain, $\boldsymbol{\sigma}$ is a vector of squashing functions $\boldsymbol{\sigma}(\cdot)$, $\hat{\boldsymbol{\sigma}} = \boldsymbol{\sigma}\left(\hat{N}^T\boldsymbol{\eta}\right)$, $\hat{\sigma}'$ denotes the Jacobian matrix computed at the estimate: $\hat{\boldsymbol{\sigma}}' = \boldsymbol{\sigma}'\left(\hat{N}^T\boldsymbol{\eta}\right)$.

A linear observer is introduced to estimate the tracking error dynamics in (2.12) as

$$\begin{aligned} \dot{\hat{\boldsymbol{E}}} &= A_m\hat{\boldsymbol{E}} + K\left(y - \hat{y}\right) \\ \hat{y} &= \boldsymbol{c}_m^T\hat{\boldsymbol{E}} \end{aligned} \tag{2.17}$$

Theorem 2.2. Consider the system (2.3) under the control of (2.14) with (2.1), (2.15), and (2.16). Let Assumptions 2.1 and 2.4 hold. Then all the signals in the system including $\boldsymbol{E}$, $\tilde{\boldsymbol{E}} \triangleq \hat{\boldsymbol{E}} - \boldsymbol{E}$, $\boldsymbol{x}$, $\boldsymbol{x}_m$, u_{ec}, u_{ad}, $\hat{M}$ and $\hat{N}$ are uniformly ultimately bounded.

Proof. Theorem 4.1.1 in [23] guarantees uniform ultimate boundedness of $\boldsymbol{E}$, $\tilde{\boldsymbol{E}}$, $\hat{M}$, $\hat{N}$, and u_{ad}. Since y_c is bounded and the reference model is stable, $\boldsymbol{x}_m$ is bounded. Bounded $\boldsymbol{x}_m$ and $\boldsymbol{E}$ imply bounded $\boldsymbol{x}$. Given bounded $\boldsymbol{E}$ and y_c, Assumption 2.4 ensures boundedness of u_{ec}. ■

2.3 Simulation Example

Trajectory control of direct fire spinning projectiles using on board control mechanisms proved to be an effective method for accommodating errors caused by calculated trajectory approximation [50]. The guidance law developed in [50] for the

horizontal and vertical plane motion of a spinning projectile shown in Figure 1-6 managed to steer the projectile into achieving virtually zero miss distance with and without error in effector, which is modeled as a continuous lateral force generator. Further research has shown that the guidance law developed cannot adjust quickly enough to accommodate actuator nonlinearities and uncertainties. In addition, actuator induced moment effect causes amplification or attenuation of the control force depending on its direction and this leads to increased target misses and peak control force [50]. Target misses caused by wind disturbances are expected to further deteriorate the performance. At the stage where flight tests are to be performed, actuator characteristics will add to the uncertainties in the system. Using Micro Adaptive Flow Control (MAFC) actuators appears to be one of the most suitable ways of generating the desired forces. MAFC actuators generate aerodynamic forces and moments by altering the axially symmetric base flow, and the apparent aerodynamic cross section of the projectile, with very modest control effort [47]. It is unlikely that a complete and accurate model of MAFC actuators will be available. To deal with these uncertainties, the guidance law has been augmented with a NN based adaptive element [25].

We augmented the guidance law with an adaptive controller following the approach in [16] and tested it in simulation with discrete firing logic and a static synthetic jet model [25]. Control hedging proved to be crucial in this case for protecting the adaptive controller against the jet model, discrete firing, and most importantly low rate update of control. In order to prevent feedback of the precession mode through the guidance loop, control was updated once every 25 revolutions, which promptly destabilized the system with adaptive controller without control hedging.

In the following sections, we first give an overview of the guidance law and firing logic, followed by simulation results. Guidance law is improved compared to the one used in [50] and [25], where some velocity terms in the linear point mass model were assumed constant. These simplifications are now removed, and the firing logic is also

improved to provide the desired impulse in the correct direction over one spin cycle. In the previous firing logic, an approximate value was used to set the impulse direction.

2.3.1 Guidance Law Overview

The idea of the guidance law is to use a model of the projectile dynamics to calculate the miss distance that would result if the projectile were allowed, at any point in its trajectory, to freely fly the remaining range to target. The miss distance calculated in this manner is called the zero effort miss (ZEM). The time the projectile requires to fly the range to target distance is called the time to go (t_{go}). The guidance law calculates a constant acceleration needed to cancel the ZEM in a time t_{go}. This form of guidance should minimize the peak force required over the trajectory.

A point mass model of the projectile is used for guidance law derivation [51]

$$\dot{V}_{x_m} = \alpha V_{x_m} \tag{2.18}$$

$$\dot{V}_{z_m} = \alpha V_{z_m} + g + u_z \tag{2.19}$$

$$\dot{V}_{y_m} = \alpha V_{y_m} + \beta V_{x_m} - \delta V_{y_m} V_{z_m} + u_y \tag{2.20}$$

where $\alpha = -\dfrac{QSC_D}{mV}$, $\beta = \dfrac{C_{L_\alpha} I_x pg}{C_{m_\alpha} dmV^2}$, and $\delta = \dfrac{C_{N_{p\alpha}} p^2 I_x g}{C_{m_\alpha} mV^4}$. Here, V_{x_m}, V_{z_m}, and V_{y_m} are the velocities of the linear projectile model in the inertial *x*, *z*, and *y* axes respectively, *Q* is the dynamic pressure, *g* is the acceleration due to gravity, I_x is the central moment of inertia about the axis of rotation of the projectile, *p* is the spin rate of the projectile, and u_z and u_y are the acceleration control commands along *z* and *y* axes. Time-to-go is computed by integrating (2.18) twice as

$$t_{go} = \frac{\log\left(1 + \dfrac{\alpha\left(x_T - x(0)\right)}{V_x(0)}\right)}{\alpha}. \tag{2.21}$$

with x_T being the x coordinate of the target. Integrating (2.19) and (2.20) twice gives z and y components of the projectile position as

$$z(t)=z(0)+\left[\frac{V_z(0)}{\alpha}+\frac{g+u_{ec,z}}{\alpha^2}\right]\left(e^{\alpha t}-1\right)-\frac{g+u_{ec,z}}{\alpha}t \tag{2.22}$$

$$y(t)=y(0)+\left[\frac{V_y(0)}{\alpha}-\frac{\beta V_x(0)}{\alpha^2}\right]\left(e^{\alpha t}-1\right)+\frac{\beta V_x(0)}{\alpha}te^{\alpha t} \tag{2.23}$$

The constant guidance commands $u_{ec,z}$ and $u_{ec,y}$ required to cancel ZEM's are solved from (2.22) and (2.23) by equating $z\left(t_{go}\right)=z_T$ and $y\left(t_{go}\right)=y_T$ with z_T and y_T being the z and y coordinates of the target:

$$u_{ec,z}=\frac{z_T-z(0)-\left[\frac{V_z(0)}{\alpha}+\frac{g}{\alpha^2}\right]\left(e^{\alpha t_{go}}-1\right)+\frac{g}{\alpha}t_{go}}{-\frac{1}{\alpha}t_{go}+\frac{1}{\alpha^2}\left(e^{\alpha t_{go}}-1\right)} \tag{2.24}$$

$$u_{ec,y}=\frac{y_T-y(0)-\left[\frac{V_y(0)}{\alpha}-\frac{\beta V_x(0)}{\alpha^2}\right]\left(e^{\alpha t_{go}}-1\right)-\frac{\beta V_x(0)}{\alpha}t_{go}e^{\alpha t_{go}}}{\left(-\frac{1}{\alpha}t_{go}+\frac{1}{\alpha^2}\left(e^{\alpha t_{go}}-1\right)\right)} \tag{2.25}$$

Every time the guidance law is updated, time-to-go from that instant to the end of the flight and the necessary corrective commands are computed from (2.21), (2.24), and (2.25) by using the current state of the projectile as the initial condition. Hence $t=0$ in (2.21), (2.24), and (2.25) refers to the current time.

Remark 2.1. Notice that t_{go} that appears nonlinearly in (2.24) and (2.25) is a nonlinear function of position and velocity in x direction and consequently the existing guidance controller is a static nonlinear controller. For bounded target position $\left(x_T, y_T, z_T\right)$, (2.24) and (2.25) generate bounded corrective acceleration commands $u_{ec,y}$ and $u_{ec,z}$ for $t<t_{go}$, which in turn yields to bounded reference model output V_{x_m}, V_{z_m}, and V_{y_m} for $t<t_{go}$. Therefore the reference model, comprised of the point mass model (2.18)–(2.20) with the nonlinear coupling term in (2.20) removed under the control of guidance law (2.24),

(2.25) is finite time bounded input-bounded output stable with $\tau = t_{go}$. Consequently stability of the closed loop system is guaranteed for the finite time interval $t \in [0, \tau)$ subject to the assumptions and conditions in Theorem 2.1 and [20].

2.3.2 Actuation via Flow Control

The actuator is modeled as a single synthetic jet effector fixed to the projectile body. In order to approximately achieve the continuous force commands given in a non-rotating body frame, the jet has to be fired in a discrete manner. Following sections discuss actuator modeling and jet firing logic.

2.3.2.1 Actuator modeling

The actuator is modeled as a single synthetic jet effector that fires once per revolution of the projectile. Figure 2-3 shows an experimentally obtained response of an MAFC actuator [48]. The incremental change in circulation (with respect to the baseline flow) about a stalled 2-D airfoil is shown in Figure 2-3 (a). Figure 2-3 (b) shows flow visualization images taken during actuation. To model the transient response observed in Figure 2-3 (a), we use a time domain model depicted in Figure 2-4. Figure 2-4 (a) shows the force profile of the actuator jet model. Figure 2-4 (b) shows the y and z axis components of the force acting on the projectile with respect to a body fixed non-spinning frame, and Figure 2-4 (c) shows the polar firing plot. The jet is modeled as follows:

$$F_{jet} = \begin{cases} F_0 & 0 < t \le T_0 \\ F_0 + \dfrac{(F_1 - F_0)\left(1 - e^{-a(t-T_0)}\right)}{1 - e^{-a(T_1 - T_0)}} & T_0 < t \le T_1 \\ F_1 e^{-b(t-T_1)} & T_1 < t \le T_2 \end{cases}$$

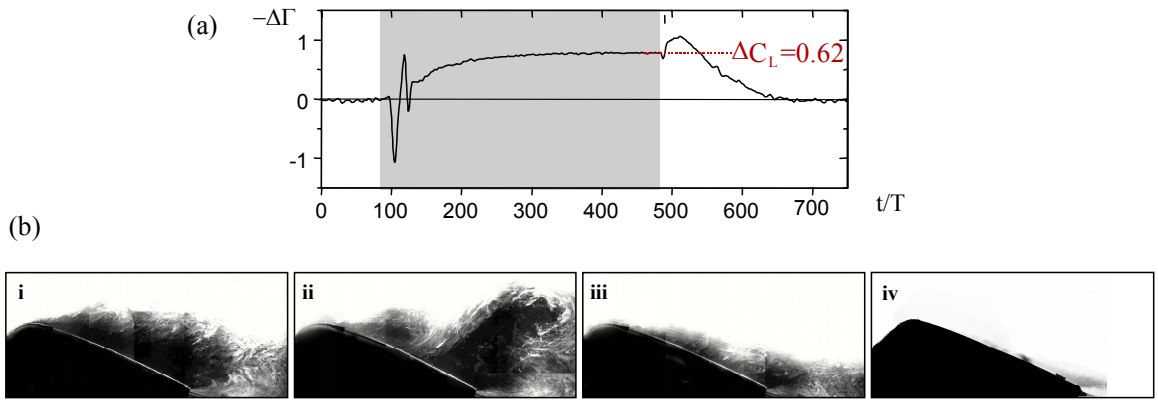

Figure 2-3. Transient control with an active flow actuator: a) Time history of the circulation when control is activated, b) Flow visualization images during flow reattachment: i. separated flow, ii. collapse of the separation domain, iii. beginning of full reattachment, and iv. full reattachment [48].

where $t = 0$ is the start of a new firing cycle corresponding to $\phi = 0$ shown in Figure 2-4 (c), a and b are empirical constants, F_0 is the jet force at $t = 0$, T_0 and T_1 designate the time at which the jet force starts rising and decaying, T_2 designates the end of the jet firing interval and the start of a new one, F_s is the force F_{jet} would reach as $t \to \infty$,

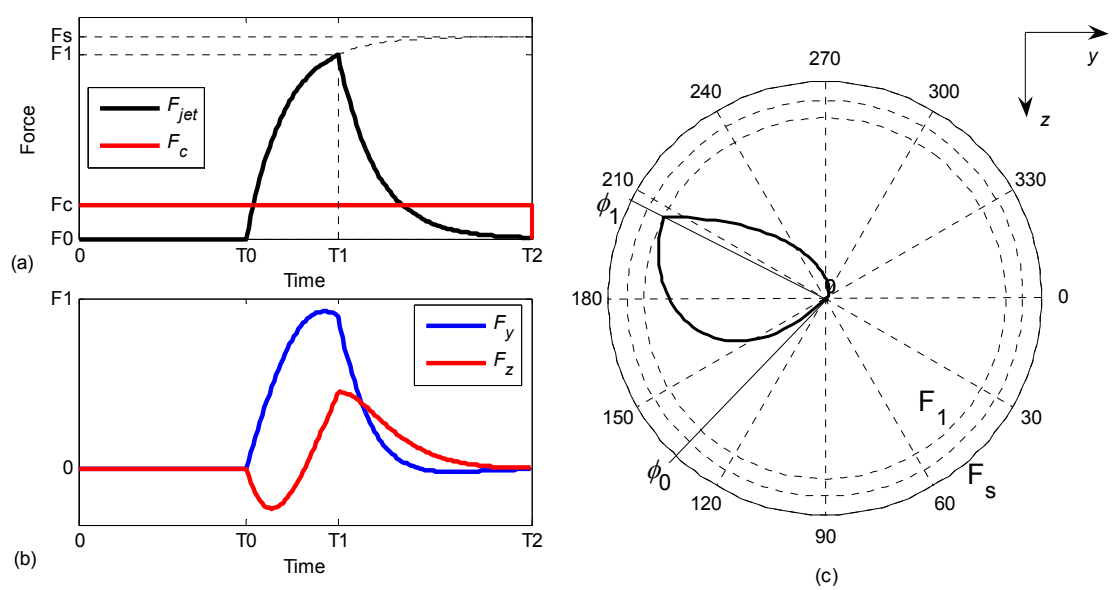

Figure 2-4. Modeling of Jet force Profile.

which is assumed fixed, and F_1 is the actual peak force achieved at $t = T_1$.

2.3.2.2 Jet firing law

Figure 2-5 is a representation of the firing process. At point '*a*' the angle of rotation of the projectile, ϕ, is equal to zero and is considered the start of a new spin cycle. At each such point '*a*' the firing law samples the required forces F_z and F_y. The goal is to find the firing start and end times T_0 and T_1 (or equivalently the corresponding roll angles ϕ_0 and ϕ_1) so that the impulses of the jet firing in one cycle along *z* and *y* axes are equal to those of the commanded forces $T_2 F_z$ and $T_2 F_y$. First, assuming $T_0 = 0$, total firing duration $T_1 - T_0$ that gives the magnitude of the desired total impulse $I_c = \sqrt{(T_2 F_z)^2 + (T_2 F_y)^2}$ is found by using a one dimensional search algorithm. Then T_0 and T_1 are shifted to equate the direction of the jet impulse to the desired direction, $\phi_{force} = \tan^{-1}(F_z / F_y)$. Since we assume that F_s is fixed, maximum impulse of the jet is limited. In case the desired impulse is greater than the maximum achievable impulse, $T_1 - T_0$ is set to produce the maximum impulse and T_0 and T_1 are shifted to give the

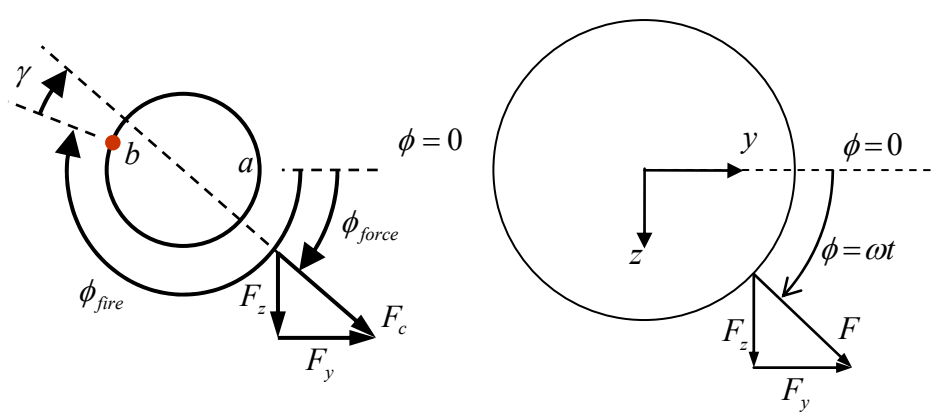

Figure 2-5. Schematic of the jet firing process.

correct direction.

2.3.3 Adaptive controller augmentation

The point mass model (2.18)-(2.20) with the nonlinear coupling term $\delta V_y V_z$ in (2.20) removed is used as a linear model of the system. The nonlinear guidance law (2.24) and (2.25) is augmented using the open-loop reference model-following controller architecture with control hedging [17], [18]. The adaptive controller has to compensate for the unmodeled rigid body dynamics of the projectile, parameter uncertainties, and nonlinear discrete actuation process. Control hedging is introduced to protect the adaptive process from the effects of actuation nonlinearities. Actuator saturation and the difference between a continuous jet force profile and the actual jet force profile (Figure 2-4 (a)) are modeled in the hedging loop. A discussion on the role of control hedging in the arbitrary reference model augmenting approach can be found in Section 4.2.

2.3.4 Simulation Results

For simulation testing, we employ the nonlinear 6-DOF spinning projectile simulation code called 'BOOM' [52]. The jet can produce a maximum force of 0.2 lbf, which is overestimated in the firing law computations by 50%. An effector that produces less force than the commanded causes an error build-up in ZEM, which leads to increasingly large commanded control forces and eventually control saturation. We also introduce uncertainty by assuming that the control force effector also induces a moment. The effector is modeled as producing a moment proportional to the force with a negative proportionality constant l. The dynamics are much more sensitive in the negative l direction, for which the induced moment opposes the applied force.

Figure 2-6 shows the simulation results with guidance law only. The plots in the first row show the trajectory in the vertical and horizontal plane in comparison with the uncontrolled trajectory. The effects of parametric uncertainty and unmodeled dynamics

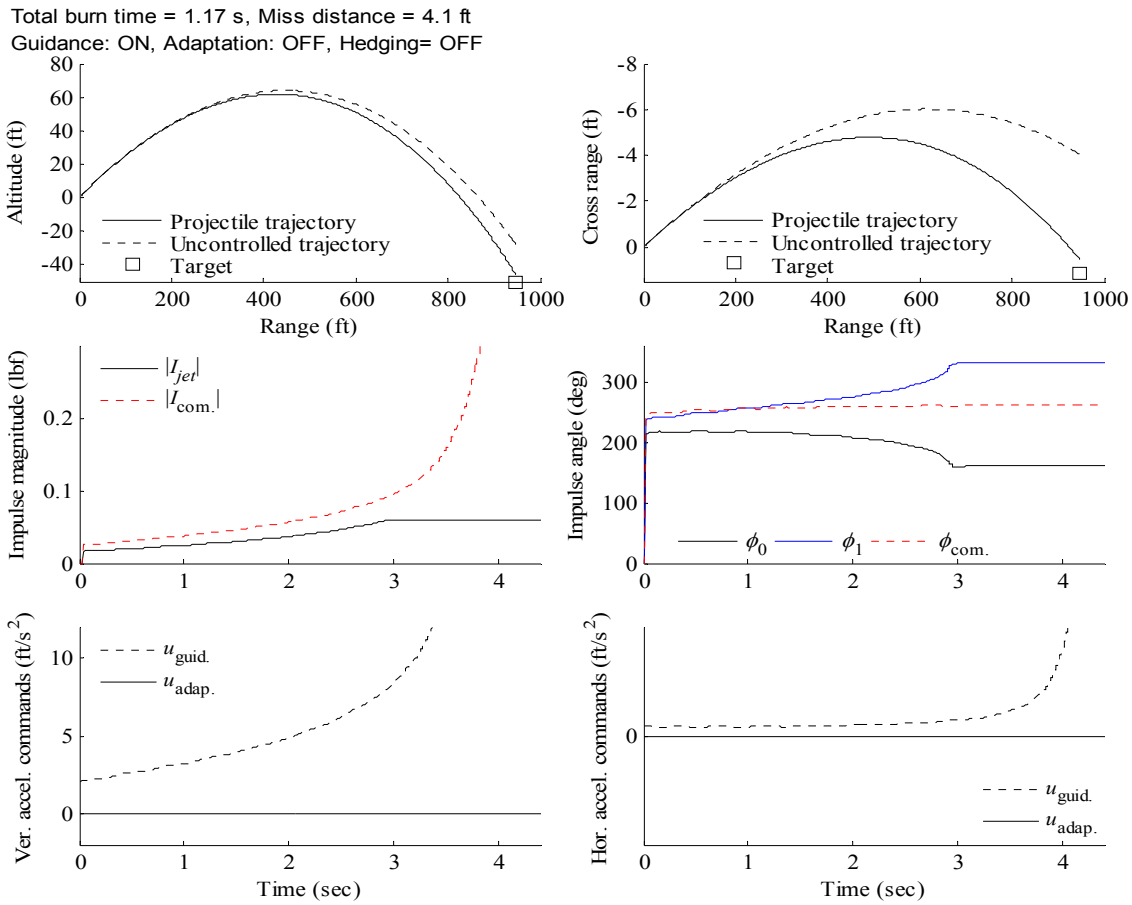

Figure 2-6. Simulation results without adaptation.

can be observed in the second row plots. The plot on the left shows the magnitudes of the commanded and achieved impulses and the second plot shows the jet turn-on and turn-off angles ϕ_0, ϕ_1 together with the direction of the commanded impulse, $\phi_{\text{com.}}$. The offset in the magnitude curve is due to the fact that the jet produces less force than expected from the model for the actuator predicts. Without the uncertainties, a constant control input would be able to steer the projectile to the target. As mentioned before, guidance commands increase as the effects of the uncertainties build up and eventually saturation occurs around $t = 3$ s. Projectile misses the target by 4.1 ft, as indicated on the top of the figure. Guidance law and adaptive components of the control signal u_{ec} and u_{ad} are shown on the bottom plots.

Results with adaptation but without hedging are shown in Figure 2-7. Adaptation significantly cancels the effects of the uncertainties as the trajectory and guidance law commands show (the guidance command no longer saturates). The projectile practically hits the target with near zero error, and the guidance law commands remain fairly constant, which they were designed to do in the absence of modeling error. However, the adaptive signals in both channels are highly oscillatory. This is because discrete firing excites the precession mode of the projectile, and the adaptive controller attempts to respond to this excitation. This is an effect of nonlinear actuation that can not be removed by adaptation, and therefore the effect should be hedged (removed for the error signal) so that the adaptive process will not perceive it as modeling error. Simulation results with hedging support this claim, as shown in Figure 2-8. The trajectory is nearly identical to the one without hedging. However, the oscillation and saturations in control are nearly completely eliminated.

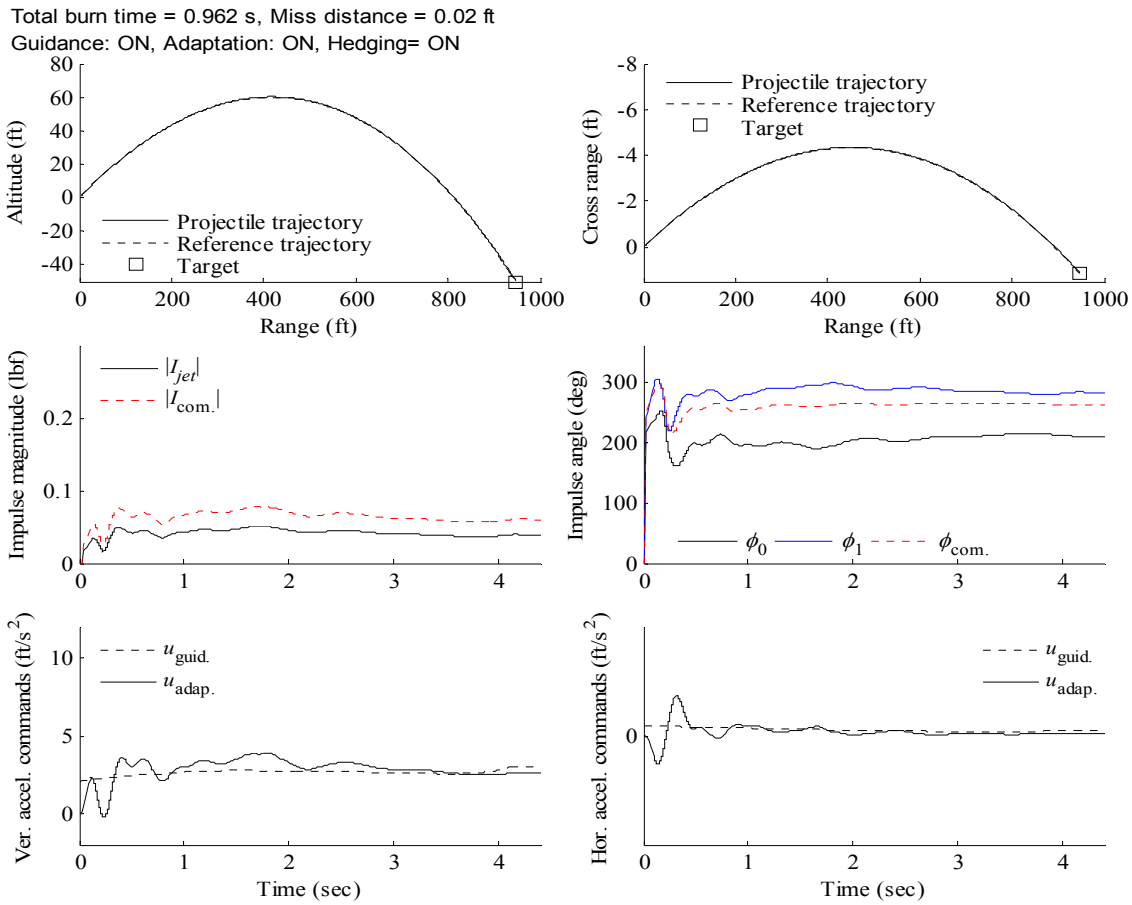

Figure 2-7.8 Simulation results with adaptation without hedging.

Precession is a rotation of the axis of symmetry of the projectile around a cone whose axis coincides with the velocity vector. This motion is best illustrated by plotting angle-of-attack versus sideslip. Figure 2-9 shows the α vs. β plots for the three controlled flights corresponding to Figure 2-6 through Figure 2-8. When adaptation is turned on without hedging, the precession cone gets bigger compared to the case without adaptation. The smallest cone is achieved with both adaptation and hedging active, showing that adaptation can reduce the magnitude of the precession mode with the help of hedging.

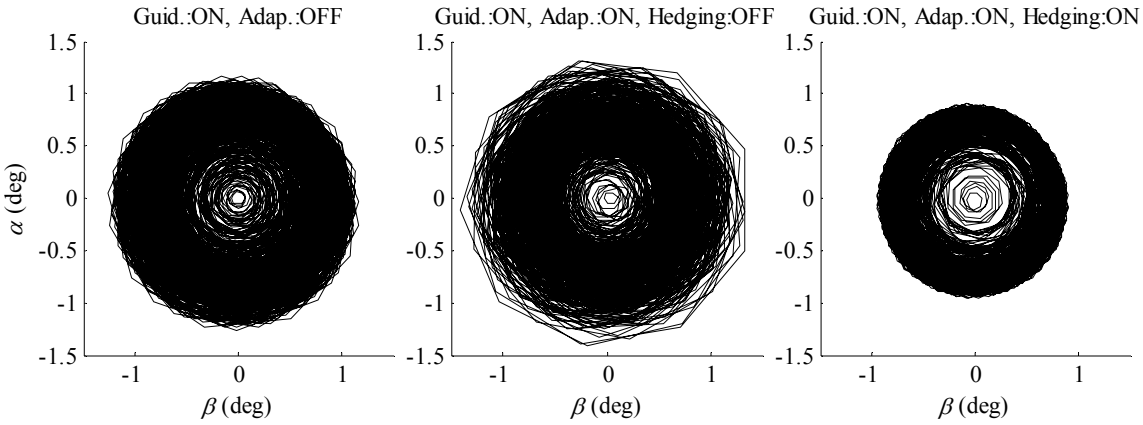

Figure 2-9. Precession motion for three controlled cases.

2.4 Conclusions

In this chapter we derived the conditions for stability of the closed loop system when the adaptive augmenting controllers of [16] and [20] are applied to systems with nonlinear existing controllers. Then we applied the controller of [16] to augment the nonlinear guidance law of a spinning projectile. The baseline guidance law aims to minimize the peak control force required over the trajectory. Effects of various uncertainties in the system can build up before the guidance law can act to compensate for them. This can lead to increasing control force and saturation. Adaptive augmentation successfully removes the effects of the uncertainties from the system leading the projectile to follow the ideal trajectory of a point mass. Consequently the guidance law can steer to the target with a more evenly distributed force profile. Discrete firing of the jet interacts with the precession mode of the projectile in a manner that causes an oscillatory response from the adaptive process. This also can lead to control saturation. Hedging is employed to prevent adaptive process from reacting to the effect of nonlinear actuation, and significantly improves the overall response.

CHAPTER 3

ARBITRARY REFERENCE MODEL-FOLLOWING ADAPTIVE AUGMENTING CONTROL FOR NON-MINIMUM PHASE SYSTEMS

This chapter addresses augmentation of an existing controller of a non-minimum phase system with an adaptive output feedback element in the framework of arbitrary reference model-following control. The recently developed closed loop reference model-following adaptive augmenting controller does not rely on feedback inversion and hence is applicable to non-minimum phase systems [19]. It is important to note that in this approach the adaptive controller does not attempt to control unstable internal dynamics of the system. Stability of the overall closed loop system is ensured by introducing an assumption that non-minimum phase zeros of the true plant are represented in the linear model with sufficient accuracy and the existing linear controller design takes into account the presence of these zeros. However the approach relies on the use of a reference model that is constructed using the existing controller and the plant model used to design the existing controller. There are many applications in which the existing controller is tuned from experiments performed on the actual system, and therefore the plant model cannot be used to construct a suitable reference model. In this chapter, to handle adaptive augmentation of non-minimum phase systems for which accurate linear models are not available, we adopt the formulation of [19] regarding internal dynamics of the system to the arbitrary reference model-following approach of Ref. [23].

3.1 Background

Control of nonlinear non-minimum phase systems is a challenging problem, particularly in an output feedback setting. Among several efforts in the literature that address this problem [53]-[56], the adaptive augmentation approach developed in Ref. [19] suits our purposes. In [19], an existing controller is assumed to be designed using a linear model of the plant that models the zero dynamics with sufficient accuracy. By this it is meant that the unstable zero dynamics are recognized and addressed in the design of the existing controller. To compensate for the modeling errors that arise from linear approximation of the nonlinear system, a NN-based adaptive element is introduced to augment the existing controller. The approach is then extended to multi-input multi-output systems in [20], [21].

In this chapter we similarly assume that non-minimum phase zeros of the true plant are recognized and addressed in the design of the existing controller, and that the modeling error of the non-minimum phase internal dynamics satisfies a conic sector bound. This assumption permits these dynamics to be managed by a robust control component.

As discussed in Section 1.1, requiring availability of a linear model of the true plant, and further assuming that the closed loop system formed by the linear model and the existing controller has satisfactory dynamics, may impose a significant restriction on controller design for real world problems. Our goal in this chapter is to relax this requirement by introducing an arbitrary stable model as the reference model. The word "arbitrary" is used in a weaker sense here since the zeros of the reference model are determined by the internal dynamics model of the true plant and only the poles can be selected arbitrarily within physical limitations of the plant. Moreover, the relative degree of the reference model has to match that of the regulated output (within the bandwidth of interest). In this architecture error dynamics for the adaptive controller are formed based on the reference model dynamics and do not involve dynamics of the existing controller.

One direct implication is that the linearity requirement of the existing controller is relaxed subject to the conditions in Chapter 2. Another difference between the development here and the one in References [19]–[21] is that states of the unstable zero dynamics of the true plant and the reference model are considered individually in the error analysis whereas in [19]–[21] only the error between them is considered. Validity of the approach is demonstrated on the numerical example of Ref. [19]. Results show substantial improvements in transient dynamics.

3.2 Problem Formulation

Consider the following *observable* and *stabilizable* nonlinear single-input single-output (SISO) system in normal form

$$\begin{aligned} \dot{\boldsymbol{z}} &= \boldsymbol{f}\left(\boldsymbol{z}, \xi_1, \ldots, \xi_r\right) \\ \dot{\xi}_1 &= \xi_2 \\ &\vdots \\ \dot{\xi}_{r-1} &= \xi_r \\ \dot{\xi}_r &= h_r\left(\boldsymbol{z}, \xi_1, \ldots, \xi_r, u\right) \\ y &= \xi_1 \end{aligned} \tag{3.1}$$

where $\boldsymbol{z} \in \mathcal{D}_z \subset \Re^{n-r}$ and $\boldsymbol{\xi} = \begin{bmatrix} \xi_1 & \cdots & \xi_r \end{bmatrix}^T \in \mathcal{D}_\xi \subset \Re^r$ are the states of the internal dynamics and output dynamics respectively, $u \in \mathcal{D}_u \subset \Re$, $y \in \Re$ are control and measurement variables, $\boldsymbol{f}$ is a partially known sufficiently smooth function, h is an unknown sufficiently smooth function with know sign of control effectiveness $\partial h_r / \partial u$, and r is the relative degree of the regulated output.

A linear model for the unstable portion of the zero dynamics in (3.1) is available as

$$\dot{\boldsymbol{z}}_m = F_0 \boldsymbol{z}_m + \boldsymbol{g}_0 y_m \tag{3.2}$$

where $\boldsymbol{z}_m \in \Re^{m-r}$ are the states of the zero dynamics that are modeled, $m \le n$ is the dimension of the plant model, and F_0 is *not* Hurwitz. It is assumed that there exists a controller represented by

$$\begin{aligned} \dot{\boldsymbol{x}}_c &= \boldsymbol{f}_c\left(\boldsymbol{x}_c, y, y_c\right) \\ u_{ec} &= h_c\left(\boldsymbol{x}_c, y, y_c\right) \end{aligned} \tag{3.3}$$

where $y_c \in \Re$ is a command signal and $\boldsymbol{x}_c \in \Re^{n_c}$ is the state vector of the existing controller.

Assumption 3.1. The existing controller given in (3.3) is bounded input-bounded output stable (see Section 2.2.2).

The objective is to augment the nonlinear control law u_{ec} in (3.3) with an adaptive element so that when applied to the system (3.1) the output y tracks y_c.

3.3 Controller Architecture

The conceptual layout for augmenting an existing controller of a non-minimum phase system in the arbitrary reference model-following control architecture is depicted in Figure 3-1. The shaded portions of the diagram highlight the elements to be added. The reference model specifies the desired performance to be achieved by the adaptive control design. Teaching signals for the NN are generated by using an estimate of the states of the error dynamics that include tracking error states, states of the reference model, and states of the zero dynamics of the true plant. The NN reconstructs the modeling uncertainty in output dynamics from a finite history of available system inputs and outputs. To further enhance tracking performance, a linear error compensator can be employed.

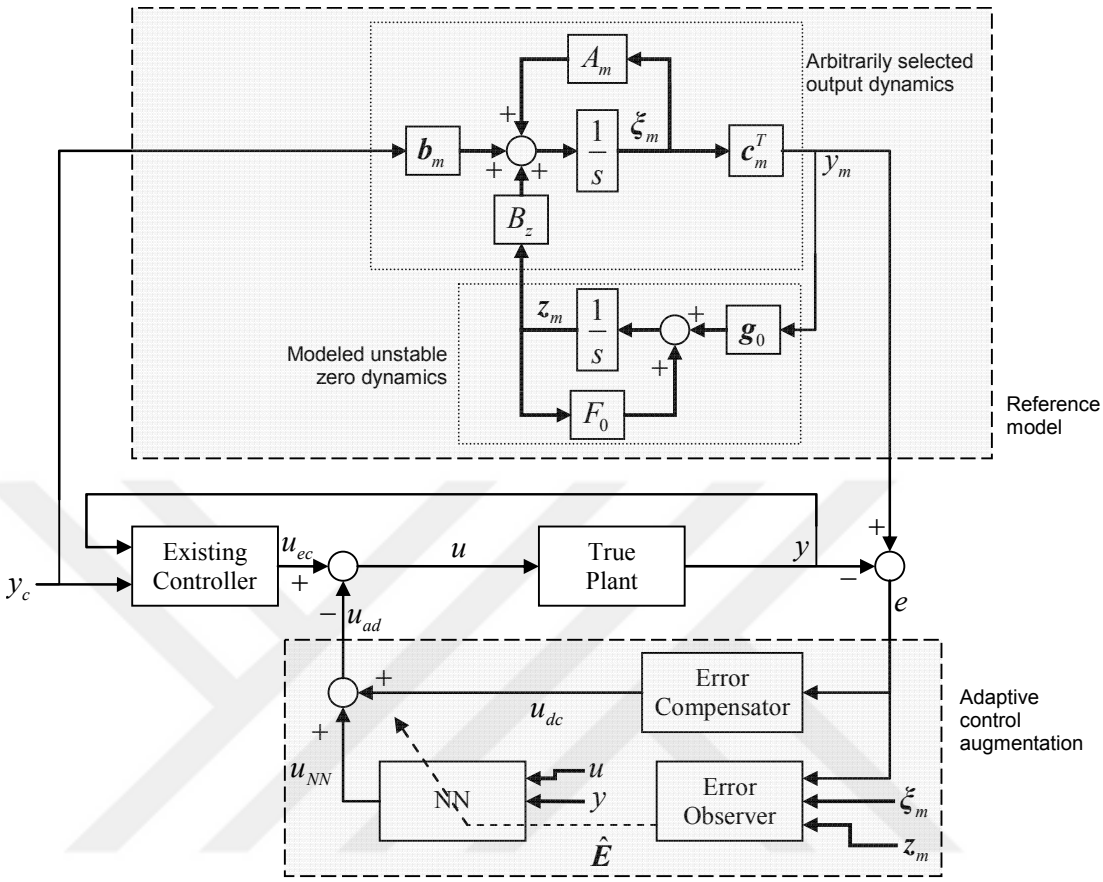

Figure 3-1. Arbitrary reference model-following control architecture for non-minimum phase systems.

3.3.1 Reference Model

The linear model of the zero dynamics given in (3.2) forms the numerator of the reference model. As for the denominator, we select a polynomial of order m with poles arbitrarily placed on the open left half plane. The reference model can be represented in normal form as

$$
\begin{aligned}
\dot{\boldsymbol{z}}_m &= F_0 \boldsymbol{z}_m + \boldsymbol{g}_0 y_m \\
\dot{\xi}_{m_1} &= \xi_{m_2} \\
&\vdots \\
\dot{\xi}_{m_{r-1}} &= \xi_{m_r} \\
\dot{\xi}_{m_r} &= \boldsymbol{h}_0^T \boldsymbol{z}_m - a_1 \xi_{m_1} - \cdots - a_r \xi_{m_r} + b_1 y_c \\
y_m &= \xi_{m_1}
\end{aligned}
\tag{3.4}
$$

and can be written in compact form as

$$
\begin{aligned}
\dot{\boldsymbol{\xi}}_m &= A_m \boldsymbol{\xi}_m + B_z \boldsymbol{z}_m + \boldsymbol{b}_m y_c \\
\dot{\boldsymbol{z}}_m &= \boldsymbol{g}_0 \boldsymbol{c}_m^T \boldsymbol{\xi}_m + F_0 \boldsymbol{z}_m \\
y_m &= \xi_{m_1} = \boldsymbol{c}_m^T \boldsymbol{\xi}_m
\end{aligned}
\tag{3.5}
$$

where

$$
A_m = \begin{bmatrix} 0 & 1 & 0 & \cdots \\ 0 & 0 & 1 & \cdots \\ \vdots & \vdots & \vdots & \vdots \\ -a_1 & -a_2 & \cdots & -a_r \end{bmatrix}, \quad B_z = \begin{bmatrix} 0 \\ 0 \\ \vdots \\ \boldsymbol{h}_0^T \end{bmatrix}, \quad \boldsymbol{b}_m = \begin{bmatrix} 0 \\ 0 \\ \vdots \\ b_1 \end{bmatrix}, \quad \boldsymbol{c}_m = \begin{bmatrix} 1 \\ 0 \\ \vdots \\ 0 \end{bmatrix}.
$$

The command to the system is assumed to be bounded:

$$
\left\| y_c(t) \right\| \le y_c^* \tag{3.6}
$$

3.3.2 Modeling Uncertainties

We establish the relationship between the internal dynamics in (3.1) and linear model in (3.2) by recalling the following assumption and remark from [19]

Assumption 3.2. The $\boldsymbol{z}$ dynamics in (3.1) can be rearranged as

$$
\dot{\boldsymbol{z}}_1 = \boldsymbol{f}_1(\boldsymbol{z}_1, \boldsymbol{z}_2, \boldsymbol{\xi}), \qquad \boldsymbol{z}_1 \in \Re^{m-r} \tag{3.7}
$$

$$
\dot{\boldsymbol{z}}_2 = \boldsymbol{f}_2(\boldsymbol{z}_1, \boldsymbol{z}_2, \boldsymbol{\xi}), \qquad \boldsymbol{z}_2 \in \Re^{n-m} \tag{3.8}
$$

where the zero solution of $\dot{z}_2 = \boldsymbol{f}_2(0, z_2, 0)$ is globally exponentially stable, the function $\boldsymbol{f}_2(z_1, z_2, \boldsymbol{\xi})$ is locally Lipschitz in its arguments in $\mathcal{D}_z \times \mathcal{D}_\xi \times \mathcal{D}_u$, and the z_1 dynamics can be written as

$$\dot{z}_1 = \boldsymbol{f}_1(z_1, z_2, \boldsymbol{\xi}) = F_0 z_1 + \boldsymbol{g}_0 y + \Delta_2(z_1, z_2, \boldsymbol{\xi}) \tag{3.9}$$

where $\Delta_2 = \boldsymbol{f}_1(z_1, z_2, \boldsymbol{\xi}) - F_0 z_1 - \boldsymbol{g}_0 y$ is the unmatched modeling error in the dynamics of z_1, satisfying the following upper bound with known constants [57]

$$\|\Delta_2\| \le \beta_0 \|\boldsymbol{\xi}\| + \beta_1 \|z_1\| + \beta_2 \|z_2\| + \beta_3, \quad \beta_0, \beta_1, \beta_2, \beta_3 > 0. \tag{3.10}$$

Remark 3.1. From a converse Lyapunov theorem, one can deduce that there exists a Lyapunov function $V_z(z_2)$ satisfying the following conditions [7]

$$\begin{gathered} c_1 \|z_2\|^2 \le V_z(z_2) \le c_2 \|z_2\|^2 \\ \frac{\partial V_z}{\partial z_2} f_2(0, 0, z_2) \le -c_3 \|z_2\|^2 \\ \left\| \frac{\partial V_z}{\partial z_2} \right\| \le c_4 \|z_2\|^2 \end{gathered} \tag{3.11}$$

implying that the $\dot{z}_2 = \boldsymbol{f}_2(z_1, z_2, \boldsymbol{\xi})$ dynamics with $z_1, \boldsymbol{\xi}$ viewed as inputs, are input-to-state stable. The following upper bound can be immediately derived

$$\begin{aligned} \dot{V}_z(z_2) &= \frac{\partial V_z}{\partial z_2} \boldsymbol{f}_2(z_1, z_2, \boldsymbol{\xi}) = \frac{\partial V_z}{\partial z_2} \boldsymbol{f}_2(0, 0, \boldsymbol{\xi}) + \frac{\partial V_z}{\partial z_2} \left(\boldsymbol{f}_2(z_1, z_2, \boldsymbol{\xi}) - \boldsymbol{f}_2(0, 0, \boldsymbol{\xi}) \right) \\ &\le -c_3 \|z_2\|^2 + c_4 c_5 \|z_2\| \|\bar{\boldsymbol{\xi}}\| \le -\frac{3c_3}{4} \|z_2\|^2 + \frac{(c_4 c_5)^2}{c_3} \|\bar{\boldsymbol{\xi}}\|^2 \end{aligned} \tag{3.12}$$

where c_5 is the Lipschitz constant of $\boldsymbol{f}_2(z_1, z_2, \boldsymbol{\xi})$ in $\bar{\boldsymbol{\xi}} = \begin{bmatrix} \boldsymbol{\xi}^T & z_1^T \end{bmatrix}^T$.

Using (3.5), (3.9), and (3.8), the nonlinear system in (3.1) can be written as

$$
\begin{aligned}
\dot{\boldsymbol{\xi}} &= A_m \boldsymbol{\xi} + B_z \boldsymbol{z}_1 + \boldsymbol{b}_m \left(y_c - u_{ad} + \Delta_1 \right) \\
\dot{\boldsymbol{z}}_1 &= \boldsymbol{g}_0 \boldsymbol{c}_m^T \boldsymbol{\xi} + F_0 \boldsymbol{z}_1 + \Delta_2 \\
\dot{\boldsymbol{z}}_2 &= \boldsymbol{f}_2 \left(\boldsymbol{z}_1, \boldsymbol{z}_2, \boldsymbol{\xi} \right) \\
y &= \xi_1 = \boldsymbol{c}_m^T \boldsymbol{\xi},
\end{aligned}
\tag{3.13}
$$

in which

$$
\Delta_1 \left(\boldsymbol{z}, \boldsymbol{\xi}, u \right) = \frac{1}{b_1} \left(h_r \left(\boldsymbol{z}, \xi_1, \ldots, \xi_r, u \right) - \boldsymbol{h}_0^T \boldsymbol{z}_1 + a_1 \xi_1 + \cdots + a_r \xi_r \right) + u_{ad} - y_c \,. \tag{3.14}
$$

Notice that the existing linear control signal u_{ec} that appears in u in h_r does not appear explicitly in (3.13). Its effect is embedded in matched uncertainty defined in (3.14).

3.3.3 Error Dynamics

The goal in adaptive controller design is to make the regulated output track output of the reference model while keeping all the other signals in the system bounded. By assumption, the nominal controller already satisfies this requirement for the internal dynamics of the system. Of particular interest on a non-minimum phase system are states of the internal dynamics. While the zero dynamics states of both the true plant and reference model are required to be bounded, the former does not necessarily need to track the latter. Therefore, to prove stability of internal dynamics, instead of the zero dynamics error term $\boldsymbol{z}_m - \boldsymbol{z}_1$ used in [19]–[21] we consider terms $\boldsymbol{z}_m$ and $\boldsymbol{z}_1$ separately. This modification relaxes the adaptive controller design by removing the unnecessary enforcement of control of zero dynamics error and guarantees stability of the internal dynamics of both the true plant and reference model explicitly. To keep terminology consistent with adaptive controller literature, with a slight abuse of language, the following vector is defined as the error vector:

$$
\boldsymbol{E}^T \triangleq \begin{bmatrix} \left(\boldsymbol{\xi}_m - \boldsymbol{\xi} \right)^T & \boldsymbol{\xi}_m^T & \boldsymbol{z}_m^T & \boldsymbol{z}_1^T \end{bmatrix}. \tag{3.15}
$$

Then the error dynamics can be written using (3.5) and (3.13) as

$$\underbrace{\begin{bmatrix} \dot{\boldsymbol{\xi}}_m - \dot{\boldsymbol{\xi}} \\ \dot{\boldsymbol{\xi}}_m \\ \dot{\boldsymbol{z}}_m \\ \dot{\boldsymbol{z}}_1 \end{bmatrix}}_{\dot{\boldsymbol{E}}} = \underbrace{\begin{bmatrix} A_m & 0 & B_z & -B_z \\ 0 & A_m & B_z & 0 \\ 0 & \boldsymbol{g}_0\boldsymbol{c}_m^T & F_0 & 0 \\ -\boldsymbol{g}_0\boldsymbol{c}_m^T & \boldsymbol{g}_0\boldsymbol{c}_m^T & 0 & F_0 \end{bmatrix}}_{\bar{A}} \underbrace{\begin{bmatrix} \boldsymbol{\xi}_m - \boldsymbol{\xi} \\ \boldsymbol{\xi}_m \\ \boldsymbol{z}_m \\ \boldsymbol{z}_1 \end{bmatrix}}_{\boldsymbol{E}} + \underbrace{\begin{bmatrix} 0 \\ \boldsymbol{b}_m \\ 0 \\ 0 \end{bmatrix}}_{\bar{B}} y_c + \underbrace{\begin{bmatrix} \boldsymbol{b}_m \\ 0 \\ 0 \\ 0 \end{bmatrix}}_{B_1} \left(u_{ad} - \Delta_1\right) + \underbrace{\begin{bmatrix} 0 \\ 0 \\ 0 \\ \Delta_2 \end{bmatrix}}_{\bar{\Delta}_2}$$

$$\dot{\boldsymbol{z}}_2 = \boldsymbol{f}_2\left(\boldsymbol{z}_1, \boldsymbol{z}_2, \boldsymbol{\xi}\right) \tag{3.16}$$

$$\boldsymbol{s} = \underbrace{\begin{bmatrix} \boldsymbol{c}_m^T & 0 & 0 & 0 \\ 0 & I & 0 & 0 \\ 0 & 0 & I & 0 \end{bmatrix}}_{\bar{C}} \begin{bmatrix} \boldsymbol{\xi}_m - \boldsymbol{\xi} \\ \boldsymbol{\xi}_m \\ \boldsymbol{z}_m \\ \boldsymbol{z}_1 \end{bmatrix}$$

where $\boldsymbol{s}$ is the vector of available measurements. The dynamics in (3.16) can also be written in the following compact form

$$\begin{aligned} \dot{\boldsymbol{E}} &= \bar{A}\boldsymbol{E} + \bar{B}y_c + B_1\left(u_{ad} - \Delta_1\right) + \bar{\Delta}_2 \\ \dot{\boldsymbol{z}}_2 &= \boldsymbol{f}_2\left(\boldsymbol{z}_1, \boldsymbol{z}_2, \boldsymbol{\xi}\right) \\ \boldsymbol{s} &= \bar{C}\boldsymbol{E} \end{aligned} \tag{3.17}$$

Notice that by selection of the reference model (3.5) the matrix $\bar{A}$ is Hurwitz. We immediately note that there exists a positive definite matrix $\bar{P} = \bar{P}^T$ that solves the following Lyapunov equation

$$\bar{A}^T\bar{P} + \bar{P}\bar{A} = -\bar{Q} \tag{3.18}$$

for arbitrary $\bar{Q} > 0$.

3.3.4 Adaptive Controller Design

The existing controller (3.3) is augmented with an adaptive signal

$$u = u_{ec} - u_{ad} \tag{3.19}$$

where the adaptive signal u_{ad} is designed to approximately cancel Δ_1. As defined in (3.14), Δ_1 depends on u_{ad} through u. Therefore the following assumption is introduced to guarantee existence and uniqueness of a solution for u_{ad}.

Assumption 3.3. The mapping $u_{ad} \mapsto \Delta_1$ is a contraction over the entire input domain of interest.

A contraction is defined by the condition $\left|\frac{\partial \Delta_1}{\partial u_{ad}}\right| < 1$. Using (3.14), this implies [12]

$$\operatorname{sgn}(b_1) = \operatorname{sgn}(\partial h_r / \partial u), \tag{3.20}$$

$$|\partial h_r / \partial u| / 2 < |b_1| < \infty. \tag{3.21}$$

The first condition states that unmodeled control reversal is not permissible. The second condition places a lower bound on the estimate of control effectiveness, b_1.

A SHL NN is used to approximate Δ_1 in (3.14). The modeling error Δ_1 is a function of states and control. The following theorem from [31], [32] enables us to reconstruct Δ_1 using available measurements.

Theorem 3.1. For arbitrary $\varepsilon^* > 0$, there exist bounded constant weights M, N and a positive time delay $d > 0$ such that the modeling error $\Delta_1(z, \boldsymbol{\xi}, u)$ in (3.14) can be approximated over a compact set $\mathcal{D}_z \times \mathcal{D}_\xi \times \mathcal{D}_u$ by a SHL NN

$$\Delta_1 = M^T \boldsymbol{\sigma}\left(N^T \boldsymbol{\eta}\right) + \varepsilon(\boldsymbol{\eta}), \qquad \|\varepsilon(\boldsymbol{\eta})\| \le \varepsilon^*, \tag{3.22}$$

where $\varepsilon(\boldsymbol{\eta})$ is the NN reconstruction error and $\boldsymbol{\eta}$ is the network input vector

$$\boldsymbol{\eta}(t)=\begin{bmatrix}1 & \bar{\boldsymbol{u}}^T(t) & \bar{\boldsymbol{y}}^T(t)\end{bmatrix}^T,\quad \|\boldsymbol{\eta}\|\le\eta^*$$
$$\bar{\boldsymbol{u}}^T(t)=\begin{bmatrix}u(t) & u(t-d) & \cdots & u(t-(k-r-1)d)\end{bmatrix}^T$$
$$\bar{\boldsymbol{y}}^T(t)=\begin{bmatrix}y(t) & y(t-d) & \cdots & y(t-(k-1)d)\end{bmatrix}^T$$

with $k\ge n$ and $d>0$, $\boldsymbol{\sigma}$ being a vector of squashing functions $\boldsymbol{\sigma}(\cdot)$, its jth element being defined like $\left[\boldsymbol{\sigma}\left(N^T\boldsymbol{\eta}\right)\right]_j=\left[\boldsymbol{\sigma}\left(N^T\boldsymbol{\eta}\right)_j\right]$.

The adaptive signal u_{ad} is designed as

$$u_{ad}=\hat{M}^T\boldsymbol{\sigma}\left(\hat{N}^T\boldsymbol{\eta}\right) \tag{3.23}$$

where $\hat{M}$ and $\hat{N}$ are estimates of the ideal weights M and N to be adapted online.

3.3.5 Error Observer

For the NN weight adaptation laws the error vector defined in (3.15) is required. In the absence of full state feedback, a linear observer is introduced to estimate the error vector [13], [19]–[21]

$$\begin{aligned}\dot{\hat{\boldsymbol{E}}}&=\bar{A}\hat{\boldsymbol{E}}+\bar{B}y_c+K\left(\boldsymbol{s}-\hat{\boldsymbol{s}}\right)\\ \hat{\boldsymbol{s}}&=\bar{C}\hat{\boldsymbol{E}}\end{aligned} \tag{3.24}$$

where K is chosen to make $\bar{A}-K\bar{C}$ Hurwitz. Then the observer error dynamics $\dot{\tilde{\boldsymbol{E}}}=\dot{\hat{\boldsymbol{E}}}-\dot{\boldsymbol{E}}$ can be written as

$$\dot{\tilde{\boldsymbol{E}}}=\tilde{A}\tilde{\boldsymbol{E}}-B_1\left(u_{ad}-\Delta_1\right)-\bar{\Delta}_2 \tag{3.25}$$

with $\tilde{A}=\bar{A}-K\bar{C}$. For Hurwitz $\tilde{A}$ there exists a positive definite matrix $\tilde{P}=\tilde{P}^T$ that solves the following Lyapunov equation

$$\tilde{A}^T\tilde{P}+\tilde{P}\tilde{A}=-\tilde{Q} \tag{3.26}$$

for arbitrary $\tilde{Q}>0$.

3.3.6 NN Adaptation Laws

Based on Lyapunov's direct method that will be detailed below, we introduce the following adaptation laws

$$\begin{aligned} \dot{\hat{M}} &= -\Gamma_M \left[2\left(\hat{\boldsymbol{\sigma}} - \hat{\sigma}' \hat{N}^T \boldsymbol{\eta} \right) \hat{\boldsymbol{E}}^T \bar{P} B_1 + k\hat{M} \right] \\ \dot{\hat{N}} &= -\Gamma_N \left[2\boldsymbol{\eta} \hat{\boldsymbol{E}}^T \bar{P} B_1 \hat{M}^T \hat{\sigma}' + k\hat{N} \right], \end{aligned} \tag{3.27}$$

in which Γ_M, Γ_N are positive definite adaptation gain matrices, $k > 0$ is a σ – modification gain, $\hat{\boldsymbol{\sigma}} = \boldsymbol{\sigma}\left(\hat{N}^T \boldsymbol{\eta} \right)$, $\hat{\sigma}'$ denotes the Jacobian matrix computed at the estimate: $\hat{\boldsymbol{\sigma}}' = \boldsymbol{\sigma}'\left(\hat{N}^T \boldsymbol{\eta} \right)$.

3.4 Stability Analysis

In this section we will show through Lyapunov's direct method that the error vector $\boldsymbol{E}$, observation error vector $\tilde{\boldsymbol{E}}$, and the NN weight errors $\tilde{M} \triangleq \hat{M} - M$ and $\tilde{N} \triangleq \hat{N} - N$ are ultimately bounded. Consider the following composite error vector

$$\boldsymbol{\zeta} = \begin{bmatrix} \boldsymbol{E}^T & \tilde{\boldsymbol{E}}^T & z_2 & \operatorname{vec} \tilde{Z} \end{bmatrix}^T$$

where $\tilde{Z} \triangleq \begin{bmatrix} \tilde{M} & 0 \\ 0 & \tilde{N} \end{bmatrix}$. Using the upper bounds on the Frobenius norms of the weights in (3.22):

$$\|M\| < M^*, \quad \|N\|_F < N^*, \tag{3.28}$$

we can write the following upper bounds

$$\|\hat{M}\| < \|\tilde{M}\| + M^*, \qquad \|\hat{N}\|_F < \|\tilde{N}\|_F + N^*. \tag{3.29}$$

With (3.29), $u_{ad} - \Delta_1$ can be upper bounded as

$$\|u_{ad} - \Delta_1\| = \left\| \hat{M}^T \boldsymbol{\sigma}\left(\hat{N}^T \boldsymbol{\eta} \right) - M^T \boldsymbol{\sigma}\left(N^T \boldsymbol{\eta} \right) - \varepsilon \right\| \le \alpha_1 \|\tilde{Z}\|_F + \alpha_2 \tag{3.30}$$

with some $\alpha_1 > 0,\ \alpha_2 > 0$. For the stability proof we will need the following representation:

$$u_{ad} - \Delta_1 = \tilde{M}^T \left(\hat{\boldsymbol{\sigma}} - \hat{\sigma}' \hat{N}' \boldsymbol{\eta} \right) + \hat{M}^T \hat{\sigma}' \tilde{N}^T \boldsymbol{\eta} + \omega - \varepsilon \,, \tag{3.31}$$

where $\omega = \tilde{M}^T \hat{\sigma}' N^T \boldsymbol{\eta} - M^T \mathcal{O}\left(\tilde{N}^T \boldsymbol{\eta} \right)^2$. Such a representation is achieved via Taylor series expansion of $\boldsymbol{\sigma}\left(N^T \boldsymbol{\eta} \right)$ around the estimates $\hat{N}^T \boldsymbol{\eta}$ (refer to [58] for more details). Over the compact set $\mathcal{D}_z \times \mathcal{D}_\xi \times \mathcal{D}_u$ the following upper bounds can be derived [58]

$$|\omega - \varepsilon| \le \gamma_1 \left\| \tilde{Z} \right\|_F + \gamma_2 \,, \tag{3.32}$$

where $\gamma_1 > 0,\ \gamma_2 > 0$ are constants such that γ_1 depends on η^* and γ_2 depends on ε.

The upper bound introduced in (3.10) can be further upper bounded

$$\left\| \Delta_2 \right\| \le \delta_1 \left\| \boldsymbol{E} \right\| + \beta_2 \left\| \boldsymbol{z}_2 \right\| + \delta_2 \,. \tag{3.33}$$

Similarly, the relation in (3.12) can be upper bounded as

$$\dot{V}_z \left(\boldsymbol{z}_2 \right) \le -\frac{3c_3}{4} \left\| \boldsymbol{z}_2 \right\|^2 + \frac{\left(c_4 c_5 \right)^2}{c_3} \left\| \boldsymbol{E} \right\|^2 + \frac{\left(c_4 c_5 \right)^2}{c_3} \beta_4^2 \tag{3.34}$$

With the upper bounds given in (3.29)–(3.34), using Lyapunov's direct method, we will prove that the error signals and states of the true plant and reference model zero dynamics are ultimately bounded. First we will introduce a positive invariant set to which the initial errors can belong. Next we will show that given an initial condition in that set, the error signals will be ultimately bounded.

Notice that the NN approximation is valid in the compact set $\mathcal{D}_z \times \mathcal{D}_\xi \times \mathcal{D}_u$. Based on the definition of the error variables and continuity of solutions of differential equations, this set maps onto a bounded set Ω_ζ in the error space. Let

$$B_R \triangleq \left\{ \boldsymbol{\zeta} \middle| \left\| \boldsymbol{\zeta} \right\| \le R \right\}, \qquad R > 0$$

be the largest hypersphere in Ω_ζ. For every $\boldsymbol{\zeta} \in B_R$, $(z, \xi, u) \in \mathcal{D}_z \times \mathcal{D}_\xi \times \mathcal{D}_u$ holds, ensuring that the NN approximation in (3.22) remains valid. Consider the matrices

$$T_1 \triangleq \frac{1}{2}\begin{bmatrix} 2\bar{P} & 0 & 0 & 0 & 0 \\ 0 & 2\tilde{P} & 0 & 0 & 0 \\ 0 & 0 & \Gamma_M^{-1} & 0 & 0 \\ 0 & 0 & 0 & \Gamma_N^{-1} & 0 \\ 0 & 0 & 0 & 0 & c_1 I \end{bmatrix}, \quad T_2 \triangleq \frac{1}{2}\begin{bmatrix} 2\bar{P} & 0 & 0 & 0 & 0 \\ 0 & 2\tilde{P} & 0 & 0 & 0 \\ 0 & 0 & \Gamma_M^{-1} & 0 & 0 \\ 0 & 0 & 0 & \Gamma_N^{-1} & 0 \\ 0 & 0 & 0 & 0 & c_2 I \end{bmatrix} \tag{3.35}$$

where I is the identity matrix of dimension $(n-m)\times(n-m)$ and the following Lyapunov function candidate:

$$V(\boldsymbol{\zeta}) = \boldsymbol{E}^T \bar{P} \boldsymbol{E} + \tilde{\boldsymbol{E}}^T \tilde{P} \tilde{\boldsymbol{E}} + \frac{1}{2}\operatorname{tr}\left(\tilde{M}^T \Gamma_M^{-1} \tilde{M}\right) + \frac{1}{2}\operatorname{tr}\left(\tilde{N}^T \Gamma_N^{-1} \tilde{N}\right) + V_z(z_2).$$

Note that the bounds in (3.11) imply

$$\boldsymbol{\zeta}^T T_1 \boldsymbol{\zeta} \le V(\boldsymbol{\zeta}) \le \boldsymbol{\zeta}^T T_2 \boldsymbol{\zeta}. \tag{3.36}$$

Let

$$\alpha \triangleq \min_{\|\boldsymbol{\zeta}\|=R} \boldsymbol{\zeta}^T T_1 \boldsymbol{\zeta} = R^2 T_{1_m},$$

where T_{1_m} is the minimum eigenvalue of T_1. Introduce the following set:

$$\Omega_\alpha \triangleq \left\{\boldsymbol{\zeta} \in B_R \middle| V(\boldsymbol{\zeta}) \le \alpha\right\}.$$

Assumption 3.4. Assume

$$R > \gamma\sqrt{\frac{T_{2_M}}{T_{1_m}}} \ge \gamma, \tag{3.37}$$

where T_{2_M} is the maximum eigenvalue of T_2, γ is defined as

$$\gamma = \max\left(C_1, C_2, C_3, C_4\right)$$

$$C_1 = \sqrt{\frac{\left\|\bar{P}B_1\right\|^2 \gamma_2^2 + \kappa_2^2 + \bar{Z} + \delta_2^2\left(\left\|\tilde{P}\right\|^2 + \left\|\bar{P}\right\|^2\right) + \frac{\left(c_4 c_5\right)^2}{c_3}\beta_4^2 + \left(\left\|\bar{P}B\right\| y_c^*\right)^2}{\bar{Q}_m - 4 - 2\delta_1\left\|\bar{P}\right\| - \frac{\left(c_4 c_5\right)^2}{c_3} - \frac{\left(2\left\|\bar{P}\right\|\beta_2\right)^2}{c_3}}} \tag{3.38}$$

$$C_2 = \sqrt{\frac{\left\|\bar{P}B_1\right\|^2 \gamma_2^2 + \kappa_2^2 + \bar{Z} + \delta_2^2\left(\left\|\tilde{P}\right\|^2 + \left\|\bar{P}\right\|^2\right) + \frac{\left(c_4 c_5\right)^2}{c_3}\beta_4^2 + \left(\left\|\bar{P}B\right\| y_c^*\right)^2}{\tilde{Q}_m - 3 - 2\delta_1\left\|\tilde{P}\right\| - \frac{\left(2\left\|\tilde{P}\right\|\beta_2\right)^2}{c_3}}} \tag{3.39}$$

$$C_3 = \sqrt{\frac{\left\|\bar{P}B_1\right\|^2 \gamma_2^2 + \kappa_2^2 + \bar{Z} + \delta_2^2\left(\left\|\tilde{P}\right\|^2 + \left\|\bar{P}\right\|^2\right) + \frac{\left(c_4 c_5\right)^2}{c_3}\beta_4^2 + \left(\left\|\bar{P}B\right\| y_c^*\right)^2}{\frac{k}{2} - \kappa_1^2 - \left(\gamma_1\left\|\bar{P}B_1\right\|\right)^2}} \tag{3.40}$$

$$C_4 = 2\sqrt{\frac{\left\|\bar{P}B_1\right\|^2 \gamma_2^2 + \kappa_2^2 + \bar{Z} + \delta_2^2\left(\left\|\tilde{P}\right\|^2 + \left\|\bar{P}\right\|^2\right) + \frac{\left(c_4 c_5\right)^2}{c_3}\beta_4^2 + \left(\left\|\bar{P}B\right\| y_c^*\right)^2}{c_3}} \tag{3.41}$$

where $\bar{Z} = \frac{k}{2}\left(\left\|M\right\|_F^2 + \left\|N\right\|_F^2\right)$, $\kappa_1 = \left\|\bar{P}B_1\right\|\gamma_1 + \Theta\alpha_1$, $\kappa_2 = \left\|\bar{P}B_1\right\|\gamma_2 + \Theta\alpha_2$, $\Theta = \left\|\bar{P}B_1 + \tilde{P}B_1\right\|$.

Further assume that δ_1 is such that the matrices $\bar{Q}$ and $\tilde{Q}$ in the Lyapunov equations in (3.18) and (3.26) can be chosen to satisfy the following conditions

$$\bar{Q}_m > 4 + 2\delta_1\left\|\bar{P}\right\| + \frac{\left(c_4 c_5\right)^2}{c_3} + \frac{\left(2\left\|\bar{P}\right\|\beta_2\right)^2}{c_3} \tag{3.42}$$

$$\tilde{Q}_m > 3 + 2\delta_1\left\|\tilde{P}\right\| + \frac{\left(2\left\|\tilde{P}\right\|\beta_2\right)^2}{c_3} \tag{3.43}$$

And finally let the σ- modification gain satisfy the lower bound $k > 2\kappa_1^2 + 2\left(\gamma_1\left\|\bar{P}B_1\right\|\right)^2$.

We are now ready to state the main result of this chapter.

Theorem 3.2. Let Assumptions 3.1–3.4 hold. Then, if the initial error $\boldsymbol{\zeta}(0)$ belongs to the compact set Ω_α, the feedback control law given by (3.19), (3.23), along with (3.27), guarantees that the signals $\boldsymbol{E}, \tilde{\boldsymbol{E}}, \boldsymbol{z}_2, \tilde{M}, \tilde{N}$ in the closed loop system are ultimately bounded.

Proof. See APPENDIX A.

Remark 3.2. The error bounds in (A.9)-(A.12) are very similar to the corresponding bounds in [20]. The only difference in numerators is the term $\left(\left\|\overline{P}B\right\| y_c^*\right)^2$ which is added due to inclusion of $\boldsymbol{\xi}_m$ states in the error dynamics. Denominators of the bounds for $\left\|\tilde{\boldsymbol{E}}\right\|$, $\left\|\tilde{Z}\right\|_F$, and $\left\|\boldsymbol{z}_2\right\|$ are the same as those in [20]. The constant in the denominator of the bound for $\left\|\boldsymbol{E}\right\|$ has decreased from –3 to –4. Although these differences increase the bound on the error vector compared to that in [20], this does not necessarily translate into poorer tracking performance. The error vector defined in (3.15) includes output dynamics error vector and states of the reference model and true plant zero dynamics while the error vector in [20], [21] contains only error signals. Consequently under nominal system operation conditions, the error vector (3.15) is a vector of a larger magnitude depending on the magnitude of the command input y_c^*, compared to the error vector in [20], [21] and hence larger bounds are expected.

3.5 Performance Improvement

The arbitrary reference model introduced in (3.5) has to be selected carefully considering physical limitations of the system. If for a reasonably selected reference model it cannot be ensured that conditions (3.37)-(3.43) are satisfied, then an additional linear error compensator can be introduced to "speed up" the error dynamics and improve

the tracking performance [19]–[21]. In this case the control signal in (3.19) can further be augmented as

$$u = u_{ec} - \left(u_{ad} + u_{dc}\right) \tag{3.44}$$

where u_{dc} is linear compensator output defined by

$$\begin{aligned} \dot{\boldsymbol{x}}_{dc} &= A_{dc}\boldsymbol{x}_{dc} + B_{dc}\boldsymbol{s} \\ u_{dc} &= C_{dc}\boldsymbol{x}_{dc} + D_{dc}\boldsymbol{s}. \end{aligned} \tag{3.45}$$

With (3.44) and (3.45), the dynamics in (3.17) can be rewritten as

$$\begin{aligned} \begin{bmatrix} \dot{\boldsymbol{E}} \\ \dot{\boldsymbol{x}}_{dc} \end{bmatrix} &= \begin{bmatrix} \overline{A} + B_1 D_{dc}\overline{C} & B_1 C_{dc} \\ B_{dc}\overline{C} & A_{dc} \end{bmatrix} \begin{bmatrix} \boldsymbol{E} \\ \boldsymbol{x}_{dc} \end{bmatrix} + \begin{bmatrix} \overline{B} \\ 0 \end{bmatrix} y_c + \begin{bmatrix} B_1 \\ 0 \end{bmatrix} \left(u_{ad} - \Delta_1\right) + \begin{bmatrix} \overline{\Delta}_2 \\ 0 \end{bmatrix} \\ \dot{z}_2 &= \boldsymbol{f}_2\left(z_1, z_2, \boldsymbol{\xi}\right) \end{aligned} \tag{3.46}$$

The dynamics in (3.46) are similar to those in (3.17) except for the dimension of the error vector. Thus the stability analysis presented in Section 3.4 can be used to show boundedness with small modifications.

3.6 Simulation Example

The arbitrary reference model-following controller developed in this chapter is tested on the numerical example of [19]:

$$\begin{aligned} \dot{\xi} &= -2\xi - 0.9z_1 - 0.5z_2 + u \\ \dot{z}_1 &= 0.9z_1 + 0.1z_1 z_2^2 + 1.7\xi \\ \dot{z}_2 &= -3z_2 + z_1 + \frac{3}{2}\xi \\ y &= \xi \end{aligned} \tag{3.47}$$

The reference model is selected as

$$\begin{aligned} \dot{\xi}_m &= -4.5\xi_m - 8.75z_m - 1.33y_c \\ \dot{z}_m &= 1.5z_m + \xi_m \\ y_m &= \xi_m \end{aligned}$$

or, equivalently in s domain as

$$G_{rm}(s) = \frac{-1.33s + 2}{s^2 + 3s + 2}. \tag{3.48}$$

The existing controller is given by [19]:

$$\frac{u_{ec}(s)}{y_c(s) - y(s)} = -\frac{s+1}{s+2.6}. \tag{3.49}$$

The error observer in (3.24) is designed such that poles eigenvalues of $\tilde{A}$ are five times faster than the eigenvalues of $\bar{A}$. An additional error compensator with an integrator is introduced to remove the steady state error in tracking as suggested in Section 3.5.

For comparison, results from [19] are presented in Figure 3-2. Results obtained with the arbitrary reference model-following control are given in Figure 3-3. The response obtained with the arbitrary reference model approach has better transient

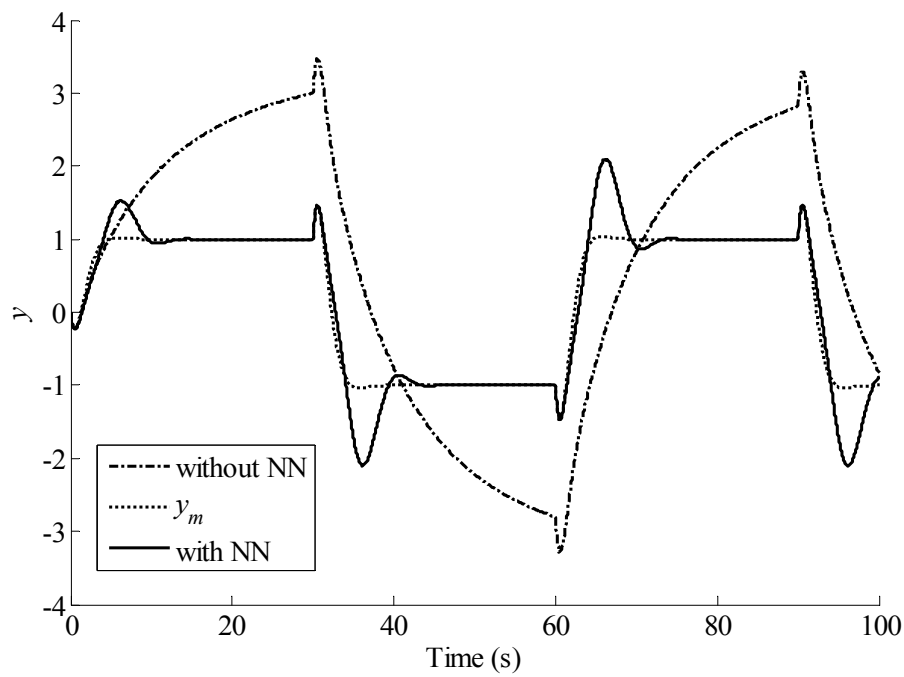

Figure 3-2. Comparison of step responses with the closed-loop reference model approach, [17].

characteristics compared to the one with the closed-loop reference model approach. The response with NN in Figure 3-2 exhibits approximately 100% overshoot while the one in Figure 3-3 exhibits no overshoot at all. The improvement in transient response is mostly attributed to the new definition of the error vector in (3.15). Using the definition of the error vector in [17] in the arbitrary reference model-following approach produces a response similar to that in Figure 3-2 with overshoots, which is not shown here. Figure 3-4 shows Δ_1 and u_{ad} and Δ_2. In the upper plot we see that Δ_1 shows a non-minimum phase type transient response, but the NN does not respond to that. This behavior shows that non-minimum phase dynamics are controlled by the existing controller and not by the NN. Lower plot shows that the unmatched uncertainty Δ_2 is bounded.

3.7 Conclusions

This chapter extends the formulation of the augmenting arbitrary reference model-following controller to non-minimum phase systems. Following the idea in [17] we

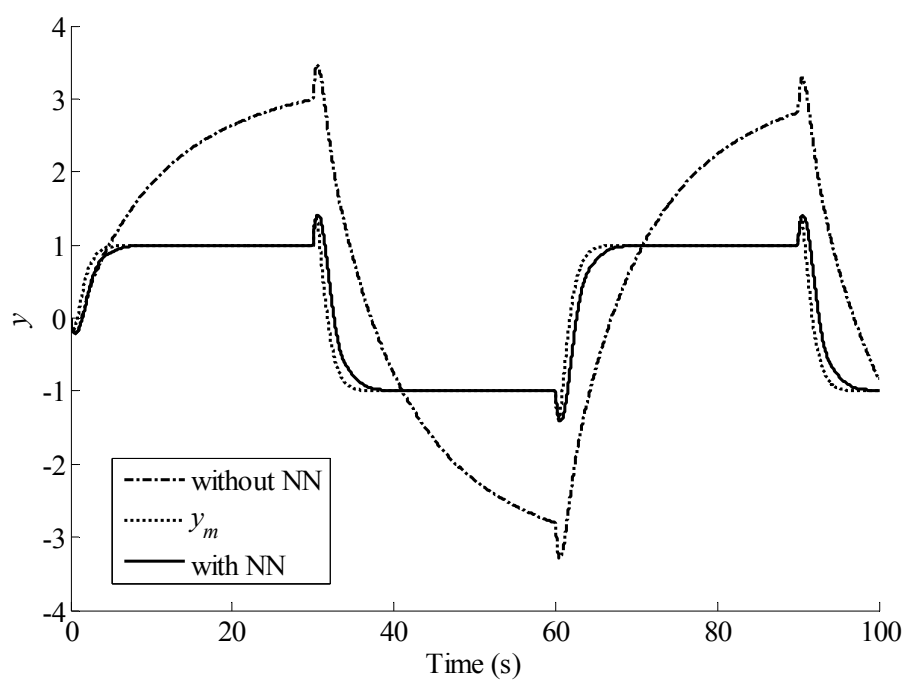

Figure 3-3. Comparison of step responses with the arbitrary reference model approach.

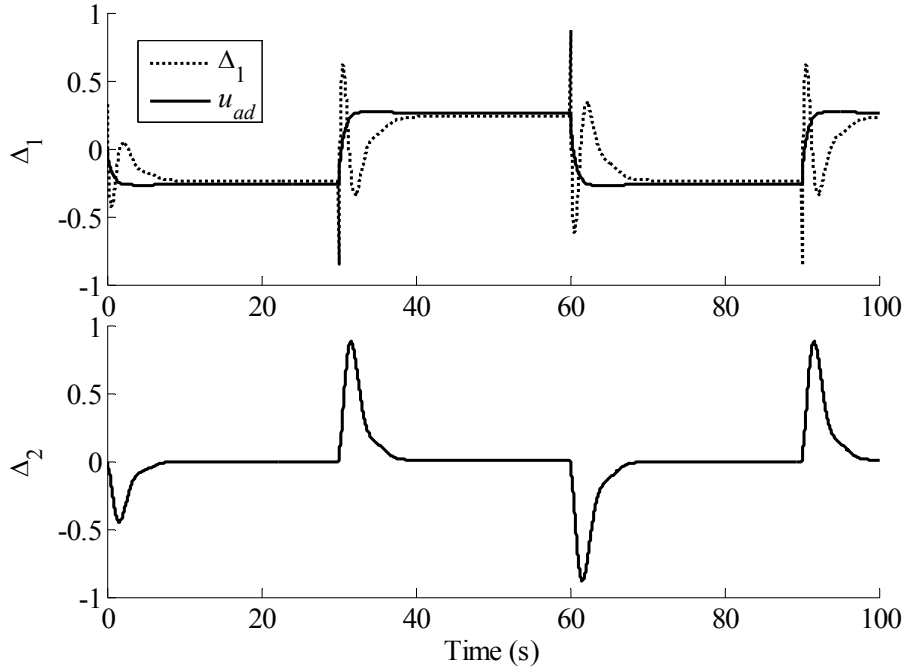

Figure 3-4. Matched and unmatched modeling errors and adaptive signal.

assumed that unstable internal dynamics of the plant are modeled with sufficient accuracy and the existing controller design addresses these dynamics. We also redefined the error vector to include internal dynamics states of the reference model and the true plant separately. Simulation results on the example of [17] show improved transient performance.

CHAPTER 4

ARBITRARY REFERENCE MODEL-FOLLOWING ADAPTIVE AUGMENTING CONTROL FOR SYSTEMS WITH INPUT NONLINEARITIES

This chapter addresses augmentation of an existing controller of a nonlinear system with input nonlinearities with an adaptive output feedback element in the framework of arbitrary reference model-following control. It is difficult to cope with input nonlinearities in an adaptive control system. When the commanded control cannot be precisely applied because of actuator characteristics such as position and/or rate limits, response of the system deviates from the ideal response that would be achieved without these characteristics. Adaptive controllers interpret changes in the response due to control deficiencies as changes in system dynamics and attempt to adapt to them. In order to protect the adaptive element in the arbitrary reference model-following architecture from input nonlinearities, we condition the command input to the reference model by subtracting a so-called hedge signal in a way similar to the control hedging implementation on the open loop reference model-following architecture developed in Ref. [17]. We show that if the system without input nonlinearities is stable, then the system with input nonlinearities will also be stable with the proposed hedging implementation. We demonstrate the effectiveness of the method on a simulation example.

4.1 Background

We start with a brief development of the arbitrary reference model-following adaptive augmenting control architecture [23]. The architecture is schematically depicted

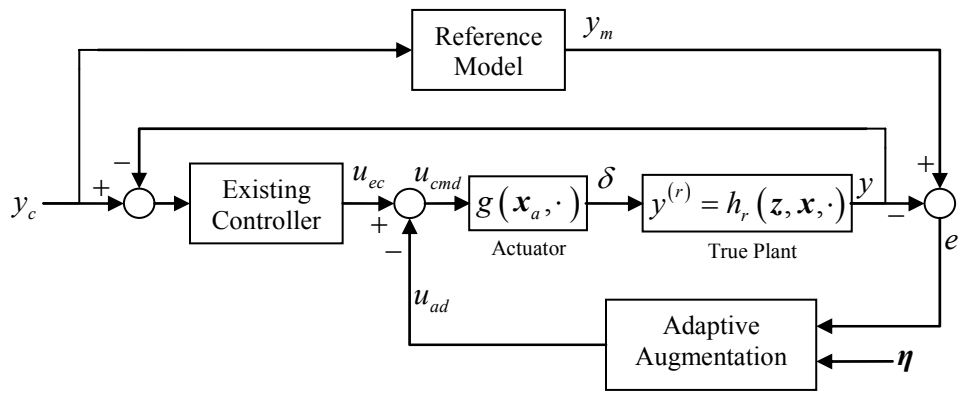

Figure 4-1. Arbitrary reference model-following adaptive augmenting control architecture.

in Figure 4-1. Consider the following *observable* and *stabilizable* nonlinear single-input single-output (SISO) system in normal form

$$\begin{aligned} \dot{z} &= \boldsymbol{f}(z, \boldsymbol{x}) \\ \dot{x}_1 &= x_2 \\ &\vdots \\ \dot{x}_{r-1} &= x_r \\ \dot{x}_r &= h_r(z, \boldsymbol{x}, \delta) \\ y &= x_1 \end{aligned} \tag{4.1}$$

where $z \in \mathbb{R}^{n-r}$ and $\boldsymbol{x} = \begin{bmatrix} x_1 & \cdots & x_r \end{bmatrix}^T \in \mathbb{R}^r$ are the states of the internal and output dynamics respectively, $\delta, y \in \mathbb{R}$ are control and measurement variables, $\boldsymbol{f}$ and h are sufficiently smooth partially known functions, and r is the relative degree of the regulated output including the dynamics of the actuator defined below. We assume that the true plant is minimum phase, i.e., the internal dynamics $\dot{z} = \boldsymbol{f}(z, \boldsymbol{x})$ with $\boldsymbol{x} = 0$ are asymptotically stable.

Control input to the system is realized by a nonlinear dynamic actuator represented by

$$\begin{aligned} \dot{\boldsymbol{x}}_a &= \boldsymbol{f}_a\left(\boldsymbol{x}_a, u_{cmd}\right) \\ \delta &= g\left(\boldsymbol{x}_a, u_{cmd}\right) \end{aligned} \tag{4.2}$$

where $u_{cmd} \in \mathbb{R}$ is the commanded control input, $\boldsymbol{x}_a \in \mathbb{R}^{n_a}$ is the actuator state vector and $\boldsymbol{f}_a$ and g are partially known functions. The actuator in (4.2) may have dynamics and/or exhibit nonlinear characteristics such as position and rate saturation, dead zone, backlash, etc. Such input characteristics degrade overall system performance and may even cause instability if not treated properly. We assume that an actuator model is available and given by

$$\begin{aligned} \dot{\hat{\boldsymbol{x}}}_a &= \hat{\boldsymbol{f}}_a\left(\hat{\boldsymbol{x}}_a, u_{cmd}\right) \\ \hat{\delta} &= \hat{g}\left(\hat{\boldsymbol{x}}_a, u_{cmd}\right) \end{aligned} \tag{4.3}$$

which contains any input characteristics present in the system that could effect system performance. The following assumption is required for proving stability of the closed loop system and holds true for all practical actuators.

Assumption 4.1. The actuator (4.2) and the actuator model (4.3) are bounded input-bounded output stable.

It is assumed that there already exists a stable linear dynamic compensator designed for the plant (4.1)

$$\begin{aligned} \dot{\boldsymbol{x}}_c &= A_c \boldsymbol{x}_c + b_c\left(y_c - y\right) \\ u_{ec} &= c_c^T \boldsymbol{x}_c + d_c\left(y_c - y\right). \end{aligned} \tag{4.4}$$

where y_c is an external command signal. Stability of the dynamic compensator is required for proving boundedness of the closed loop system. Refer to Section 2.1 and Figure 2-2 for a discussion regarding the necessity of this assumption.

A simple linear performance model with relative degree r is selected as a reference model

$$G(s) = \frac{b_1}{s^r + a_r s^{r-1} + \cdots + a_1} \tag{4.5}$$

which can also be written in state space form as

$$\begin{aligned}
\dot{x}_{m_1} &= x_{m_2} \\
&\vdots \\
\dot{x}_{m_{r-1}} &= x_{m_r} \\
\dot{x}_{m_r} &= -a_1 x_{m_1} - \cdots - a_r x_{m_r} + b_1 y_c \\
&= C_r \boldsymbol{x}_m + b_1 y_c \\
&= \hat{h}_r\left(\boldsymbol{x}_m, y_c\right) \\
y_m &= x_{m_1}
\end{aligned} \tag{4.6}$$

where $\boldsymbol{x}_m = \begin{bmatrix} x_{m_1} & \cdots & x_{m_r} \end{bmatrix}^T$ is the reference model state vector and $C_r = -\begin{bmatrix} a_1 & \cdots & a_r \end{bmatrix}^T$. The existing controller (4.4) is augmented by introducing an adaptive signal u_{ad} as follows:

$$u_{cmd} = u_{ec} - u_{ad}\,. \tag{4.7}$$

Using the reference model dynamics (4.6), the true plant dynamics (4.1) can equivalently be written as

$$\begin{aligned}
y^{(r)} &= C_r \boldsymbol{x} + b_1 y_c - \hat{b}_u\left(u_{ad} - \Delta\right) \\
&= \hat{h}_r\left(\boldsymbol{x}, y_c\right) - \hat{b}_u\left(u_{ad} - \Delta\right)
\end{aligned} \tag{4.8}$$

where $\hat{b}_u$ is a scalar term introduced for dimension matching. For problems where the input to the system has the same dimension as $y^{(r)}$, such as guidance problems, this term is not needed. For other systems a conversion factor needs to be used that has the same dimension as the control effectiveness of the actuator, or $b_u = \partial h_r / \partial u_{cmd}$. The factor $\hat{b}_u$ in **Error! Reference source not found.** is an estimate of b_u. The modeling error Δ is defined as

$$\begin{aligned}\Delta\left(z,\boldsymbol{x},\boldsymbol{x}_a,y_c,u_{cmd},u_{ad}\right) &= \frac{1}{\hat{b}_u}\left[h_r\left(z,\boldsymbol{x},g\left(\boldsymbol{x}_a,u_{cmd}\right)\right)-C_r\boldsymbol{x}-b_1y_c\right]+u_{ad} \\ &= \frac{1}{\hat{b}_u}\left[h_r\left(z,\boldsymbol{x},g\left(\boldsymbol{x}_a,u_{ec}-u_{ad}\right)\right)-\hat{h}_r\left(\boldsymbol{x},y_c\right)\right]+u_{ad}.\end{aligned} \tag{4.9}$$

Defining the tracking error as $e = y_m - y$, we can write the error dynamics as

$$e^{(r)} = y_m^{(r)} - y^{(r)} = C_r\left(\boldsymbol{x}_m - \boldsymbol{x}\right) + \hat{b}_u\left(u_{ad} - \Delta\right). \tag{4.10}$$

Notice that the reference model (4.6) specifies the desired system trajectory regardless of the input characteristics. Expressing the true system dynamics with respect to reference model (4.6) results in the dynamics in (4.8) where the modeling error Δ is given in (4.9). The purpose of the adaptive signal u_{ad} in (4.8) is to cancel Δ, in which u_{ad} appears explicitly and also implicitly in $g\left(\boldsymbol{x}_a,u_{cmd}\right)$. If u_{ad} successfully cancels Δ, or in other words if u_{ad} solves for $u_{ad} = \Delta\left(z,\boldsymbol{x},\boldsymbol{x}_a,y_c,u_{cmd},u_{ad}\right)$, the regulated output y will track the reference command y_c with the dynamics specified by the reference model (4.5). From (4.7) and (4.9), the condition for $u_{ad} = \Delta\left(z,\boldsymbol{x},\boldsymbol{x}_a,y_c,u_{cmd},u_{ad}\right)$ can be written as

$$h_r\left(z,\boldsymbol{x},g\left(\boldsymbol{x}_a,u_{ec}-u_{ad}\right)\right) = C_r\boldsymbol{x} + b_1y_c. \tag{4.11}$$

When the controller is not in direct control of the system, such as during rate or position saturation, the applied control input to the system $g\left(\boldsymbol{x}_a,u_{ec}-u_{ad}\right)$ is not a function of u_{ad}. In these circumstances there is no solution to (4.11) and hence adaptive cancellation of the modeling error cannot take place. As detailed in the next section we introduce command hedging to permit the adaptive controller to continue to estimate the modeling error even when not in direct control of the system.

4.2 Command Hedging Formulation

Pseudo control hedging was first introduced in [26]–[28] in the setting of augmenting an inverting controller to condition the reference model based on pseudo control signals. The approach was then modified so that it could be applied in a setting of augmenting a linear controller and was simply called control hedging in [17], [18]. The idea in control hedging is to replace the commanded control signals appearing in the modeling error expression by estimates of the corresponding applied control inputs. In other words, we want to apply hedging so that the modeling error in (4.9) becomes

$$\Delta_h = \frac{1}{\hat{b}_u}\left[h_r\left(z, \boldsymbol{x}, g\left(\boldsymbol{x}_a, u_{ec} - u_{ad}\right)\right) - \hat{h}_r\left(\boldsymbol{x}, y_c\right)\right] + \hat{g}\left(\boldsymbol{x}_a, u_{ad}\right) \tag{4.12}$$

where the last term u_{ad} in (4.9) is replaced with an estimate of the applied adaptive control $\hat{g}\left(\boldsymbol{x}_a, u_{ad}\right)$. The benefit of this modification is that during times when the control input applied to the system is not effective, or $g\left(x_a, u_{cmd}\right)$ and $\hat{g}\left(\boldsymbol{x}_a, u_{ad}\right)$ are not functions of their second arguments, Δ_h is not a function of u_{ad} anymore. This means that there is no fixed point issue and there always exists a unique solution to $u_{ad} - \Delta_h$. Consequently adaptive cancellation of the modeling error Δ_h can continue even during times when the adaptive control is not in command of the system. Notice however that replacing u_{ad} in Δ with $\hat{g}\left(\boldsymbol{x}_a, u_{ad}\right)$ removes the difference between u_{ad} and $\hat{g}\left(\boldsymbol{x}_a, u_{ad}\right)$ from the modeling error and as a result the adaptive controller does not adapt to the portion of the modeling error due to this difference. Since the other sources of nonlinearities and modeling error still appear in Δ_h, the NN continues to compensate for them.

In general, if the map $u_{ad} \mapsto \Delta_h$ is a contraction, existence and uniqueness of a solution to $u_{ad} - \Delta_h$ is guaranteed. In the ideal case where both the true actuator and

actuator model are identity, or $g\left(\boldsymbol{x}_a, u_{cmd}\right) = u_{cmd}$ and $\hat{g}\left(\hat{\boldsymbol{x}}_a, u_{cmd}\right) = u_{cmd}$, the contraction condition requires that $\operatorname{sgn}\left(b_1\right) = \operatorname{sgn}\left(\partial h_r / \partial u\right)$ and $\left|\partial h_r / \partial u\right| / 2 < \left|b_1\right| < \infty$ [12]. For non ideal actuators, conditions that guarantee existence and uniqueness of a solution can be derived from the contraction condition $\left|\partial \Delta_h / \partial u_{ad}\right| < 1$. For a linear actuator with output saturation, contraction condition leads to the conclusion that it is desirable to underestimate the control limit, and overestimate the control effectiveness [18].

Our goal is to modify the input to the reference model (4.6) so that the modeling error (4.9) is replaced with (4.12) while the error dynamics (4.10) remain the same. Based on the control hedging implementation in [17], we modify the input y_c to the reference model in (4.6) so that

$$y_m^{(r)} = C_r \boldsymbol{x}_m + b_1\left(y_c - y_h\right) \tag{4.13}$$

where y_h is the hedge signal, yet to be determined. Since the hedge signal is injected at the command level, this modification can be referred to as "command hedging". The objective is to select y_h so that form of the error dynamics in (4.10) is recovered. To achieve this form we use (4.12) and (4.13) in (4.10) and solve for y_h:

$$\underbrace{y_m^{(r)}}_{\substack{C_r\boldsymbol{x}_m + b_1\left(y_c - y_h\right) \\ (4.13)}} \underbrace{-y^{(r)}}_{\substack{-h_r\left(z, \boldsymbol{x}, g\left(\boldsymbol{x}_a, u_{ec} - u_{ad}\right)\right) \\ (4.1),(4.2)}} = C_r \boldsymbol{x}_m - C_r \boldsymbol{x} + b_1 y_c - b_1 y_c + \hat{b}_u u_{ad} \underbrace{-\hat{b}_u \Delta}_{\substack{-h_r\left(z, \boldsymbol{x}, g\left(\boldsymbol{x}_a, u_{ec} - u_{ad}\right)\right) + C_r\boldsymbol{x} + b_1 y_c - \hat{b}_u \hat{g}\left(\hat{\boldsymbol{x}}_a, u_{ad}\right) \\ (4.12)}}$$

$$\begin{aligned}
\cancel{C_r \boldsymbol{x}_m} + \cancel{b_1 y_c} - b_1 y_h - \cancel{h_r\left(z, \boldsymbol{x}, g\left(\boldsymbol{x}_a, u_{ec} - u_{ad}\right)\right)} &= \cancel{C_r \boldsymbol{x}_m} + \cancel{b_1 y_c} - \cancel{C_r \boldsymbol{x}} - \cancel{b_1 y_c} \\
&\quad + \hat{b}_u u_{ad} - \cancel{h_r\left(z, \boldsymbol{x}, g\left(\boldsymbol{x}_a, u_{ec} - u_{ad}\right)\right)} \\
&\quad + \cancel{C_r \boldsymbol{x}} + \cancel{b_1 y_c} + \hat{b}_u \hat{g}\left(\hat{\boldsymbol{x}}_a, u_{ad}\right)
\end{aligned}$$

$$-b_1 y_h = \hat{b}_u u_{ad} + \hat{b}_u \hat{g}\left(\hat{\boldsymbol{x}}_a, u_{ad}\right)$$

$$y_h = \frac{\hat{b}_u}{b_1}\left(\hat{g}\left(\hat{\boldsymbol{x}}_a, u_{ad}\right) - u_{ad}\right) \tag{4.14}$$

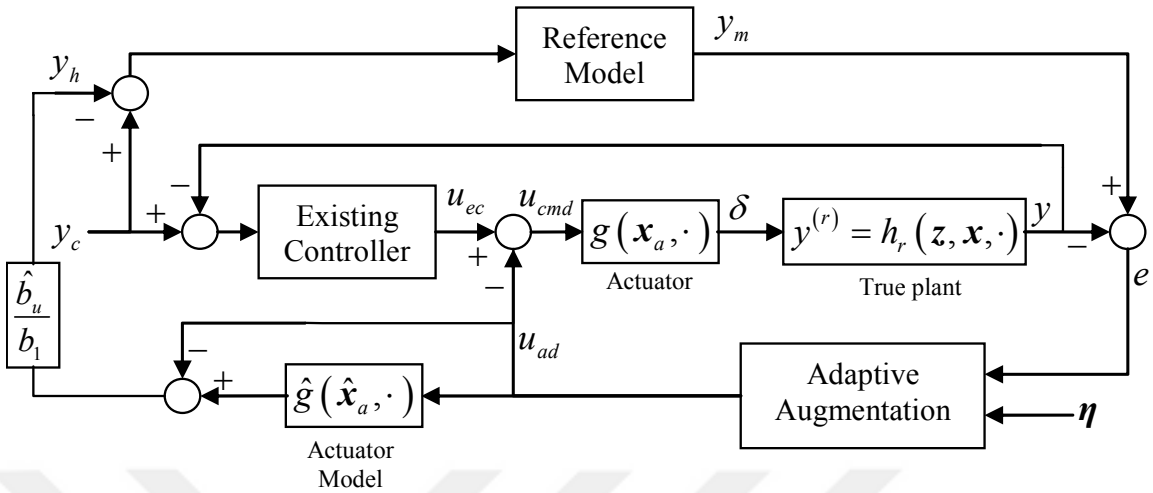

Figure 4-2. Implementation of command hedging in the arbitrary reference model-following adaptive augmenting control architecture.

Implementation of command hedging is schematically shown in Figure 4-2.

In the open loop reference model architecture of [17] the problem is formulated in such a way that in the modeling error expression, the input to the reference model is the augmented control input $u_{ec} + u_{ad}$. Consequently the augmented control signal is hedged in [17]. Since only the adaptive portion of the control signal u_{ad} appears as an input to the reference model in the modeling error expression (4.9) in the arbitrary reference model approach, only that part needs to be hedged. This difference in formulation leads to an easier stability analysis as discussed in the proof of Theorem 4.1.

4.3 Stability with Command Hedging

Stability of the closed loop system with the arbitrary reference model-following adaptive augmenting controller has been proven for systems without input nonlinearities in Section 4.1 of [23] subject to certain conditions on adaptive controller design parameters and initial conditions. It is shown through Lyapunov's direct method that the tracking error vector $\boldsymbol{e}$ remains bounded together with errors on the states associated with the adaptive augmentation. Since the reference model (4.6) without command hedging is a stable linear system driven by a bounded reference command, boundedness of $\boldsymbol{e}$ directly

implies boundedness of system output y. With the command hedging implementation developed in Section 4.2, we show in this section that all the signals in the closed loop system remain bounded. We construct the stability analysis over the existing stability result for the problem without command hedging.

Assumption 4.2. Assume that for the system (4.1) with an ideal actuator ($\delta = \hat{\delta} = u_{cmd}$), the controller (4.7) with (4.4) and u_{ad} as described in (3.23) with reference model (4.6), satisfies all the conditions of uniform ultimate boundedness laid out in Section 4.1 of [23] (a special case of the stability analysis in Section 3.4 of this thesis can also be considered here by removing the z_1 dynamics in the system).

Theorem 4.1. Consider the nonlinear system (4.1), (4.2) under the control of (4.7) with (4.4) and u_{ad} as described in (3.23) with the modified reference model (4.13). Let Assumptions 4.1 and 4.2 hold. Then all the error signals in the closed loop system are uniformly ultimately bounded.

Proof. Without command hedging, boundedness of the tracking error $e = y_m - y$ implies boundedness of the system output y since as long as y_c is bounded y_m is a bounded signal regardless of the other signals in the system. With command hedging, input to the reference model is modified by adding a hedge signal and boundedness of the reference model has to be shown explicitly. In the proof of boundedness with command hedging in the open loop reference model approach, states of the modified reference model are shown to be bounded together with other signals in the system through Lyapunov like stability analysis in [18]. In the arbitrary reference model approach, proving boundedness of the modified reference model is easier since the reference model dynamics are not coupled with the linear error dynamics of the system and the linear

control signal u_{ec} is not fed into the reference model through the hedge signal. This allows us to study the boundedness of the reference model separately.

Ultimate boundedness of the closed loop system with command hedging can be shown in two steps. First, boundedness of the errors in plant states, and states associated with the adaptive augmentation can be shown using the analysis in [23] regardless of boundedness of the reference model states. Assumption 4.2 states that this is granted for the case without command hedging and when hedging is introduced, the same analysis can be used since equation (4.10) that governs error dynamics of the system and other equations regarding dynamics of the adaptive controller ((3.25) with $\Delta_2 = 0$ and (3.27)) are the same with and without command hedging. As a second step, it is straight forward to show boundedness of the reference model states using the already proven boundedness property of the adaptive signal u_{ad}. Assumption 4.1 ensures that hedge signal u_h in (4.14) is bounded for bounded u_{ad}. Since the reference model (4.13) is stable by design, given bounded y_c and u_h, y_m is bounded. ■

4.4 Simulation Example

We test the command hedging implementation developed in the preceding sections on a nonlinear system, consisting of a modified van der Pol oscillator coupled to a lightly damped mode:

$$\begin{aligned}
\dot{x}_1 &= x_2 \\
\dot{x}_2 &= -2\left(x_1^2 - 1\right)x_2 - x_1 + u \\
\dot{x}_3 &= x_4 \\
\dot{x}_4 &= -x_3 - 0.2x_4 + x_1 \\
y &= x_1 + x_3
\end{aligned} \tag{4.15}$$

The output y has a relative degree of $r = 2$. From a practical perspective, the system can be thought of as a second order nonlinear plant model, whose realization consists of

states x_1 and x_2, in which the output is modeled as $y = x_1$. However, the system also contains a very lightly damped unmodeled mode, with a natural frequency equal to that of the linearized plant. This mode is excited by the plant displacement state x_1 and is coupled to the measurement.

The low natural frequency of the unmodeled mode is encompassed by the bandwidth of the controlled system. This represents a challenging control problem. Moreover a dynamic actuator with rate and position saturation is introduced as shown in Figure 4-3. The time constant of the actuator is selected as $\tau = 0.01$ s. Rate limit and position limit are set as $|\mathrm{d}\delta/\mathrm{d}t| \le 15$ and $|\delta| \le 10$ respectively.

We assume the following linear controller has been designed for the system:

$$G_{ec}(s) = \frac{s+1.44}{s+1.80} + \frac{0.56}{s} \tag{4.16}$$

The method by which the above controller has been designed is immaterial to the adaptive controller design. We simply select an $r = 2$ reference model as

$$y_m = \frac{1}{s^2 + 1.8s + 1} y_c \tag{4.17}$$

with a pair of complex conjugate poles with natural frequency 1 rad/s and damping 0.9.

Simulation results without adaptive augmentation are shown in Figure 4-4 where the first row shows plots of y_c and y and the second row shows plots of u_{cmd} and $g(u_{cmd})$. The system is unstable and the command is almost always position and rate

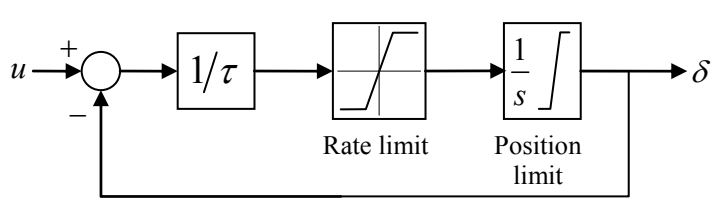

Figure 4-3. Nonlinear actuator model.

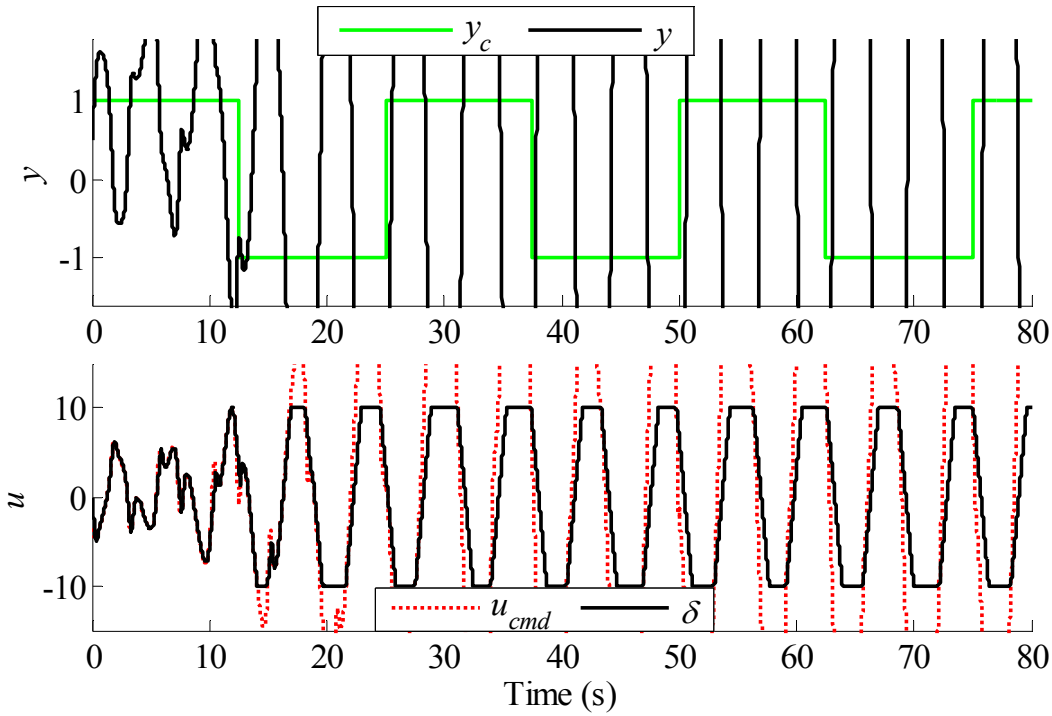

Figure 4-4. Simulation results without adaptive augmentation.

saturated after $t = 15$ s.

Figure 4-5 shows the results with the adaptive controller without command hedging. The system is still unstable. In addition to y_c and y, the top row also shows the y_m plot. NN learning performance is shown at the bottom row. The control signal goes into rate and position saturation as soon as the simulation starts and stays saturated throughout the simulation. The NN attempts to learn the uncertainty and respond to that very quickly, faster than the actuator allows. However it cannot learn the actuator characteristics and the system quickly goes unstable.

Results with the adaptive controller with command hedging are shown in Figure 4-6. In the top row there are four curves; y_c , y_m without command hedging modification plotted for reference to evaluate command hedging's effect on the performance, y_m with command hedging modification, and y. We see that hedging has a dramatic effect on the reference model output in first five seconds. It immediately

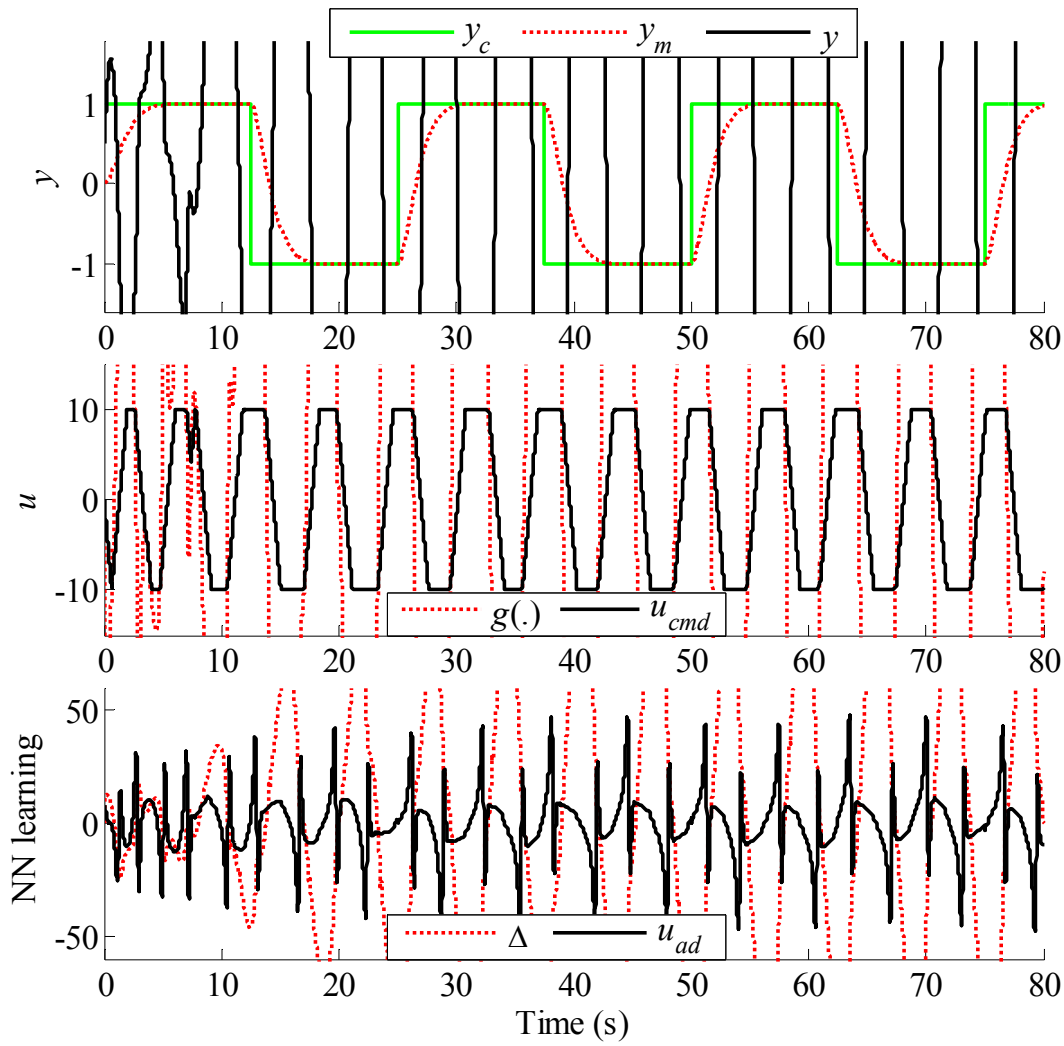

Figure 4-5. Simulation results with adaptive augmentation without command hedging.

detects actuator position and rate saturation and modifies the reference model such that it generates a response that the system can track with the given actuator limitations. This time is enough for the NN to learn the modeling error. Once it starts approximating the modeling error sufficiently well, the system can track the reference model without the actuator exceeding its limits and hence no further modification to the reference model is needed.

4.5 Conclusions

In this chapter we developed command hedging implementation for the arbitrary reference model-following adaptive augmenting control architecture. Similar to previous command hedging implementations, input to the reference model is modified by subtracting a so called hedge signal. The difference is that the hedge signal is computed based on the adaptive component of the control signal and not the total control signal. Simulation results demonstrate that command hedging modifies the reference command is such a way that the NN continues to learn the modeling error in the system during times when it would fail to do so without hedging.

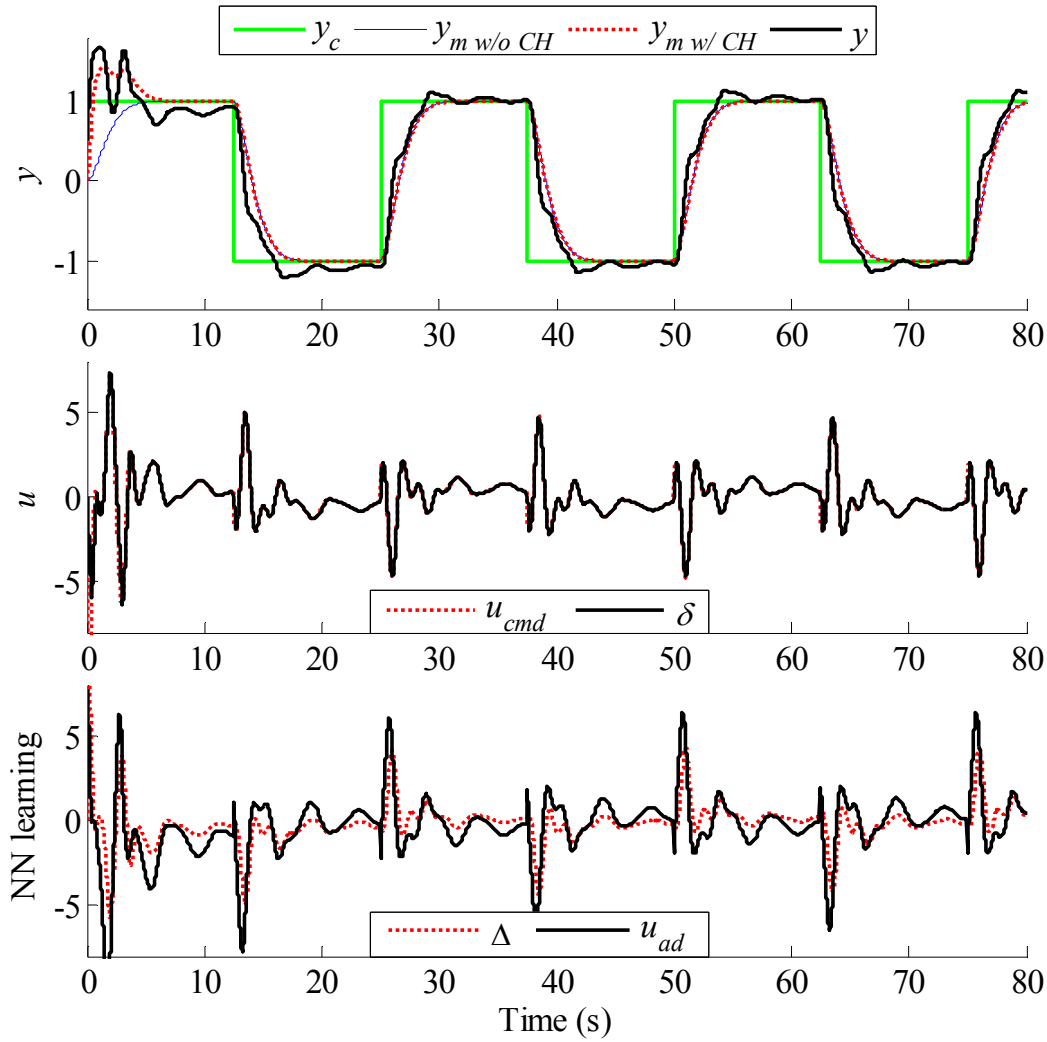

Figure 4-6. Simulation results with adaptive augmentation with command hedging.

CHAPTER 5

DISTRIBUTED CONTROL OF STRUCTURED INTERCONNECTED SYSTEMS

This chapter extends the formulation of the arbitrary reference model-following adaptive augmenting architecture to MIMO systems for distributed control of large-scale interconnected systems. It is assumed that the controllers are interconnected in the same way as the plant. Based on available measurements, a SHL NN is introduced for each subsystem to partially cancel the effects of the sub-system interconnections and modeling errors on tracking performance. Boundedness of error signals is shown through Lyapunov's direct method. Effectiveness of the approach is demonstrated on a wind tunnel experiment representing aerial vehicles flying in a highly aerodynamically coupled formation [59].

5.1 Background

The motivation for extending the open loop reference model approach to MIMO systems has been the formation flight wind tunnel experiment test bed at Cornell University. The experiment setup consists of four 2-DOF wings in a half-vee formation. Due to the complexity of vortex generation and shedding, and the resulting interaction between a shed vortex and a downstream lifting surface, it is difficult to obtain a first principles quantitative model that accurately captures the dynamics of the overall system (see [60], for example). Furthermore, the non-linearity of the inter-aircraft effects [61] makes accurate system identification more difficult.

Consequently the formation flight system held promise as an application for adaptive control. The adaptive control presented here improves the effectiveness of

lower-level controllers by modifying the plant behavior toward that assigned by the reference model. In particular, it can alleviate nonlinearities that would otherwise be treated as disturbances in linear control methods. Similarly, these adaptive control methods eliminate any linear modeling error.

Analysis of the experiment setup has revealed that the aerodynamic interaction between the wings has a quadratic nature, which cannot be captured by the algorithms outlined in [45] and [46]. Modeling the interactions as large disturbances allows use of the tools in [45] and [46] at the expense of performance, and the resulting controller requires further tuning on the experiment. When applied to the experimentally identified model of the wings, the hand tuned controller does not provide satisfactory dynamics. Therefore, the open loop and closed loop reference model-following adaptive augmenting controllers are not applicable.

Open loop analysis of the experiment setup has further revealed that coupling from downstream wing to upstream wing is negligible compared to the coupling from upstream to downstream [62]. Based on this observation, distributed controllers were designed for each wing using the local measurements and measurements of the upstream wing. In the following we augment the hand tuned controllers with adaptive controllers in the framework of arbitrary reference model-following control. We then provide a stability analysis that shows boundedness of the overall system.

5.2 System Description and Problem Formulation

Let the formation be composed of *m stabilizable* nonlinear subsystems obeying the following differential equations:

$$
\begin{aligned}
\dot{\boldsymbol{x}}_{p_1} &= \boldsymbol{f}_{p_1}\left(\boldsymbol{x}_{p_1}, u_1, \boldsymbol{\delta}_1\right) \\
y_1 &= h_{p_1}\left(\boldsymbol{x}_{p_1}, \boldsymbol{\delta}_1\right) \\
\dot{\boldsymbol{x}}_{p_i} &= \boldsymbol{f}_{p_i}\left(\boldsymbol{x}_{p_{i-1}}, \boldsymbol{x}_{p_i}, u_i, \boldsymbol{\delta}_i\right), \qquad i = 2, \ldots, m \\
y_i &= h_{p_i}\left(\boldsymbol{x}_{p_{i-1}}, \boldsymbol{x}_{p_i}, \boldsymbol{\delta}_i\right)
\end{aligned}
\tag{5.1}
$$

where $\boldsymbol{x}_{p_i} \in \mathbb{R}^{n_{p_i}}$ is the state vector of the ith subsystem, $u_i \in \mathbb{R}$ and $y_i \in \mathbb{R}$ are the control and regulated output of the ith subsystem, $\boldsymbol{\delta}_i \in \mathbb{R}^{n_{\delta_i}}$ are bounded external disturbances, $\boldsymbol{f}_{p_1} : \mathbb{R}^{n_{p_1}} \times \mathbb{R} \times \mathbb{R}^{n_{e_1}} \to \mathbb{R}^{n_1}$, $h_{p_1} : \mathbb{R}^{n_{p_1}} \times \mathbb{R}^{n_{\delta_1}} \to \mathbb{R}$, $\boldsymbol{f}_{p_i} : \mathbb{R}^{n_{p_{i-1}}} \times \mathbb{R}^{n_{p_i}} \times \mathbb{R} \times \mathbb{R}^{n_{\delta_i}} \to \mathbb{R}^{n_i}$, $h_{p_i} : \Re^{n_{p_{i-1}}} \times \mathbb{R}^{n_{p_i}} \times \mathbb{R}^{n_{\delta_i}} \to \mathbb{R}$, are unknown but otherwise sufficiently smooth and bounded functions.

Assumption 5.1. *Bounded* disturbances $\boldsymbol{\delta}_i$ belong to a class of continuous time functions describable by

$$
\begin{aligned}
\dot{\boldsymbol{x}}_{d_i} &= \boldsymbol{f}_{d_i}\left(\boldsymbol{x}_{d_i}\right), \boldsymbol{x}_{d_i}(0) = \boldsymbol{x}_{d_i}^0 \\
\boldsymbol{\delta}_i &= \boldsymbol{h}_{d_i}\left(\boldsymbol{x}_{d_i}\right)
\end{aligned}
\tag{5.2}
$$

where $\boldsymbol{x}_{d_i} \in \mathbb{R}^{n_{d_i}}$. The functions $\boldsymbol{f}_{d_i}$ and $\boldsymbol{h}_{d_i}$ are also unknown.

The augmented subsystem dynamics consisting of the plant and disturbance dynamics can be expressed in compact form as

$$
\begin{aligned}
\dot{\boldsymbol{x}}_{s_1} &= \boldsymbol{f}_{s_1}\left(\boldsymbol{x}_{s_1}, u_1\right) \\
y_1 &= h_{s_1}\left(\boldsymbol{x}_{s_i}\right) \\
\dot{\boldsymbol{x}}_{s_i} &= \boldsymbol{f}_{s_i}\left(\boldsymbol{x}_{s_{i-1}}, \boldsymbol{x}_{s_i}, u_i\right), \; i = 2, \ldots, m \\
y_i &= h_{s_i}\left(\boldsymbol{x}_{s_{i-1}}, \boldsymbol{x}_{s_i}\right)
\end{aligned}
\tag{5.3}
$$

where $\boldsymbol{x}_{s_i} \in \mathbb{R}^{n_i}$, $n_i = n_{p_i} + n_{d_i}$ is the combined state vector of the subsystem i and external disturbance dynamics.

Assumption 5.2. Each of the subsystems satisfies the conditions for output feedback linearization with known strong relative degree $r_i, r_i \le n_i$, achieved by its own control.

Assumption 5.2 allows us to represent the system dynamics (5.3) under the regulation of (5.6) with (5.5) in normal form as

$$\begin{aligned} \dot{\boldsymbol{\chi}}_1 &= \boldsymbol{f}_{\chi_1}\left(y_o, \boldsymbol{\chi}_1, \boldsymbol{y}_1\right) \\ y_1^{(r_1)} &= h_1\left(y_o, \boldsymbol{x}_i, u_1\right) \\ \dot{\boldsymbol{\chi}}_i &= \boldsymbol{f}_{\chi_i}\left(\boldsymbol{x}_{i-1}, \boldsymbol{\chi}_i, \boldsymbol{y}_i\right), \quad i = 1, \ldots, m \\ y_i^{(r_i)} &= h_i\left(\boldsymbol{x}_{i-1}, \boldsymbol{x}_i, u_i\right) \end{aligned} \tag{5.4}$$

where $\boldsymbol{y}_i \triangleq \begin{bmatrix} y_i & \dot{y}_i & \cdots & y_i^{(r_i-1)} \end{bmatrix}^T$, $\boldsymbol{x}_i = \begin{bmatrix} \boldsymbol{x}_{s_i}^T & \boldsymbol{x}_{c_i}^T \end{bmatrix}^T \in \mathbb{R}^{n_i + n_{c_i}}$, and $\boldsymbol{\chi}_i$ are the states associated with the internal dynamics for each subsystem. From this point on we will not treat the first subsystem separately with the understanding that for $i = 1$, input argument $\boldsymbol{x}_0$ of $\boldsymbol{f}_{\chi_1}$ and h_1 is replaced with y_0.

Assumption 5.3. The internal dynamics of the closed loop system in (5.4) with $\boldsymbol{y}_i$ and $\boldsymbol{x}_{i-1}$ viewed as inputs are input to state stable [7].

Existing controllers designed to stabilize the system in (5.1) are represented by

$$\begin{aligned} \dot{\boldsymbol{x}}_{c_i} &= \boldsymbol{f}_{c_i}\left(\boldsymbol{x}_{c_i}, y_{i-1}, y_i\right) \\ u_{ec_i} &= \boldsymbol{h}_{c_i}\left(\boldsymbol{x}_{c_i}, y_{i-1}, y_i\right) \end{aligned} \tag{5.5}$$

for $i = 1, \ldots, m$ with y_0 being an external command signal for the first (leading) subsystem. Notice that the dependence of the controller on system structure matches that of the system in (5.3), except that instead of the full state information, only measured outputs are assumed available.

Assumption 5.4. The existing controller for the ith subsystem given in (5.5) for $i = 1, \ldots, m$ is input-to-state stable [7].

The objective is to synthesize distributed adaptive output feedback control laws u_{ad_i} that augment existing controllers as

$$u_i = u_{ec_i} - u_{ad_i} \tag{5.6}$$

such that the synchronization errors $\tilde{y}_i = y_{i-1} - y_i$ remain bounded under the assumption that the ith controller has access to its own measurements y_i and measurements of the upstream subsystem, y_{i-1}.

5.3 Controller Architecture

The conceptual layout for augmenting existing distributed controller designs for large-scale interconnected systems with NN based adaptive elements in the framework of arbitrary reference model-following control is depicted in Figure 5-1. The shaded blocks represent the elements to be added. The reference model specifies the desired performance for the ith subsystem. Input vector to the NN includes signals from the local subsystem as well as measurements from other subsystems that the local one is dynamically connected to. Here the formulation is developed for the special case of a

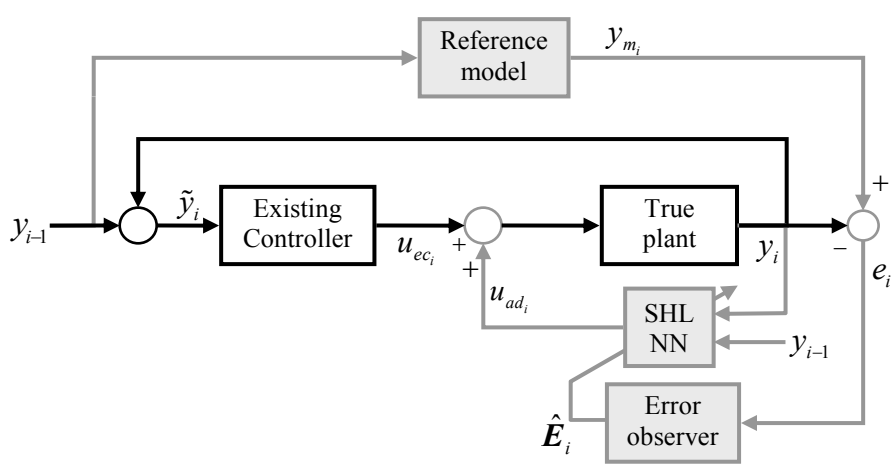

Figure 5-1. Augmenting adaptive controller architecture for the ith subsystem.

formation of aerial vehicles where every vehicle i is dynamically affected by its nearest upstream vehicle, $i-1$.

5.3.1 Reference Model

We choose a simple linear performance model for each subsystem as a reference model [23]:

$$G_i(s) = \frac{y_{m_i}(s)}{y_{i-1}(s)} = \frac{b_i}{s^{r_i} + a_{i,r_i} s^{r_i - 1} + \cdots + a_{i,1}} \tag{5.7}$$

where $y_{i-1}(s)$ is the output of the subsystem $i-1$ given as input command to the ith subsystem. $G_i(s)$ for $i = 1, \ldots, m$ should be designed to have relative degree r_i and to satisfy the performance requirements of the closed-loop system with all the poles in the open left half plane. It can be expressed in time domain as

$$y_{m_i}^{(r_i)} = -a_{i,1} y_{m_i} - a_{i,2} \dot{y}_{m_i} - \cdots - a_{i,r_i} y_{m_i}^{(r_i - 1)} + b_i y_{i-1}(t) \tag{5.8}$$

and in state space form as

$$\begin{aligned} \dot{\boldsymbol{y}}_{m_i} &= A_{m_i} \boldsymbol{y}_{m_i} + \boldsymbol{b}_{m_i} y_{i-1} \\ y_{m_i} &= \boldsymbol{c}_{m_i}^T \boldsymbol{y}_{m_i} \end{aligned} \tag{5.9}$$

where $\boldsymbol{y}_{m_i} \triangleq \begin{bmatrix} y_{m_i} & \dot{y}_{m_i} & \cdots & y_{m_i}^{(r_i - 1)} \end{bmatrix}^T$ and

$$A_{m_i} = \begin{bmatrix} 0 & 1 & 0 & \cdots & 0 \\ 0 & 0 & 1 & \cdots & 0 \\ \vdots & \vdots & \vdots & \ddots & \vdots \\ 0 & 0 & & \cdots & 1 \\ -a_{i,1} & -a_{i,2} & -a_{i,3} & \cdots & -a_{i,r_i} \end{bmatrix}, \quad \boldsymbol{b}_{m_i} = \begin{bmatrix} 0 \\ 0 \\ 0 \\ \vdots \\ b_i \end{bmatrix}, \quad \boldsymbol{c}_{m_i} = \begin{bmatrix} 1 \\ 0 \\ 0 \\ \vdots \\ 0 \end{bmatrix}$$

5.3.2 Modeling Uncertainties

The output dynamics of the ith system given in (5.4) can be written using (5.8) as

$$
\begin{aligned}
y_i^{(r_i)} &= h_i\left(\boldsymbol{x}_{i-1}, \boldsymbol{x}_i, u_i\right) \\
&= -a_{i,1}y_i - a_{i,2}\dot{y}_i - \cdots - a_{i,r_i}y_i^{(r_i-1)} + b_i\left(y_{i-1} - u_{ad_i} + \Delta_i\right)
\end{aligned}
\tag{5.10}
$$

where Δ_i represents the modeling error and interconnection effects and is given by

$$
\Delta_i = \frac{1}{b_i}\left(h_i\left(\boldsymbol{x}_{i-1}, \boldsymbol{x}_i, u_i\right) + a_{i,1}y_i + a_{i,2}\dot{y}_i + \cdots + a_{i,r_i}y_i^{(r_i-1)}\right) + u_{ad_i} - y_{i-1}. \tag{5.11}
$$

Notice that the existing linear control signal u_{ec_i} that appears in u_i in h_i does not appear explicitly in (5.10). Its effect is embedded in the uncertainty defined in (5.11).

5.3.3 Error Dynamics

Defining tracking error as $e_i = y_{m_i} - y_i$, we can write error dynamics for the ith subsystem from (5.8) and (5.10) as

$$
\begin{aligned}
e_i^{(r_i)} &= -a_{i,1}y_{m_i} + a_{i,1}y_i - a_{i,2}\dot{y}_{m_i} + a_{i,2}\dot{y}_i - \cdots - a_{i,r_i}y_{m_i}^{(r_i-1)} + a_{i,r_i}y_i^{(r_i-1)} + b_i\left(u_{ad_i} - \Delta_i\right) \\
&= -a_{i,1}\left(y_{m_i} - y_i\right) - a_{i,2}\left(\dot{y}_{m_i} - \dot{y}_i\right) - \cdots - a_{i,r_i}\left(y_{m_i}^{(r_i-1)} - y_i^{(r_i-1)}\right) + b_i\left(u_{ad_i} - \Delta_i\right) \\
&= -a_{i,1}e_i - a_{i,2}\dot{e}_i - \cdots - a_{i,r_i}e_i^{(r_i-1)} + b_i\left(u_{ad_i} - \Delta_i\right)
\end{aligned}
\tag{5.12}
$$

Error dynamics in (5.12) can be represented in state space form as follows:

$$
\begin{aligned}
\dot{\boldsymbol{E}}_i &= A_{m_i}\boldsymbol{E}_i + \boldsymbol{b}_{m_i}\left(u_{ad_i} - \Delta_i\right) \\
e_i &= \boldsymbol{c}_{m_i}\boldsymbol{E}_i
\end{aligned}
\tag{5.13}
$$

where

$$
\boldsymbol{E}_i \triangleq \boldsymbol{y}_{m_i} - \boldsymbol{y}_i = \begin{bmatrix} e_i & \dot{e}_i & \cdots & e_i^{(r_i-1)} \end{bmatrix}^T. \tag{5.14}
$$

5.3.4 Adaptive Controller Design

The adaptive control signal u_{ad_i} that augments the existing control signal will be designed to approximately cancel Δ_i, which depends on u_{ad_i} through u_i. The following

assumption introduces a sufficient condition for the existence and uniqueness of a solution for u_{ad_i}.

Assumption 5.5. The mapping $u_{ad_i} \to \Delta_i$ is a contraction.

Assumption 5.5 is equivalent to [12]:

$$sign(b_i) = sign\left(\frac{\partial h_i}{\partial u}\right)$$
$$\left|\frac{\partial h_i}{\partial u}\right| / 2 < |b_i| < \infty$$

These conditions imply that control reversal is not permitted, and that there is a lower bound on the estimate of control effectiveness b_i.

A SHL NN is used to approximate Δ_i in (5.11). Notice that Δ_i is a nonlinear function of the states of the subsystems i and $i-1$ and input u_i. Following assumption is required to approximate Δ_i using available measurements:

Assumption 5.6. The modeling error Δ_i, which represents the interconnection effects between subsystems i and $i-1$ and modeling errors of subsystem i, is observable from the measurements of subsystems i and $i-1$.

Then, using the main result of [32], Δ_i can be written as

$$\Delta_i = M_i^T \boldsymbol{\sigma}_i \left(N_i^T \boldsymbol{\eta}_i\right) + \varepsilon_i(\boldsymbol{\eta}),\ \left\|\varepsilon_i(\boldsymbol{\eta})\right\| \le \varepsilon_i^* \tag{5.15}$$

where $M_i \in \mathbb{R}^{l_i \times 1}$ and $N_i \in \mathbb{R}^{m_i \times l_i}$ are constant weight matrices with l_i being the number of neurons in the hidden layer, $\varepsilon^* > 0$ is arbitrary, $\varepsilon(\boldsymbol{\eta})$ is the NN reconstruction error, and $\boldsymbol{\eta} \in \mathbb{R}^{m_i \times 1}$ is the input vector

$$
\begin{aligned}
\boldsymbol{\eta}_i(t) &= \begin{bmatrix} 1 & \bar{u}_{ad_i}^T(t) & \bar{y}_{i-1}^T(t) & \bar{y}_i^T(t) \end{bmatrix}^T, \qquad i = 1,\ldots,m \\
\bar{u}_{ad_i}^T(t) &= \begin{bmatrix} u_{ad_i}(t) & u_{ad_i}(t-d) & \cdots & u_{ad_i}\left(t-\left(j_i-r_i-1\right)d\right) \end{bmatrix}^T \\
\bar{y}_i^T(t) &= \begin{bmatrix} y_i(t) & y_i(t-d) & \cdots & y_i\left(t-\left(j_i-1\right)d\right) \end{bmatrix}^T, \; i = 1,\ldots,m \\
\bar{y}_0^T(t) &= y_0(t)
\end{aligned}
$$

with $j_i \geq n_i$ and $d > 0$, $m_i = 3k_i - r_i + 1$, $\boldsymbol{\sigma}_i$ being a vector of squashing functions $\boldsymbol{\sigma}_i(\cdot)$, its jth element being defined like $\left[\boldsymbol{\sigma}_i\left(N_i^T\boldsymbol{\eta}_i\right)\right]_j = \left[\boldsymbol{\sigma}_i\left(N_i^T\boldsymbol{\eta}_i\right)_j\right]$. The adaptive signal u_{ad_i} is designed as

$$
u_{ad_i} = \hat{M}_i^T \boldsymbol{\sigma}_i\left(\hat{N}_i^T \boldsymbol{\eta}_i\right) \tag{5.16}
$$

where $\hat{M}_i$ and $\hat{N}_i$ are estimates of the ideal weights M_i and N_i to be adapted online.

5.3.5 Error Observer

For full-state feedback applications, Lyapunov-like stability analysis of the error dynamics in (5.13) results in update laws for the adaptive control parameters in terms of the error vector, $\boldsymbol{E}$. Following the approach in [13], we introduce a simple linear observer for the interconnection error dynamics (5.13), assuming that the adaptive signal can compensate for the modeling error $\left(u_{ad_i} = \Delta_i\right)$:

$$
\begin{aligned}
\dot{\hat{\boldsymbol{E}}}_i &= A_{m_i}\hat{\boldsymbol{E}}_i + K_i\left(e_i - \hat{e}_i\right) \\
\hat{e}_i &= \boldsymbol{c}_{m_i}\hat{\boldsymbol{E}}_i
\end{aligned} \tag{5.17}
$$

where K_i is a gain matrix, and should be chosen such that $A_{m_i} - K_i\boldsymbol{c}_{m_i}$ is asymptotically stable. This observer design ignores the nonlinearities that enter the interconnection error dynamics (5.13) as a forcing function. This can be justified by the fact that u_{ad_i} nearly cancels Δ_i, as will be demonstrated by using Lyapunov stability analysis. Let $\tilde{A}_i = A_{m_i} - K_i\boldsymbol{c}_{m_i}$ and $\tilde{\boldsymbol{E}}_i = \hat{\boldsymbol{E}}_i - \boldsymbol{E}_i$. Then the observer error dynamics can be written as:

$$\dot{\tilde{\boldsymbol{E}}} = \tilde{A}_i \tilde{\boldsymbol{E}}_i - \boldsymbol{b}_{m_i}\left(u_{ad_i} - \Delta_i\right). \tag{5.18}$$

5.3.6 NN Adaptation Laws

Based on Lyapunov's direct method that will be detailed below, we introduce the following adaptation laws [13]:

$$\begin{aligned} \dot{\hat{M}}_i &= -\Gamma_{M_i}\left[2\left(\hat{\boldsymbol{\sigma}}_i - \hat{\sigma}_i' \hat{N}_i^T \boldsymbol{\eta}_i\right)\hat{E}_i^T P_i b_{m_i} + k_i \hat{M}_i\right] \\ \dot{\hat{N}}_i &= -\Gamma_{N_i}\left[2\boldsymbol{\eta}_i \hat{E}_i P_i b_{m_i} \hat{M}_i^T \hat{\sigma}_i' + k_i \hat{N}_i\right] \end{aligned} \tag{5.19}$$

in which $\Gamma_{M_i}, \Gamma_{N_i}$ are positive definite adaptation gain matrices, $k_i > 0$ are σ − modification gains, $\hat{\boldsymbol{\sigma}}_i = \boldsymbol{\sigma}_i\left(\hat{N}_i^T \boldsymbol{\eta}_i\right)$, $\hat{\sigma}_i'$ denotes the Jacobian matrix computed at the estimate: $\hat{\boldsymbol{\sigma}}_i' = \boldsymbol{\sigma}_i'\left(\hat{N}_i^T \boldsymbol{\eta}_i\right)$ and P_i is the solution of the Lyapunov equation

$$A_{m_i}^T P_i + P_i A_{m_i} = -Q_i, \qquad i = 1, \ldots, m$$

for some $Q_i > 0$ with $\lambda_{\min}\left(Q_i\right) > 2$.

5.4 Stability Analysis

In this section we show through Lyapunov's direct method that the error signals in the large scale interconnected system are ultimately bounded. Consider the following composite error vector

$$\boldsymbol{\zeta} = \begin{bmatrix} \boldsymbol{E}_1^T & \cdots & \boldsymbol{E}_m^T & \tilde{\boldsymbol{E}}_1^T & \cdots & \tilde{\boldsymbol{E}}_m^T & \operatorname{vec}\left(\tilde{Z}_1\right)^{\boldsymbol{T}} & \cdots & \operatorname{vec}\left(\tilde{Z}_m\right)^{\boldsymbol{T}} \end{bmatrix}^T$$

where $\tilde{Z}_i \triangleq \begin{bmatrix} \tilde{M}_i & 0 \\ 0 & \tilde{N}_i \end{bmatrix}$ and consider the following positive definite function

$$V\left(\boldsymbol{\zeta}\right) = \boldsymbol{\zeta}^T T \boldsymbol{\zeta}$$

where

$$T = \text{blockdiag}\left(\begin{bmatrix} P_1 & \cdots & P_m & \tilde{P}_1 & \cdots & \tilde{P}_m & \Gamma_{M_1}^{-1} & \cdots & \Gamma_{M_m}^{-1} & \Gamma_{N_1}^{-1} & \cdots & \Gamma_{N_m}^{-1} \end{bmatrix}\right)$$

in which $\tilde{P}_i$ satisfies

$$\tilde{A}_i^T \tilde{P}_i + \tilde{P}_i \tilde{A}_i = -\tilde{Q}_i$$

for some $\tilde{Q}_i > 0$ with minimum eigenvalue $\lambda_{\min}\left(\tilde{Q}_i\right) > 2$.

Notice that the NN approximation is valid in a compact set. Based on the definition of the error variables and continuity of solutions of differential equations, this set maps onto a bounded set Ω_ζ in the error space. Let

$$B_R \triangleq \left\{\boldsymbol{\zeta} \middle| \|\boldsymbol{\zeta}\| \le R\right\}, \qquad R > 0$$

be the largest hypersphere in Ω_ζ. Let α be the minimum value of $V(\boldsymbol{\zeta}) = \boldsymbol{\zeta}^T T \boldsymbol{\zeta}$ on the boundary of B_R

$$\alpha \triangleq \min_{\|\boldsymbol{\zeta}\|=R} V(\boldsymbol{\zeta}) = R^2 T_m,$$

where T_m is the minimum eigenvalue of T. Introduce the following set:

$$\Omega_\alpha \triangleq \left\{\boldsymbol{\zeta} \in B_R \middle| V(\boldsymbol{\zeta}) \le \alpha\right\}.$$

Assumption 5.7. Assume

$$R > \gamma \sqrt{\frac{T_M}{T_m}} \ge \gamma, \tag{5.20}$$

where T_M is the maximum eigenvalue of T, γ is defined as

$$\gamma = \max\left(\sqrt{\frac{\Omega}{Q_m}}, \sqrt{\frac{\Omega}{\tilde{Q}_m}}, \sqrt{\frac{\Omega}{\Lambda_m}}\right) \tag{5.21}$$

where Ω and Λ_m are defined in APPENDIX B.

Theorem 5.1. Consider the controlled interconnected system (5.4). Let Assumptions 5.1-5.7 hold. Then the augmenting control law (5.6), (5.16) along with (5.17), (5.19) guarantees that the signals $\boldsymbol{E}_i$, $\tilde{\boldsymbol{E}}_i$, $\tilde{\boldsymbol{M}}_i \triangleq \hat{\boldsymbol{M}}_i - \boldsymbol{M}_i$, $\tilde{\boldsymbol{N}}_i \triangleq \hat{\boldsymbol{N}}_i - \boldsymbol{N}_i$, $i = 1, \ldots, m$ in the closed loop system are ultimately bounded.

Proof. See APPENDIX B.

Remark 5.1. Assumption 5.6 is the key to the proof, enabling the SHL NN to approximate the interconnection effects and uncertainties up to arbitrary accuracy using available measurements. With this assumption, forcing terms of the error equations (5.13) and (5.18) can be upper bounded as shown in [13] and since these equations are in the same form as those in [13], stability analysis for an individual subsystem follows directly.

Remark 5.2. In the case of non-minimum phase subsystems, Assumption 5.3 can be relaxed by assuming that the internal dynamics satisfy a conic sector bound within a compact domain, in the expense of increased error bounds as detailed in Chapter 3 for a single-input single-output system.

Remark 5.3. Theorem 5.1 guarantees boundedness of the output tracking error e_i. Since the reference model is a stable linear system, boundedness of e_i also implies boundedness of synchronization error given by $\tilde{y}_i = y_{i-1} - y_i = e_i + y_{i-1} - y_{m_i}$ for bounded external input.

Remark 5.4. The problem is formulated according to the wind tunnel experiment having wings in half-vee formation, where every wing is dynamically connected only to its upstream wing. However, the method developed here remains valid for general interconnections as long as Assumption 5.6 is suitably modified for the connection

structure. Thus the control approach is valid even if there is an upstream dynamic connection so long as observability is maintained.

5.5 Description of the Wind Tunnel Experiment

The results discussed in this chapter derived from experiments on an existing apparatus. The formation flight test-bed at Cornell University [62] was conceived for study of newly developed control architectures, with the ancillary purpose of demonstrating the prospective benefits of flying aircraft in formation [63]. Airplanes flying in such a formation would enjoy a substantial reduction in induced drag, extending the range of a squadron or allowing solar powered airplanes to stay aloft indefinitely [64], [65]. This reduction in drag is thought to be the reason geese fly in formation [66].

5.5.1 Configuration design

The design of the formation flight apparatus sought to represent a realistic system as well as present a challenging control problem. In the Cornell experiment pictured in Figure 1-5, four wings are mounted in a half-vee formation. Each wing moves independently with two degrees of freedom, roll and sway (lateral motion). For reasons of manufacturability, sway was implemented as yaw about an axis some distance behind the wing. Both degrees of freedom were measured with low friction optical encoders. Control was effected with servomotor-actuated ailerons.

For a formation flight implementation, we wish to control the total induced drag. Of the six standard degrees of freedom, sway (lateral motion) is the one that most impacts the induced drag of the formation as a whole. Sway is most effectively controlled via roll. Roll is most effectively controlled with ailerons. Yaw, pitch, and heave (vertical motion) have second-order effects on the induced drag of the formation; we consider them decoupled from sway and roll, so that in a practical system they would be controlled

independently. Surge (stream-wise motion) affects the induced drag locally, but moderate surge does not affect the drag of the formation as a whole.

While a formation of two wings demonstrates the spatial coupling integral to the control problem and the drag reduction, the larger formation of four wings allows disturbances to propagate in the spatial dimension. This propagation allows for empirical observation of controller performance in a system having significant spatial structure.

The formation that maximizes drag reduction is a vee formation, not necessarily symmetric, in which each aircraft behind the leader is situated with one wing-tip directly behind the wing-tip of the next aircraft forward. The half-vee formation captures the essential dynamics of a full-vee, but allows for higher order propagation due to the limited cross section of the wind-tunnel.

5.5.2 Specifications

Each airfoil has rectangular planform of 9 cm chord and 24 cm span. The airfoil cross section, NACA 0018, has a nearly linear lift curve for moderate angles of attack at low Reynolds numbers, and it develops significant lift under such conditions [67]. The rectangular planform is actually quite inefficient and thus generates strong vortices [68], making the aerodynamic coupling among wings consistent and substantial.

The length of the cantilevered arm between the yaw axis and the wing, for effecting the sway degree of freedom, is about 50 cm. Each wing was mounted 21 cm (chord plus one half span) behind and 24 cm (one span) port side of its predecessor. The mount allows a wing to move 8 cm port or starboard (0.33 span, 0.16 radians/9° of yaw) from its nominal position, and to roll by nearly a quarter-turn in either direction.

The airfoils were rapid-prototyped from ABS plastic. Roll inertia, yaw inertia, and Coulomb friction were kept low where possible.

The 1.2 m wind-tunnel was operated at a wind speed of about 8.5 m/s, or a Reynolds number of 50 000.

Control is moderated with a real time control system from dSPACE. All control design, analysis, and implementation was performed with Matlab and Simulink. Performance was evaluated by recording yaw angles, as the lift and drag forces involved were too small at the available wind speeds for a force balance to be useful.

The apparatus is equipped with servo-controlled roll and yaw locks to facilitate system identification and system initialization. Each wing module was made to bolt to an optical table to allow for different formation configurations. The wings can be mounted with different stream-wise spacing, with different lateral spacing, or possibly in a more general formation. A formation other than a variation on a vee formation is less applicable to the practical and control problems we are studying, but may be useful for investigating alternative control problems abstracting different practical scenarios.

5.6 Experiment Results

Prior to implementing the adaptive augmenting controller, PD controllers were manually tuned with the objective of minimizing the synchronization errors with zero external command to the leading wing. In particular, the existing local control signals were generated as

$$u_{ec_i} = k_1\bar{y}_i + k_2\dot{\bar{y}}_i + k_3 y_i + k_4\dot{y}_i + k_5 y_{i-1} + k_6\dot{y}_{i-1} \tag{5.22}$$

with $k_1 = -3.110$, $k_2 = -0.851$, $k_3 = -8.050$, $k_4 = -4.590$, $k_5 = 4.000$, and $k_6 = 1.455$. Here y_i is the regulated output, yaw, and $\bar{y}_i$ is roll position, which is available for feedback but not regulated. Derivatives are obtained with a high pass filter. Both the identified local linear model and theoretical analysis show that relative degree of the regulated output is four. For the adaptive controller, a linear fourth order system is chosen as the reference model with poles located at $-2.4 \pm 1.8i$ and $-3.2 \pm 2.4i$. Error observer introduced in (5.17) is designed to be five times faster than the reference model. The SHL NNs are designed to have ten hidden neurons and the weights $\hat{M}_i$ and $\hat{N}_i$ are

initialized to zero. Adaptive law parameters are selected as $F_i = 25I$, $G_i = 15I$, and $k_i = 0.5$.

First, performances of the existing and augmented controllers are compared against disturbance rejection. In addition to the ambient disturbances in the wind tunnel, leading wing is used as a disturbance generator. Yaw axis of the first wing is locked at zero and it is given a control input so that its roll angle oscillates with a frequency of 1 rad/s and amplitude 25 deg. Formation remained stable with both controllers. On the average we observed more than 60% improvement in the synchronization error with the augmented controller.

Figure 5-2 shows yaw and roll positions of the wings when all the wings are free, $y_0 = 0$, and the only disturbance is the ambient noise in the wind tunnel. The experiment starts with adaptive controllers on, then around $t = 6\,\text{s}$ adaptive controllers are turned off, and turned back on again around $t = 16\,\text{s}$. Adaptive controllers improve robustness of the

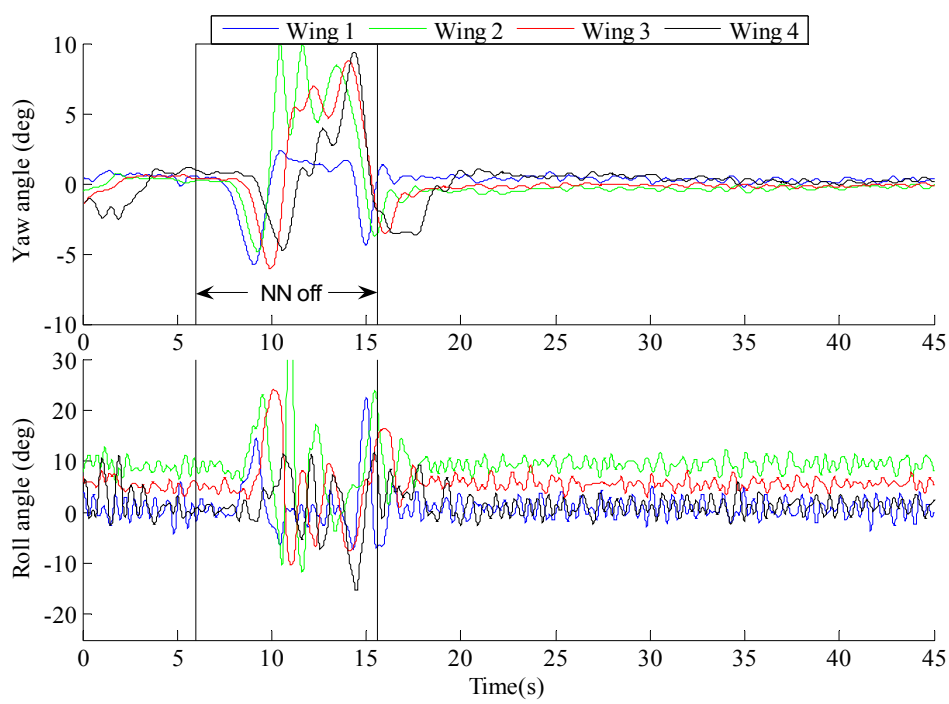

Figure 5-2. Disturbance rejection with adaptive and non-adaptive controllers.

formation to disturbance drastically. With adaptive controllers on, synchronization errors remain within 1 deg, while they grow as high as 10 deg without adaptation.

Next we compare the two controllers with a nonzero command to the leader. A rather large yaw command of -5 deg is given to the leader wing, which is more than half of the available yaw motion. Results with the existing non-adaptive controllers are given in Figure 5-3. Command is given around $t = 4\,\mathrm{s}$ and then removed around $t = 30\,\mathrm{s}$. The formation quickly gets unstable and wings start oscillating within the physical limitations. Synchronous motion of a formation is challenging since spatial instability can occur quickly due to time delays and local overshoots. Moreover, due to the fact that lateral motion is implemented as yaw, local dynamics of wings change when a nonzero command is given. For the given command, these changes come to a point where the linear controller tuned for zero yaw can no longer tolerate the ambient noise in the tunnel.

Figure 5-4 shows the results when the -5 deg command is given while the

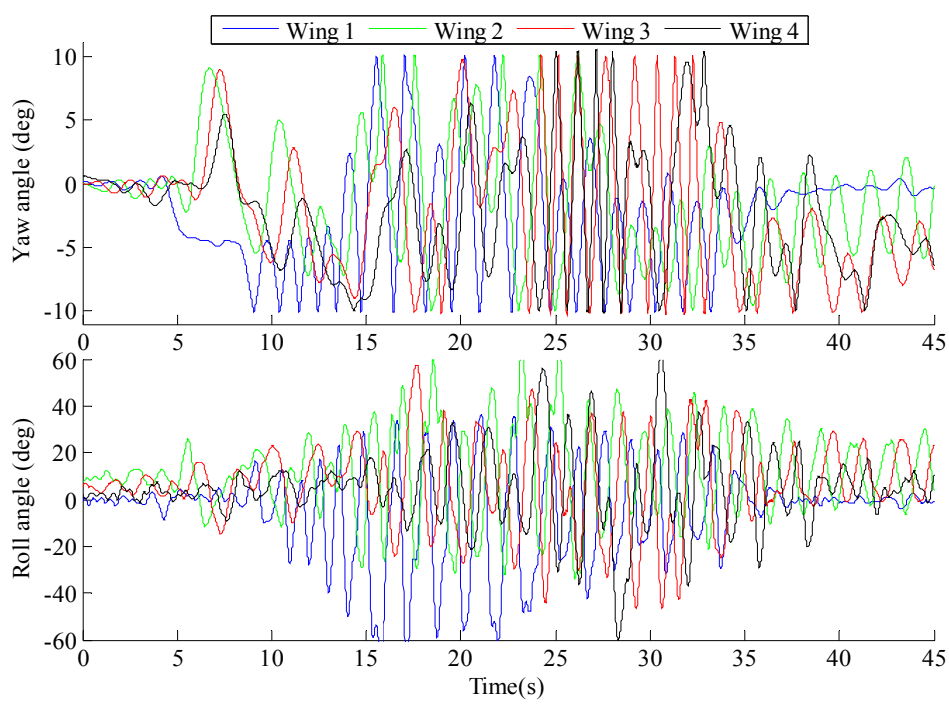

Figure 5-3. Command tracking with existing non-adaptive controllers.

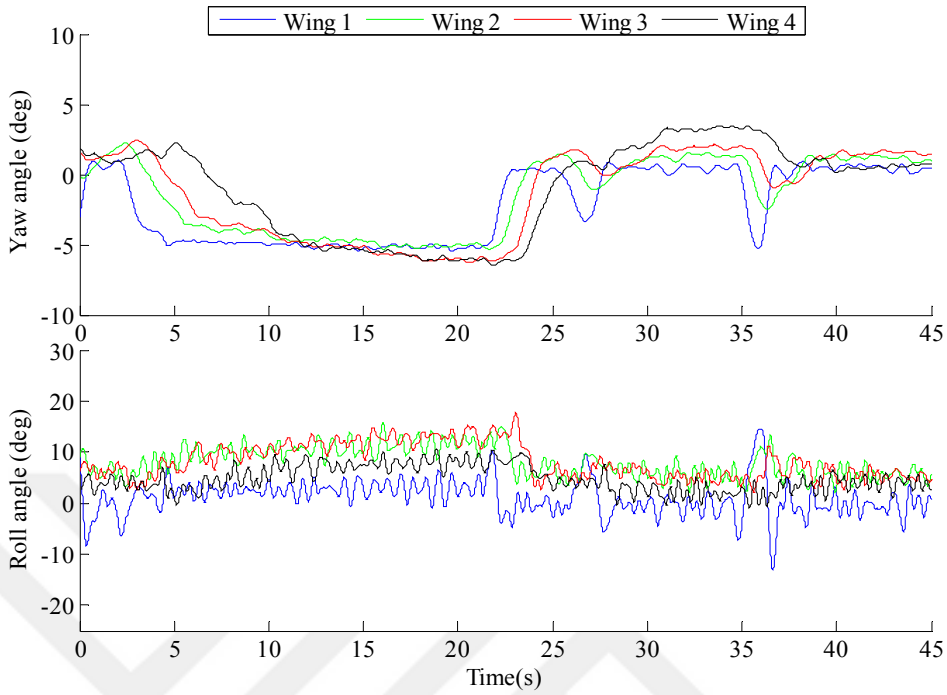

Figure 5-4. Command tracking with the augmenting adaptive controllers.

adaptive controllers are engaged. Command is given around $t = 2\,\mathrm{s}$ and then removed around $t = 22\,\mathrm{s}$. The leading wing follows the command, obeying the dynamics specified by the reference model very closely. Similarly, other wings also follow their upstream wings as commanded by their reference models. We can clearly see the time delay introduced by the chain of reference models, but no signs of spatial instability are observed. When the command is removed, the formation returns back to original configuration smoothly. Yaw position of the first wing exhibits two spikes around $t = 27\,\mathrm{s}$ and $t = 36\,\mathrm{s}$, which were caused by aerodynamic disturbances in the wind tunnel. Adaptive controllers successfully reject these disturbances as well.

5.7 Conclusions

In this chapter we have presented a methodology to augment existing distributed controllers in a large-scale interconnected system with adaptive output feedback controllers in the framework of arbitrary reference model-following control. The method

does not require the existing controller to be designed based on a linear model. A SHL NN is used to approximate the interconnection effects and modeling errors on-line. Boundedness of error signals is shown through Lyapunov's direct method. The method is validated on the Cornell formation flight experiment test-bed. Experiment results show that adaptive controllers can handle interconnection effects, external disturbances, and changes in system dynamics due to changes in the operating point.

CHAPTER 6

FLIGHT CONTROL USING MAFC ACTUATORS

The spinning projectile problem in Chapter 2 demonstrated the potential for using MAFC actuators in a closed loop control system. In order to fully exploit the potential of this flow control technology in dynamic flight control, we also employed MAFC actuators in longitudinal control of a 2-DOF model that consists of a main wing and a tail as depicted in Figure 1-7. Motion of the model is constrained to two degrees of freedom by using a vertical beam that passes through middle of the model. The model slides along the beam and has freedom to pitch and plunge. A conventional elevator is used to trim the model and change its dynamic characteristics. Once the model is trimmed the position feedback loop is opened, and the elevator controller acts like an inner loop control to alter the dynamic characteristics and to introduce disturbances. Once flow control is engaged, position control of the model is achieved by an adaptive outer loop controller that drives the flow actuators located on the tail surface. For controller design we assume full state feedback information is available, consisting of vertical position z, pitch attitude θ, and their derivatives.

The main objective of this chapter is to demonstrate closed loop adaptive flow control under a highly dynamic flight condition. The experimentally obtained response of an MAFC actuator presented in Figure 2-3 represents actuation in a stationary flow condition. Behavior of MAFC actuators in a dynamic flight condition is yet to be investigated. Here we propose a dynamic model that represents possible coupling effects between actuation, the dynamics of flow field, and the rigid body dynamics of the model. An LQR controller is designed for the outer loop to stabilize the nominal plant model and augmented with an adaptive element following the open loop reference model approach

to partially cancel the effects of parameter uncertainties and unmodeled flow actuation characteristics that are coupled with the vehicle dynamics.

6.1 Nomenclature

ρ = Air density

α = Angle of attack

ε = Downwash angle at the tail

γ = Flight path angle

θ = Pitch angle

ε_0 = Downwash angle at the tail at $\alpha = 0$

δ_e = Elevator deflection

δ_{e0} = Trim elevator deflection

δ_f = Active flow control signal

δ_i = Inner loop control elevator deflection

$\eta_s = S_t/S$ = Ratio of tail area to wing area

$\eta_t = (V'/V)^2$ = Tail efficiency factor

$\bar{c}$ = Wing chord length

C_D = Wing drag coefficient

C_{D_α} = Slope of the C_D versus α curve at $\alpha = 0$

$C_{D,t}$ = Tail drag coefficient

C_{D,t_α} = Slope of the $C_{D,t}$ versus α curve at $\alpha = 0$

$C_{D,t_{\delta_e}}$ = Slope of the $C_{D,t}$ versus δ_e curve

$C_{D,t_{\delta_f}}$ = Slope of the $C_{D,t}$ versus δ_f curve

C_{D,t_0} = Zero angle of attack tail drag coefficient

C_L = Wing lift coefficient

C_{L_α} = Slope of the C_L versus α curve at $\alpha = 0$

$C_{L,t}$ = Tail lift coefficient

C_{L,t_α} = Slope of the $C_{L,t}$ versus α curve at $\alpha = 0$

$C_{L,t_{\dot{\alpha}}}$ = Slope of the $C_{L,t}$ versus normalized $\dot{\alpha}$ curve

$C_{L,t_{\delta_e}}$ = Elevator effectiveness (slope of the $C_{L,t}$ versus δ_e curve)

$C_{L,t_{\delta_f}}$ = Active flow control actuator effectiveness (slope of the $C_{L,t}$ versus δ_f curve)

C_{L,t_0} = Zero angle of attack tail lift coefficient

C_{L,t_q} = Slope of the $C_{L,t}$ versus normalized q curve at

C_{L_0} = Zero angle of attack wing lift coefficient

C_{L_0} = Zero angle of attack wing lift coefficient

I = Moment of inertia of the model around P

$l =$ Distance from the tail aerodynamic center to P

$l_g =$ Distance from the model center of gravity to P

$L_t =$ Aerodynamic lift force acting on the tail

$L_w =$ Aerodynamic lift force acting on the wing

$m =$ Mass of the model

$P =$ Point where the model is attached to the support mechanism (assumed to be coincident with the wing aerodynamic center)

$q = \frac{1}{2}\rho V_0^2$ = Dynamic pressure

$S =$ Wing surface area

$S_t =$ Tail surface area

$V = \sqrt{V_0^2 + \dot{z}^2}$ = Air speed experienced by the model

$V' =$ Effective air speed at tail

$V_0 =$ Speed of the wind tunnel

$z =$ Vertical position of the model

6.2 Equations of Motion

A free body diagram of the model is shown in Figure 6-1. The model is constrained by the beam at point P, which is assumed to be at the aerodynamic center of the wing. It is further assumed that the beam can only exert horizontal forces to the model, which cancel the horizontal component of the aerodynamic forces. The dynamics and control problem is very similar to that encountered in conventional longitudinal aircraft control. Plunging and pitching dynamics can be written as

$$\begin{aligned} mg - L_w \cos\gamma - L_t \cos(\gamma - \varepsilon) - D_w \sin\gamma - D_t \sin(\gamma - \varepsilon) &= m\ddot{z} \\ (L_w \cos\gamma + D_w \sin\gamma) l_g \cos\theta - \left[L_t \cos(\gamma - \varepsilon) + D_t \sin(\gamma - \varepsilon) \right] (l - l_g) \cos\theta &= I\ddot{\theta} \end{aligned} \tag{6.1}$$

where ε is the downwash angle of the flow as seen at the tail surface. The flight path angle is given by

$$\gamma = \tan^{-1}\left(\frac{\dot{z}}{V_0}\right) \tag{6.2}$$

6.2.1 Aerodynamic Forces

Pitching and plunging motion are controlled by changing the lift on the tail. To this end, we assume that lift on the tail can be varied by using both a moving elevator surface and flow actuators located on the tail surface. We write lift and drag on wing and tail as

$$
\begin{aligned}
L_w &= qS\left(C_{L_0} + C_{L_\alpha}\alpha\right) \\
D_w &= qS\left(C_{D_0} + C_{D_\alpha}\alpha\right) \\
L_t &= qS\eta_s\eta_t\begin{pmatrix} C_{L,t_0} + C_{L,t_\alpha}\left(\alpha-\varepsilon\right) + C_{L,t_{\dot\alpha}}\left(\dot\alpha-\dot\varepsilon\right)\dfrac{\bar c}{2V_0} \\ +C_{L,t_q}q\dfrac{\bar c}{2V_0} + C_{L,t_{\delta_e}}\delta_e + C_{L,t_{\delta_f}}\delta_f \end{pmatrix} \\
D_t &= qS\eta_s\eta_t\left(C_{D,t_0} + C_{D,t_\alpha}\left(\alpha-\varepsilon\right) + C_{D,t_{\delta_e}}\delta_e + C_{D,t_{\delta_f}}\delta_f\right)
\end{aligned}
\tag{6.3}
$$

where $q = \frac{1}{2}\rho V^2$ is the dynamic pressure, $\eta_s = S_t/S$ and $\eta_t = \left(V'/V\right)^2$ are efficiency factors for tail that account for the velocity and surface area change at the tail, α is angle of attack, V_0 is airspeed, $C_{\cdot}$'s are aerodynamic coefficients, and δ_e and δ_f are elevator and flow actuator control commands. The downwash ε can be closely approximated as a

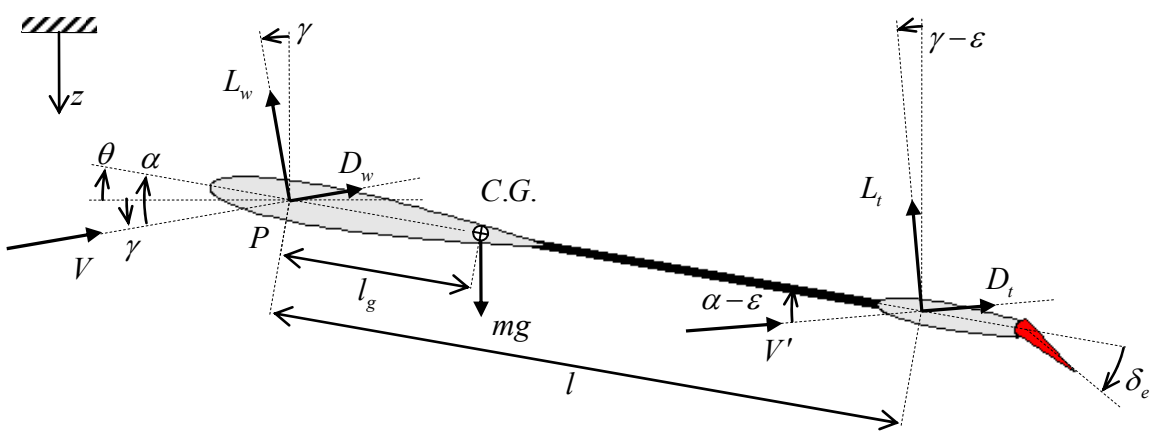

Figure 6-1. Free-body diagram of the 2-DOF wind tunnel model.

linear function of α [69]

$$\varepsilon = \varepsilon_0 + \frac{\partial \varepsilon}{\partial \alpha}\alpha \tag{6.4}$$

Using (6.4) in (6.3), we can express the aerodynamic forces as:

$$\begin{aligned}
L_w &= qS\left(C_{L_0} + C_{L_\alpha}\alpha\right) \\
D_w &= qS\left(C_{D_0} + C_{D_\alpha}\alpha\right) \\
L_t &= qS\eta_s\eta_t\left(\begin{array}{l} C_{L,t_0} - C_{L,t_\alpha}\varepsilon_0 + C_{L,t_\alpha}\left(1-\frac{\partial\varepsilon}{\partial\alpha}\right)\alpha + C_{L,t_{\dot\alpha}}\left(1-\frac{\partial\varepsilon}{\partial\alpha}\right)\dot\alpha\frac{\bar c}{2V_0} \\ +C_{L,t_q}q\frac{\bar c}{2V_0} + C_{L,t_{\delta_e}}\delta_e + C_{L,t_{\delta_f}}\delta_f \end{array}\right) \\
D_t &= qS\eta_s\eta_t\left(C_{D,t_0} - C_{D,t_\alpha}\varepsilon_0 + C_{D,t_\alpha}\left(1-\frac{\partial\varepsilon}{\partial\alpha}\right)\alpha + C_{D,t_{\delta_e}}\delta_e + C_{D,t_{\delta_f}}\delta_f\right)
\end{aligned} \tag{6.5}$$

We redefine the tail aerodynamic coefficients so that the effects of the downwash angle are included:

$$\begin{aligned}
C_{L,t_0} &= C_{L,t_0} - C_{L,t_\alpha}\varepsilon_0 \\
C_{D,t_0} &= C_{D,t_0} - C_{D,t_\alpha}\varepsilon_0 \\
C_{L,t_\alpha} &= C_{L,t_\alpha}\left(1-\frac{\partial\varepsilon}{\partial\alpha}\right) \\
C_{L,t_{\dot\alpha}} &= C_{L,t_{\dot\alpha}}\left(1-\frac{\partial\varepsilon}{\partial\alpha}\right) \\
C_{D,t_\alpha} &= C_{D,t_\alpha}\left(1-\frac{\partial\varepsilon}{\partial\alpha}\right)
\end{aligned} \tag{6.6}$$

then the expressions in (6.5) can be simplified as follows:

$$\begin{aligned}
L_w &= qS\left(C_{L_0} + C_{L_\alpha}\alpha\right) \\
D_w &= qS\left(C_{D_0} + C_{D_\alpha}\alpha\right) \\
L_t &= qS\eta_s\eta_t\left(C_{L,t_0} + C_{L,t_\alpha}\alpha + C_{L,t_{\dot\alpha}}\dot\alpha\frac{\bar c}{2V_0} + C_{L,t_q}q\frac{\bar c}{2V_0} + C_{L,t_{\delta_e}}\delta_e + C_{L,t_{\delta_f}}\delta_f\right) \\
D_t &= qS\eta_s\eta_t\left(C_{D,t_0} + C_{D,t_\alpha}\alpha + C_{D,t_{\delta_e}}\delta_e + C_{D,t_{\delta_f}}\delta_f\right)
\end{aligned} \tag{6.7}$$

6.2.2 Linearization

The equations of motion derived in the previous section are linearized for the inner loop control design using small-disturbance theory. We assume a trim condition with $z = z_0$, $\dot{z}=0$, $\theta=\theta_0$, $\dot{\theta}=0$ and consider the motion as small deviations from this reference steady condition. Since trim conditions for $\dot{z}$, and $\dot{\theta}$ are zero, and the dynamics are independent of z_0, these variables are redefined as representing small perturbations from equilibrium. For pitch angle we will use $\theta=\theta_0+\Delta\theta$ where θ_0 is the equilibrium value and $\Delta\theta$ is a small perturbation. Similarly for vertical position and elevator deflection we will use $z = z_0 + \Delta z$ and $\delta_e = \delta_{e,0} + \Delta\delta_e$. The following approximations will be used for the nonlinear terms:

$$\begin{aligned}
&\alpha \cong \theta_0 + \theta + \frac{\dot{z}}{V_0} && \dot{\alpha} \cong \dot{\theta} + \frac{\ddot{z}}{V_0} \\
&\cos\theta \cong \cos\theta_0 - \theta\sin\theta_0 && \sin\theta \cong \theta\cos\theta_0 + \sin\theta_0 \\
&q \cong \frac{1}{2}\rho\left(V_0+\dot{z}\right)^2 = \frac{1}{2}\rho V_0^2 && \sin\gamma \cong \frac{\dot{z}}{V_0} \qquad \cos\gamma \cong 1
\end{aligned} \tag{6.8}$$

For simplicity we further assume $C_{L,t_{\dot{\alpha}}}=0$ for the linear model. Flow actuation effectiveness coefficients $C_{L,t_{\delta_f}}$ and $C_{D,t_{\delta_f}}$ will be treated as constants for linearization. For simulation purposes, a nonlinear static model is developed in Section 6.4.2. These approximations and the assumption that products of small perturbations are zero lead to the following linearization of (6.1)

$$\begin{aligned}
&m\ddot{z} = mg - \left(L_w + L_t\right) - \left(D_w + D_t\right)\frac{\dot{z}}{V_0} \\
&I\ddot{\theta} = L_w l_g \cos\theta_0 - L_w l_g \sin\theta_0 \Delta\theta + \frac{D_w}{V_0}\cos\theta_0 l_g \dot{z} - L_t\left(l - l_g\right)\cos\theta_0 + \\
&\quad L_t\left(l - l_g\right)\sin\theta_0\Delta\theta - \frac{D_t}{V_0}\left(l - l_g\right)\cos\theta_0\dot{z}
\end{aligned} \tag{6.9}$$

We assume that elevator command contains a bias term to trim the model at the equilibrium point with all the perturbations at zero. The equilibrium pitch angle θ_0 needed to balance the model for a given mass and tunnel speed and the elevator trim command δ_{e0} to hold the pitch attitude at that level can be found from simultaneous solution of equations (6.9) after equating all the perturbations to zero:

$$\begin{aligned} &\frac{mg}{qS}-\left(C_{L_0}+\eta_s\eta_t C_{L,t_0}\right)=\left(C_{L_\alpha}+\eta_s\eta_t C_{L,t_\alpha}\right)\theta_0+\eta_s\eta_t C_{L,t_{\delta_e}}\delta_{e0} \\ &-C_{L_0}l_g+\eta_s\eta_t C_{L,t_0}\left(l-l_g\right)=\left[C_{L_\alpha}l_g-\eta_s\eta_t C_{L,t_\alpha}\left(l-l_g\right)\right]\theta_0-\eta_s\eta_t C_{L,t_{\delta_e}}\left(l-l_g\right)\delta_{e0} \end{aligned} \tag{6.10}$$

Since these equations and the values of the parameters are approximate, trim values for an actual experiment setup would be obtained by a closed loop controller as discussed in Section 6.3.1.

Finally, defining the states as $x_1=\Delta z$, $x_2=\dot{z}$, $x_3=\Delta\theta$, and $x_4=\dot{\theta}$, inserting the aerodynamic forces in (6.7) and removing the trim values in (6.10), and ignoring the products of perturbations we obtain the linear system model as

$$\begin{bmatrix}\dot{x}_1\\ \dot{x}_2\\ \dot{x}_3\\ \dot{x}_4\end{bmatrix}=\begin{bmatrix}0 & 1 & 0 & 0\\ 0 & a_{2,2} & a_{2,3} & a_{2,4}\\ 0 & 0 & 0 & 1\\ 0 & a_{4,2} & a_{4,3} & a_{4,4}\end{bmatrix}\begin{bmatrix}x_1\\ x_2\\ x_3\\ x_4\end{bmatrix}+\begin{bmatrix}0\\ b_{e,2}\\ 0\\ b_{e,4}\end{bmatrix}\delta_e+\begin{bmatrix}0\\ b_{f,2}\\ 0\\ b_{f,4}\end{bmatrix}\delta_f \tag{6.11}$$

with

$$a_{2,2}=-\frac{qS}{V_0 m}\left(C_{L_\alpha}+C_{D_0}+C_{D_\alpha}\theta_0+\eta\left(C_{L,t_\alpha}+C_{D,t_0}+C_{D,t_\alpha}\theta_0+C_{D,t_{\delta_e}}\delta_{e0}\right)\right)$$

$$a_{2,3}=-\frac{qS}{m}\left(C_{L_\alpha}+\eta C_{L,t_\alpha}\right)$$

$$a_{2,4}=-\frac{qS}{2V_0 m}\eta\bar{c}\left(C_{L,t_{\dot{\alpha}}}+C_{L,t_q}\right)$$

$$a_{4,2} = \frac{qS}{V_0 I}\begin{bmatrix} \left(C_{L_\alpha} + C_{D_0} + C_{D_\alpha}\theta_0\right) l_g \\ -\eta\left(C_{L,t_\alpha} + C_{D,t_0} + C_{D,t_\alpha}\theta_0 + C_{D,t_{\delta_e}}\delta_{e0}\right)\left(l - l_g\right) \end{bmatrix}\cos\theta_0$$

$$a_{4,3} = \frac{qS}{I}\left[\eta\left(C_{L,t_0} + C_{L,t_\alpha}\theta_0 + C_{L,t_{\delta_e}}\delta_{e0}\right)\left(l - l_g\right) - l_g\left(C_{L_0} + C_{L_\alpha}\theta_0\right)\right]\sin\theta_0$$
$$+\left[C_{L_\alpha} l_g - \eta C_{L,t_\alpha}\left(l - l_g\right)\right]\cos\theta_0$$

$$a_{4,4} = -\frac{qS}{2V_0 I}\eta\bar{c}\left(C_{L,t_{\dot{\alpha}}} + C_{L,t_q}\right)\left(l - l_g\right)\cos\theta_0$$

$$b_{e,2} = -\frac{qS}{m}\eta C_{L,t_{\delta_e}}$$

$$b_{e,4} = -\frac{qS}{I}\eta C_{L,t_{\delta_e}}\left(l - l_g\right)\cos\theta_0$$

$$b_{f,2} = -\frac{qS}{m}\eta C_{L,t_{\delta_t}}$$

$$b_{f,4} = -\frac{qS}{I}\eta C_{L,t_{\delta_e}}\left(l - l_g\right)\cos\theta_0$$

We will write the linear system model in the following compact form for controller design:

$$\dot{\boldsymbol{x}} = A\boldsymbol{x} + \boldsymbol{b}_e\delta_e + \boldsymbol{b}_f\delta_f \tag{6.12}$$

6.3 Controller Design

There are two control signals, one for the elevator and one for the MAFC actuators. The elevator command includes two components:

$$\delta_e = \delta_{e0} + \delta_i \tag{6.13}$$

where δ_{e0} is the trim command. We refer to this as the inner loop component because in normal operation (when the flow control devices are activated) the elevator control has its position feedback loop open. The flow controller forms the outer loop portion of the controller, which we denote as δ_f. First, only the trim controller will be active, which is

basically an LQR controller augmented by an integrator. When the model reaches the trim condition, the integrator state of this controller will be frozen to form the δ_{e0} term in (6.13). At the same time the position feedback loops are opened, and the LQR controller that remains is the δ_i term in (6.13). Shortly afterwards the outer loop controller will be engaged, which will be designed as a linear compensator augmented with an integrator and an adaptive element following the open loop reference model-following architecture. Opening the position feedbacks of the inner loop controller will ensure that the model position will be completely regulated by the adaptive outer loop controller using the active flow actuators. For controller design we assume full state feedback information is available, consisting of vertical position, pitch attitude, and their derivatives.

6.3.1 Trim Controller Design

Finding the trim condition and the required elevator trim deflection requires integral action on the vertical position. To incorporate integrator design into the LQR design, we augment the linear model (6.12) with an auxiliary state x_i as the integral of x_1 as

$$\dot{\bar{\boldsymbol{x}}} = \begin{bmatrix} \dot{\boldsymbol{x}} \\ \dot{x}_i \end{bmatrix} = \begin{bmatrix} A & 0 \\ \boldsymbol{c}_1 & 0 \end{bmatrix} \bar{\boldsymbol{x}} + \begin{bmatrix} \boldsymbol{b}_e \\ 0 \end{bmatrix} \delta_e + \begin{bmatrix} \boldsymbol{b}_f \\ 0 \end{bmatrix} \delta_f \tag{6.14}$$

where $\boldsymbol{c}_1 = \begin{bmatrix} 1 & 0 & 0 & 0 \end{bmatrix}$. LQR controller design based on the above augmented model returns the gain matrix $K_t = \begin{bmatrix} k_{i,1} & k_{i,2} & k_{i,3} & k_{i,4} & k_{i,5} \end{bmatrix}$ where $k_{i,1}$ through $k_{i,4}$ are gains on states x_1 through x_4 respectively, and $k_{i,5}$ is the gain for the integral of vertical position. Trim controller in transient is $\delta_{e0} = -K_t \bar{\boldsymbol{x}}$. When steady state is reached, δ_{e0} will be frozen and remain constant throughout the experiment.

6.3.2 Inner Loop Controller Design

The inner loop controller is the LQR controller designed for trim with integrator and position feedbacks removed:

$$\delta_i = -K_i \boldsymbol{x} \tag{6.15}$$

where $K_i = \begin{bmatrix} 0 & k_{i,2} & 0 & k_{i,4} \end{bmatrix}$. Closing the inner loop leads to the linear system

$$\dot{\boldsymbol{x}}_m = A_m \boldsymbol{x}_m + \boldsymbol{b}_f \delta_f \tag{6.16}$$

with $A_m = A - \boldsymbol{b}_e K_i$ and $\boldsymbol{x}_m$ indicating the state vector of the linear model with inner loop closed, which will be used as the plant model for the outer loop controller design.

6.3.3 Outer Loop Controller Design

The outer loop controller will be composed of a linear controller augmented with an adaptive NN in the open loop reference model-following control framework. The linear part will be an LQR controller augmented by an integrator, similar to the trim controller in transient. To compensate for the modelling errors, unmodeled dynamics, and nonlinearities of the flow actuators, an adaptive NN will be introduced as in (3.19) as

$$\delta_f = \delta_{ec} - \delta_{NN} \tag{6.17}$$

To this end, we introduce a state transformation $\xi_m = Tx_m$ to transform the plant model into normal form as

$$\begin{aligned} \dot{\boldsymbol{\xi}}_m &= A_n \boldsymbol{\xi}_m + \boldsymbol{b}_n \delta_f \\ \boldsymbol{\xi}_m &= T\boldsymbol{x}_m \end{aligned} \tag{6.18}$$

where $A_n = TA_mT^{-1}$ and $\boldsymbol{b}_n = T\boldsymbol{b}_f$. Note that the above model in normal form can also be written in the same form as the plant model in (3.4) as

$$
\begin{aligned}
\dot{\boldsymbol{z}}_l &= F_0 \boldsymbol{z}_l + \boldsymbol{g}_0 \boldsymbol{x}_{l_1} \\
\dot{x}_{l_1} &= x_{l_2} \\
&\vdots \\
\dot{x}_{l_r} &= \boldsymbol{h}_0^T \boldsymbol{z}_l + a_1 x_{l_1} + \ldots + a_r x_{l_r} + b\delta_f \\
y_l &= x_{l_1}
\end{aligned}
\tag{6.19}
$$

with $\boldsymbol{\xi}_m = \begin{bmatrix} \boldsymbol{z}_l & \boldsymbol{x}_l \end{bmatrix}^T = \begin{bmatrix} \boldsymbol{z}_l & \begin{bmatrix} x_{l_1} & \cdots & x_{l_r} \end{bmatrix} \end{bmatrix}^T$, where $\boldsymbol{z}_l$ represents the states of the internal dynamics and $\boldsymbol{x}_l$ represents the feedback linearized states. Note that the conventional longitudinal control of an airplane from tail is inherently a non-minimum phase system, which means that the matrix F_0 in (6.19) is not Hurwitz. As discussed in [19] and Chapter 3, non-minimum phase internal dynamics that are modeled with sufficient accuracy and accounted for in the linear controller design are allowed in this adaptive output feedback architecture.

6.3.3.1 <u>Linear compensator design for the outer loop</u>

The linear compensator for the outer loop is designed in the same way as the trim controller discussed previously. We first augment the model in (6.18) with an auxiliary state for the integral of the vertical position as

$$
\dot{\bar{\xi}}_m = \begin{bmatrix} A_n & 0 \\ c_1 & 0 \end{bmatrix} \bar{\xi}_m + \begin{bmatrix} b_n \\ 0 \end{bmatrix} \delta_f \tag{6.20}
$$

We obtain the full state feedback gain $K_o = \begin{bmatrix} k_{o,1} & k_{o,2} & k_{o,3} & k_{o,4} & k_{o,5} \end{bmatrix}$ from the LQR design. This time we leave all the feedbacks closed, including the integral term:

$$
\delta_{ec} = -K_o \bar{\xi}_m \tag{6.21}
$$

6.3.3.2 <u>Adaptive NN design for the outer loop</u>

Following Section 3.3.4, a SHL NN is introduced as

$$
\delta_{NN} = \hat{M}^T \boldsymbol{\sigma}\left(\hat{N}^T \boldsymbol{\eta}\right) \tag{6.22}
$$

where the adaptive gain matrices $\hat{M}$ and $\hat{N}$ are updated according (3.27) with the estimate of the tracking error vector $\hat{\boldsymbol{E}}$ replaced with the tracking error itself. The controller architecture is depicted in Figure 6-2.

6.4 Actuator and Sensor Modeling

Realistic models of both the elevator and active flow control actuator are required to evaluate the adaptive controllers in simulation. In the following we describe the models used.

6.4.1 Elevator model

Based on off-the-shelf servo specifications, elevator is modelled as a first order system with

$$G_e(s) = \frac{\delta_e(s)}{\delta_{e,com.}(s)} = \frac{15}{s+15}$$

where $\delta_{e,com.}(s)$ is the commanded deflection. Also magnitude of the elevator deflection

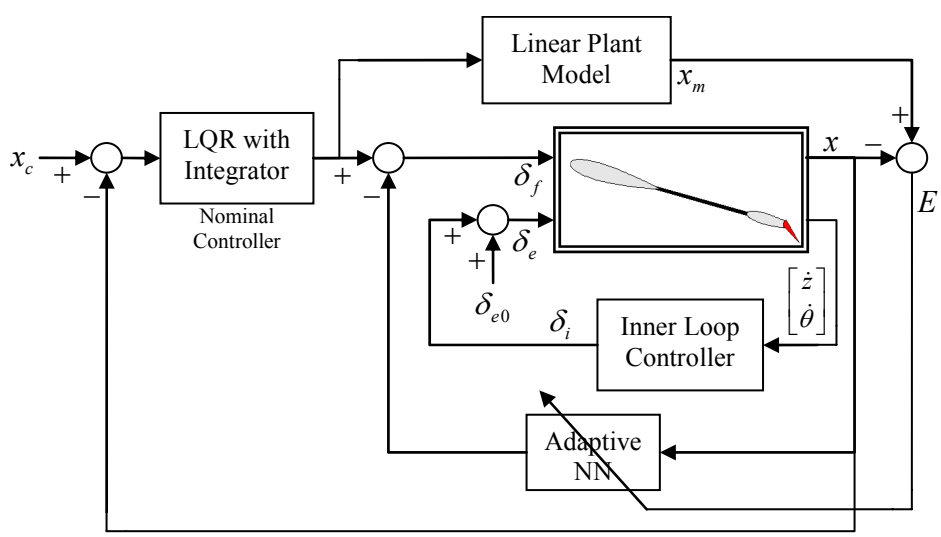

Figure 6-2. Controller architecture for closed loop flight control using MAFC actuators

is limited to be less than 45 deg.

6.4.2 MAFC Actuator Model

To simulate the flow control actuators, we refer to the experimentally obtained response of an MAFC actuator shown in Figure 2-3. The incremental change in circulation (with respect to the baseline flow) about a stalled 2-D airfoil is shown in Figure 2-3 (a). An adverse change in circulation is observed immediately following the start of the actuation, similar to the response of a non-minimum phase system to a step input. To model this transient behavior, a non-minimum phase transfer function is introduced

$$G_f(s) = \frac{\delta_f(s)}{\delta_{f,com.}(s)} = \frac{-100(s-100)}{(s+100)^2}$$

where $\delta_{f,com.}(s)$ is the commanded actuation. Response of the above model to a step input is shown in Figure 6-3.

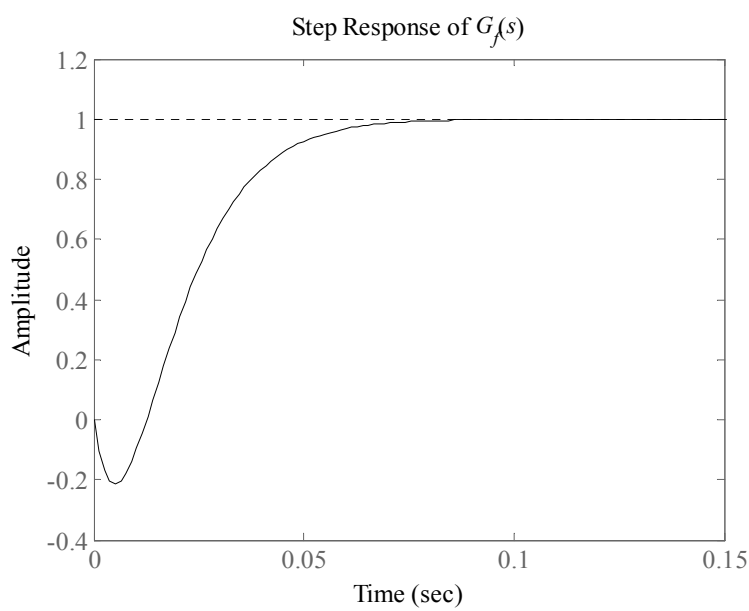

Figure 6-3. Step response of $G_f(s)$.

The response in Figure 2-3 (a) represents actuation in a stationary flow condition. Behavior of active flow actuators in a dynamic flight condition is yet to be investigated. In an attempt to represent possible coupling effects between actuation, the dynamics of flow field, and the rigid body dynamics of the model we propose the following model for the flow actuator effectiveness coefficient $C_{L,t_{\delta_f}}$:

$$C_{L,t_{\delta_f}} = C_{L,t_{\delta_{f0}}} + C_{L,t_{\delta_{f\alpha}}}\alpha + C_{L,t_{\delta_{f\alpha^2}}}\alpha^2 + C_{L,t_{\delta_{f\dot{\alpha}}}}\dot{\alpha} + C_{L,t_{\delta_{f\theta}}}\theta + C_{L,t_{\delta_{f\dot{\theta}}}}\dot{\theta} \tag{6.23}$$

For the simulation results presented below, each of these parameters has been selected to have an adverse effect on the closed loop response. That is, for each of the coefficients in (6.23), simulations have been made with both positive and negative values with reasonable magnitudes and the one with the adverse effect on the closed response has been selected. This selection therefore represents a hypothetical worst case situation.

6.4.3 Sensor Model

Vertical position and pitch attitude are measured with optical encoders. The angular encoder is modeled as having 12 bit resolution (2^{12} = 4096 count), which corresponds to 0.088 deg resolution. The linear encoder for the vertical position is modeled as having 0.1 mm resolution. It is assumed that angular velocity is directly measured using a rate sensor and that vertical velocity is obtained by differentiating the output of the linear encoder.

6.5 Simulation Results

We present simulation results with two different inner loop controller designs, comparing the responses with and without adaptation for each case. Linear controller designs for the inner and outer loops ignore the actuator models. In addition, we introduce uncertainties to aerodynamic parameters as summarized in Table 6-1.

Table 6-1. Aerodynamic parameters.

Linear Model				True Plant		
ε_0	=	0		ε_0	=	-0.05
$\frac{\partial \varepsilon}{\partial \alpha}$	=	0.05 rad^{-1}		$\frac{\partial \varepsilon}{\partial \alpha}$	=	0.05 rad^{-1}
η_s	=	0.42		η_s	=	0.42
η_t	=	1		η_t	=	0.75
$\bar{c}$	=	0.4 m		$\bar{c}$	=	0.4 m
C_{D_α}	=	4.27 rad^{-1}		C_{D_α}	=	6.41 rad^{-1}
C_{D,t_α}	=	4.06 rad^{-1}		C_{D,t_α}	=	6.08 rad^{-1}
$C_{D,t_{\delta_e}}$	=	0.03 rad^{-1}		$C_{D,t_{\delta_e}}$	=	0.05 rad^{-1}
C_{D,t_0}	=	0.1		C_{D,t_0}	=	0.15
C_{L_0}	=	0		C_{L_0}	=	0
C_{L_α}	=	5.73 rad^{-1}		C_{L_α}	=	4.30 rad^{-1}
C_{L,t_α}	=	5.44 rad^{-1}		C_{L,t_α}	=	4.08 rad^{-1}
$C_{L,t_{\dot{\alpha}}}$	=	0		$C_{L,t_{\dot{\alpha}}}$	=	-5 rad^{-1}
$C_{L,t_{\delta_e}}$	=	1 rad^{-1}		$C_{L,t_{\delta_e}}$	=	0.75 rad^{-1}
C_{L,t_0}	=	0		C_{L,t_0}	=	0
C_{L,t_q}	=	8.5 rad^{-1}		C_{L,t_q}	=	6.38 rad^{-1}
I	=	0.1 kg.m^2		I	=	0.15 kg.m^2
l	=	0.75 m		l	=	0.56 m
l_g	=	0.1 m		l_g	=	0.13 m
m	=	1 kg		m	=	0.75 kg
V_0	=	10 m/s		V_0	=	10 m/s

Uncertainties in these variables have been selected in a way similar to that used in selection of the flow actuator model parameters to represent a hypothetical worst case.

6.5.1 High Damping Inner Loop Design

First the inner loop controller is designed to make the model have satisfactory damping. The intended pole locations and the actual pole locations, which are different due to the uncertainties introduced in Table 6-1, are given in Table 6-2. We see that the uncertainties have a significant effect on the closed loop dynamics. Simulation results without adaptation in the outer loop are shown in Figure 6-4 (a). The flow control

Table 6-2. Inner loop and outer loop linear controller designs.

	Intended inner loop poles, $\hat{\lambda}(A_m)$	Actual inner loop poles, $\lambda(A_m)$	Intended outer loop poles $\hat{\lambda}(\bar{A})$	Actual outer loop poles $\lambda(\bar{A})$
High damping model	0 -5.20 -7.41 -58.75	0 $-4.04+4.55i$ $-4.04-4.55i$ -13.89	-1.07 -1.85 $-7.41+3.01i$ $-7.41-3.01i$ -65.01	-1.12 -1.50 $-4.29+9.89i$ $-4.29-9.89i$ -13.03
Low damping model	0 $-6.29+10.02i$ $-6.29-10.02i$ -52.81	0 $-1.31+10.78i$ $-1.31-10.78i$ -14.26	$-0.89+0.45i$ $-0.89-0.45i$ $-7.39+9.24i$ $-7.39-9.24i$ -59.30	$-1.07+0.19i$ $-1.07-0.19i$ $-1.98+12.22i$ $-1.98-12.22i$ -13.86

actuator causes the highly oscillatory response observed. Results for this case with adaptation are presented in Figure 6-4 (b). Adaptation successfully removes the oscillations.

6.5.2 Low Damping Inner Loop Design

Gains on the velocity feedbacks for the inner loop controller are modified manually to lower the damping of the model. Intended and actual pole locations are shown in Table 6-2. Results without adaptation are in Figure 6-5 (a). The system quickly goes unstable when a vertical position command is given. With adaptation, system remains stable as seen in Figure 6-5 (b). The response is very similar to the case with high damping, which shows that adaptation can handle significant changes in system dynamics.

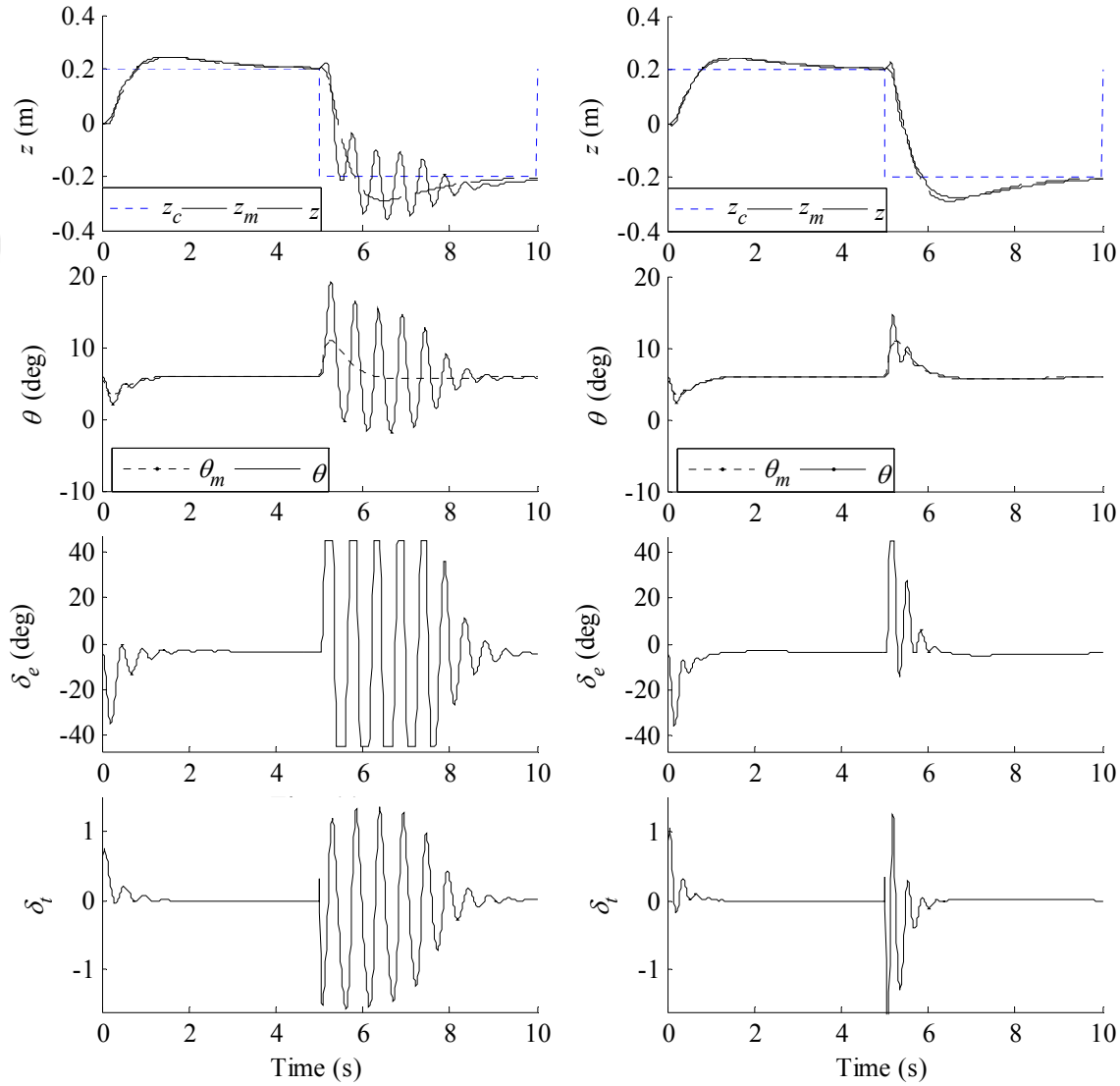

(a) Without adaptation (b) With adaptation

Figure 6-4. Simulation results with high damping model.

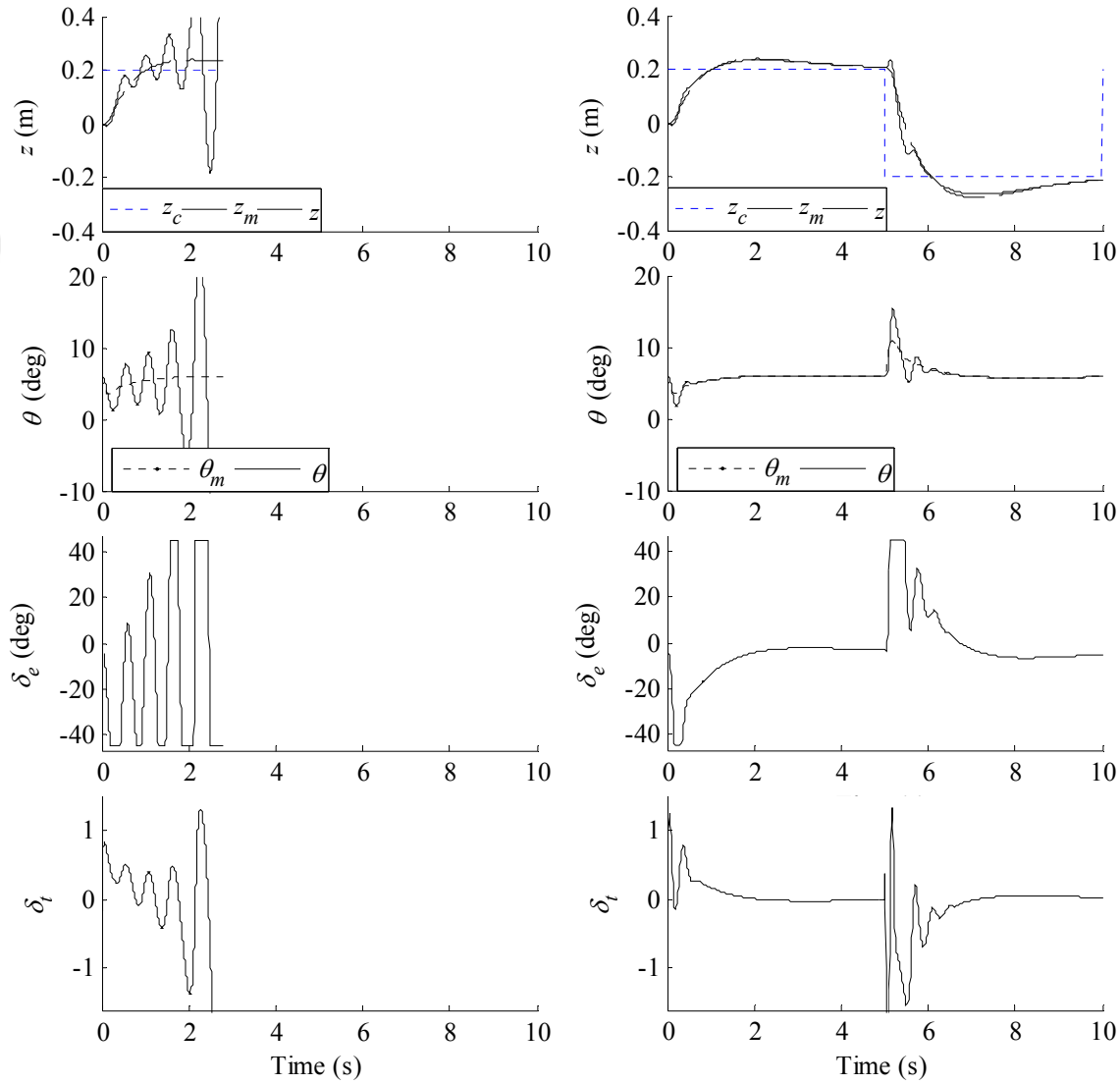

(a) Without adaptation (b) With adaptation

Figure 6-5. Simulation results with low damping model.

CHAPTER 7

ADAPTIVE OUTPUT FEEDBACK CONTROL WITH REDUCED SENSITIVITY TO SENSOR NOISE

In this chapter we address the noise sensitivity issue of the error observer based adaptive output feedback control approach of Ref. [13]. In [13], an adaptive output feedback controller has been developed based on feedback linearization in which both the dynamics and dimension of the regulated system may be unknown, and only the relative degree r of the regulated output is assumed to be known. A linear output feedback controller is used to stabilize the feedback linearized system and a SHL NN is employed to partially cancel the inversion error. For the adaptive laws, a linear observer is proposed to estimate the states of the error dynamics, which include tracking error and its time derivatives up to $r - 1$ and the dynamic compensator states. It has been observed experimentally that the resulting adaptive control architecture is sensitive to sensor noise.

Keeping the same adaptive scheme of [13], a specific reduced order error observer is proposed that eliminates the redundancy in estimating the already available compensator states. Lyapunov-like stability analysis similar to that of [13] is presented showing ultimate boundedness of all the error signals in the system. We present numerical and experimental evidence that the proposed modification significantly reduces the effect of sensor noise in the adaptive process.

7.1 Problem Formulation

Let the dynamics of an *observable* and *stabilizable* nonlinear single-input-single-output (SISO) system be given by the following equations:

$$\begin{aligned} \dot{\boldsymbol{x}} &= \boldsymbol{f}(\boldsymbol{x}, u) \\ y &= g(\boldsymbol{x}), \end{aligned} \tag{7.1}$$

where $\boldsymbol{x} \in \Omega \subset \mathbb{R}^n$ is the state of the system, $u, y \in \mathbb{R}$ are the system input (control) and output (measurement) signals, respectively, and $\boldsymbol{f}(\cdot,\cdot)$, $g(\cdot)$ are sufficiently smooth partially known functions. Moreover, n need not be known.

Assumption 7.1. The dynamical system in (7.1) satisfies the conditions for output feedback linearization with known relative degree r.

Assumption 7.1 allows us to represent the system dynamics in (7.1) in normal form [8]

$$\begin{aligned} \boldsymbol{\chi} &= \boldsymbol{f}_0(\boldsymbol{x}, \boldsymbol{\chi}) \\ \dot{\xi}_i &= \xi_{i+1}, \qquad i = 1, \ldots r-1 \\ \dot{\xi}_r &= h(\boldsymbol{\xi}, \boldsymbol{\chi}, u), \\ y &= \xi_1 \end{aligned} \tag{7.2}$$

where $\boldsymbol{\xi} = \begin{bmatrix} \xi_1 & \ldots & \xi_r \end{bmatrix}^T$, $\boldsymbol{\chi}$ represent the states associated with the internal dynamics and $\boldsymbol{f}_0$ is Lipschitz continuous in its arguments.

Assumption 7.2. The system (7.2) is minimum phase, i.e. the internal dynamics $\dot{\boldsymbol{\chi}} = \boldsymbol{f}_0(\boldsymbol{\xi}, \boldsymbol{\chi})$ while setting $\boldsymbol{\xi} = 0$ are asymptotically stable.

The objective is to synthesize a feedback control law u that utilizes the available measurement y, so that $y(t)$ tracks a smooth *bounded* reference trajectory $y_c(t)$ with bounded error.

7.2 Controller Architecture

Following Ref. [13], a linearizing feedback control law is approximated by introducing the following signal

$$u = \hat{h}^{-1}(y, \nu), \tag{7.3}$$

where

$$\nu = \hat{h}(y,u) \tag{7.4}$$

is commonly referred to as pseudo-control. The function $\hat{h}(y,u)$ represents any available approximation of $h(\xi,\chi,u)$ that is invertible with respect to its second argument. It may be constructed from approximate linear models. Additional requirements on $\hat{h}(y,u)$ will be specified in Assumption 7.3. For now it is enough to assume its invertibility. With this definition of pseudo control the output dynamics can be expressed as:

$$y^{(r)} = \nu + \Delta, \tag{7.5}$$

where

$$\Delta(\boldsymbol{x},u) = h\left(\xi,\chi,\hat{h}^{-1}(y,\nu)\right) - \hat{h}\left(y,\hat{h}^{-1}(y,\nu)\right) \tag{7.6}$$

is the difference between the possibly unknown function $h(\xi,\chi,u)$ and its approximation $\hat{h}(y,u)$ which we refer to as modeling error. The pseudo control is chosen to have the form:

$$\nu = y_c^{(r)} + \nu_{dc} - \nu_{ad}, \tag{7.7}$$

where $y_c^{(r)}$ is the r-th derivative of the input signal, generated using an r-th (or higher) order stable command filter forced by an external command input, ν_{dc} is the output of a linear output feedback dynamic compensator, and ν_{ad} is the adaptive control signal designed to approximately cancel Δ. With (7.7), the output dynamics in (7.5) becomes

$$y^{(r)} = y_c^{(r)} + \nu_{dc} - \nu_{ad} + \Delta. \tag{7.8}$$

From (7.6), notice that Δ depends on ν_{ad} through ν, whereas ν_{ad} has to be designed to cancel Δ. Therefore the following assumption is introduced to guarantee existence and uniqueness of a solution for ν_{ad}.

Assumption 7.3. The mapping $\nu_{ad} \mapsto \Delta$ is a contraction over the entire input domain of interest.

A contraction is defined by the condition $\left|\partial\Delta/\partial\nu_{ad}\right| < 1$. Using (7.6), this implies:

$$\left|\frac{\partial\Delta}{\partial\nu_{ad}}\right| = \left|\frac{\partial h/\partial u}{\partial\hat{h}/\partial u} - 1\right| < 1, \tag{7.9}$$

which can equivalently be stated as two conditions:

$$\operatorname{sgn}\left(\partial h/\partial u\right) = \operatorname{sgn}\left(\partial\hat{h}/\partial u\right), \tag{7.10}$$

$$\left|\partial\hat{h}/\partial u\right| > \left|\partial h/\partial u\right|/2 > 0. \tag{7.11}$$

The first condition states that unmodeled control reversal is not permissible. The second condition places a lower bound on our estimate of the control effectiveness in (7.3).

We assume that output measurements are corrupted by noise and denote the noisy measurements as

$$y_m = y - w. \tag{7.12}$$

where the measurement error w is subject to the bound

$$\left|w(t)\right| \le w_0,\ w_0 > 0. \tag{7.13}$$

Defining the output tracking error $\tilde{y} = y_c - y$, the dynamics in (7.8) can be written as

$$\tilde{y}^{(r)} = -\nu_{dc} + \nu_{ad} - \Delta. \tag{7.14}$$

For the case $\Delta = 0$, the adaptive term ν_{ad} in (7.7) is not required, and the error dynamics in (7.14) reduce to

$$\tilde{y}^{(r)} = -\nu_{dc}\,. \tag{7.15}$$

The following linear compensator is introduced to stabilize the dynamics in (7.15):

$$\begin{aligned} \dot{\boldsymbol{x}}_c &= A_c \boldsymbol{x}_c + \boldsymbol{b}_c \tilde{y}_m \\ \nu_{dc} &= \boldsymbol{c}_c \boldsymbol{x}_c + d_c \tilde{y}_m \end{aligned} \tag{7.16}$$

Where $\boldsymbol{x}_c \in \mathbb{R}^{n_c}$ and $\tilde{y}_m = y_c - y_m$ is the measured error signal. Using (7.12), the compensator dynamics in (7.16) can be rewritten:

$$\begin{aligned} \dot{\boldsymbol{x}}_c &= A_c \boldsymbol{x}_c + \boldsymbol{b}_c \tilde{y} + \boldsymbol{b}_c w \\ \nu_{dc} &= \boldsymbol{c}_c \boldsymbol{x}_c + d_c \tilde{y} + d_c w \end{aligned} \tag{7.17}$$

The error vector $\mathbf{e} \triangleq \begin{bmatrix} \tilde{y} & \dot{\tilde{y}} & \cdots & \tilde{y}^{(r-1)} \end{bmatrix}^T$ together with the compensator state $\boldsymbol{x}_c$ will obey the following dynamics, hereafter (with a slight abuse of language) referred to as the error dynamics:

$$\begin{aligned} \begin{bmatrix} \dot{\mathbf{e}} \\ \dot{\boldsymbol{x}}_c \end{bmatrix} &= \underbrace{\begin{bmatrix} A - d_c \mathbf{b}\mathbf{c} & -\mathbf{b}\boldsymbol{c}_c \\ \boldsymbol{b}_c \mathbf{c} & A_c \end{bmatrix}}_{\bar{A}} \begin{bmatrix} \mathbf{e} \\ \boldsymbol{x}_c \end{bmatrix} + \underbrace{\begin{bmatrix} \mathbf{b} \\ 0 \end{bmatrix}}_{\bar{\mathbf{b}}} \left[\nu_{ad} - \Delta \right] + \underbrace{\begin{bmatrix} -\mathbf{b} d_c \\ \boldsymbol{b}_c \end{bmatrix}}_{G} w \\ \boldsymbol{z} &= \begin{bmatrix} \tilde{y}_m \\ \boldsymbol{x}_c \end{bmatrix} = \underbrace{\begin{bmatrix} \mathbf{c} & 0 \\ 0 & I \end{bmatrix}}_{\bar{C}} \begin{bmatrix} \mathbf{e} \\ \boldsymbol{x}_c \end{bmatrix} + \underbrace{\begin{bmatrix} 1 \\ 0 \end{bmatrix}}_{H} w \end{aligned} \tag{7.18}$$

where

$$A = \begin{bmatrix} 0 & 1 & \cdots & 0 \\ \vdots & \vdots & \ddots & \vdots \\ 0 & 0 & \cdots & 1 \\ 0 & 0 & \cdots & 0 \end{bmatrix}, \qquad \mathbf{b} = \begin{bmatrix} 0 \\ \vdots \\ 0 \\ 1 \end{bmatrix}, \qquad \mathbf{c} = \begin{bmatrix} 1 & 0 & \cdots & 0 \end{bmatrix},$$

and $\boldsymbol{z}$ is the vector of available measurements. We can write the dynamics in (7.18) in compact from as

$$\begin{aligned} \dot{\boldsymbol{E}} &= \bar{A}\boldsymbol{E} + \bar{\mathbf{b}}\left[\nu_{ad} - \Delta \right] + Gw \\ \boldsymbol{z} &= \bar{C}\boldsymbol{E} + Hw \end{aligned} \tag{7.19}$$

where

$$\boldsymbol{E} \triangleq \begin{bmatrix} \mathbf{e}^T & \boldsymbol{x}_c^T \end{bmatrix}^T \tag{7.20}$$

is the new error vector. Note that $A_c, \boldsymbol{b}_c, \boldsymbol{c}_c, d_c$ in (7.17) should be designed such that $\bar{A}$ is Hurwitz. A linear observer for the dynamics in (7.19) is introduced in [13] as

$$\begin{aligned} \dot{\hat{\boldsymbol{E}}} &= \bar{A}\hat{\boldsymbol{E}} + K\left(z - \hat{z}\right) \\ \hat{z} &= \bar{C}\hat{\boldsymbol{E}}, \end{aligned} \tag{7.21}$$

where $\bar{A} - K\bar{C}$ is designed to be Hurwitz with dynamics faster than the dynamics of $\bar{A}$. The observer in (7.21) will be referred to as the full order observer hereafter.

7.3 Reduced Order Observer Design

When the output measurements contain sensor noise as in (7.12), the sensor noise w propagates through the linear compensator and the error observer. Improved overall performance requires faster observer dynamics. This leads to an amplification of the effect of the sensor noise, which is particularly a problem in an adaptive design since sensor noise is interpreted as modeling error. In this section we propose a reduced order observer that estimates only the **e** portion of $\boldsymbol{E}$. Since the compensator state vector $\boldsymbol{x}_c$ is known, **e** dynamics can be written from (7.18) treating $\boldsymbol{x}_c$ as a forcing input:

$$\begin{aligned} \dot{\mathbf{e}} &= \left(A - d_c\mathbf{b}\mathbf{c}\right)\mathbf{e} - \mathbf{b}\boldsymbol{c}_c\boldsymbol{x}_c + \mathbf{b}\left[\nu_{ad} - \Delta\right] - \mathbf{b}d_c w \\ z_1 &= \mathbf{c}\mathbf{e} + w. \end{aligned} \tag{7.22}$$

where $z_1 \triangleq \tilde{y}_m$ is the available error measurement. A linear observer for the **e** dynamics in (7.22) is designed as:

$$\begin{aligned} \dot{\hat{\mathbf{e}}} &= \left(A - d_c\mathbf{b}\mathbf{c}\right)\hat{\mathbf{e}} + K_r\left(z_1 - \hat{z}_1\right) \\ \hat{z}_1 &= \mathbf{c}\hat{\mathbf{e}}. \end{aligned} \tag{7.23}$$

where the gain K_r is selected such that $A - d_c\mathbf{b}\mathbf{c} - K_r\boldsymbol{c}$ is asymptotically stable. Using (7.22) and (7.23), the reduced order observer error dynamics can be expressed as

$$\dot{\tilde{\mathbf{e}}} = \tilde{A}\tilde{\mathbf{e}} + \mathbf{b}\boldsymbol{c}_c\boldsymbol{x}_c - \mathbf{b}\left[\nu_{ad} - \Delta\right] + \tilde{G}w, \tag{7.24}$$

where $\tilde{A} \triangleq A - d_c\mathbf{b}\mathbf{c} - K_r\mathbf{c}$, $\tilde{G} \triangleq \mathbf{b}d_c + K_r$. The augmented error vector $\hat{\boldsymbol{E}}$, which will be required for the adaptive laws, is obtained by augmenting the estimates of (7.23) with the true compensator states:

$$\hat{\boldsymbol{E}}_r \triangleq \begin{bmatrix} \hat{\mathbf{e}}^T & \boldsymbol{x}_c^T \end{bmatrix}^T \tag{7.25}$$

where the subscript r denotes that the error vector estimate is obtained by the reduced order observer as opposed to the one in (7.21) obtained using the full order observer. The overall controller architecture is depicted in Figure 7-1.

7.4 Numerical Noise Sensitivity Analysis

Practical experience has shown that the adaptive system is less sensitive to sensor noise when $\hat{\boldsymbol{E}}_r$ in (7.25) is used in the adaptive laws instead of $\hat{\boldsymbol{E}}$ in (7.21). The signal $\bar{E} = \hat{\boldsymbol{E}}^T P\bar{\mathbf{b}}$ is used for adaptation, where P is the solution of the Lyapunov equation

$$\bar{A}^T P + P\bar{A} = -Q, \tag{7.26}$$

for some $Q \succ 0$. The SISO systems from sensor noise w to the adaptive learning signal

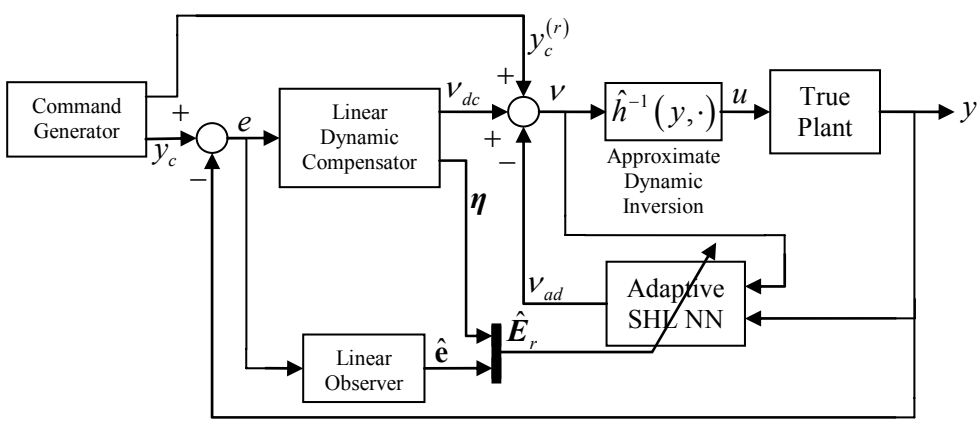

Figure 7-1. Error observer based adaptive output feedback controller with reduced order observer.

$\bar{\boldsymbol{E}}$ with the full and reduced order observers can be written as

$$\begin{bmatrix} \dot{\hat{\boldsymbol{E}}} \\ \dot{\boldsymbol{E}} \end{bmatrix} = \begin{bmatrix} \bar{A} - K\bar{C} & K\bar{C} \\ 0 & \bar{A} \end{bmatrix} \begin{bmatrix} \hat{\boldsymbol{E}} \\ \boldsymbol{E} \end{bmatrix} + \begin{bmatrix} 0 \\ \bar{\mathbf{b}} \end{bmatrix} \left[\nu_{ad} - \Delta \right] + \begin{bmatrix} KH \\ G \end{bmatrix} w$$
$$\bar{E}_f = \begin{bmatrix} \bar{\mathbf{b}}^T P & 0 \end{bmatrix} \begin{bmatrix} \hat{\boldsymbol{E}} \\ \boldsymbol{E} \end{bmatrix} \tag{7.27}$$

$$\begin{bmatrix} \dot{\hat{\mathbf{e}}} \\ \dot{\mathbf{e}} \\ \dot{\boldsymbol{x}}_c \end{bmatrix} = \begin{bmatrix} A - d_c \mathbf{bc} - K_r \mathbf{c} & K_r \mathbf{c} & 0 \\ 0 & A - d_c \mathbf{bc} & -\mathbf{b}\boldsymbol{c}_c \\ 0 & \boldsymbol{b}_c \mathbf{c} & A_c \end{bmatrix} \begin{bmatrix} \hat{\mathbf{e}} \\ \mathbf{e} \\ \boldsymbol{x}_c \end{bmatrix} + \begin{bmatrix} 0 \\ \mathbf{b} \\ 0 \end{bmatrix} \left[\nu_{ad} - \Delta \right] + \begin{bmatrix} K_r \\ -\mathbf{b} d_c \\ \boldsymbol{b}_c \end{bmatrix} w$$
$$\bar{E}_r = \begin{bmatrix} \mathbf{b}^T P_{11} & 0 & \mathbf{b}^T P_{12} \end{bmatrix} \begin{bmatrix} \hat{\mathbf{e}} \\ \mathbf{e} \\ \boldsymbol{x}_c \end{bmatrix} \tag{7.28}$$

where the solution to (7.26) is partitioned as $P = \begin{bmatrix} P_{11} & P_{12} \\ P_{12} & P_{22} \end{bmatrix}$ with appropriate dimensions.

The first step in the design of the adaptive controller is the design of the linear compensator (7.17), which gives the matrix $\bar{A}$ defined in (7.18). Next step is the design of the error observer. In the full order observer design, we solve for the gain matrix $K \in \mathbb{R}^{(r+n_c)\times(1+n_c)}$ to place the eigenvalues of $\bar{A} - K\bar{C}$ to desired locations. In the design of the reduced order observer we similarly solve for $K_r \in \mathbb{R}^{r\times 1}$ to place the eigenvalues of $A - d_c \mathbf{bc} - K_r \boldsymbol{c}$. We compare the sensitivities of the two observers to sensor noise numerically on a sample problem. We consider a system with $r = 3$ and design the output feedback compensator (7.17) by using LQR - Loop Transfer Recovery (LTR) synthesis. Then we design the full order observer such that eigenvalues of $\bar{A} - K\bar{C}$ are four times greater than the eigenvalues of $\bar{A}$. For a fair comparison of the two observers, we pick the eigenvalues of $A - d_c \mathbf{bc} - K_r \boldsymbol{c}$ for the reduced order observer design from the eigenvalues of $\bar{A} - K\bar{C}$. Figure 7-2 shows the Bode diagrams of the transfer functions $G_f(j\omega)$ and $G_r(j\omega)$ corresponding to systems (7.27) and (7.28) respectively. Both

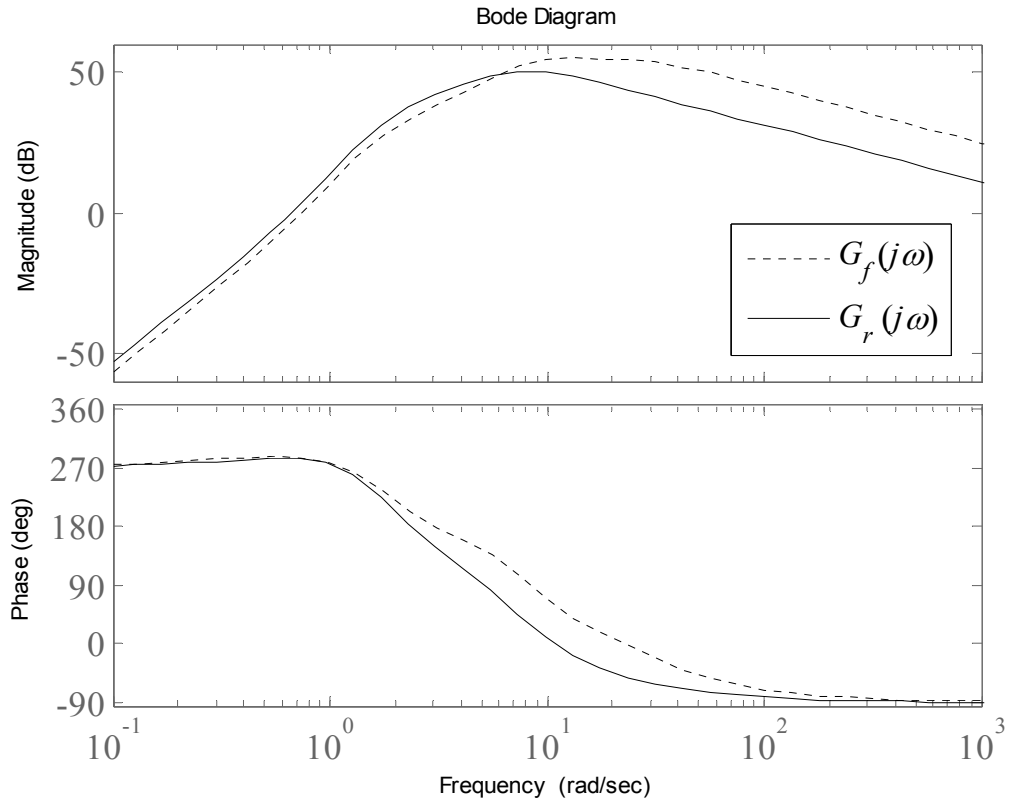

Figure 7-2. Bode diagrams of the transfer functions from sensor noise to learning signal for the full and reduced order observers.

observers cut off the low frequency range below 1 rad/s. Sensitivities of the two observers to sensor noise are close up to around 10 rad/s. For frequencies higher than 30 rad/s, the reduced order observer has approximately 15 dB less amplification effect.

Sensitivities of the two observers to sensor noise change as the linear compensator design and observer designs change. For a given compensator and full and reduced order observer designs with similar dynamics, comparison of the noise sensitivities look similar to Figure 7-2 for majority of the cases. Unfortunately we do not have a systematic way of tuning the compensator and observer designs for optimal noise rejection at present. For a given problem the linear compensator and error observer have to be designed carefully to reduce sensitivity of the adaptive controller to sensor noise.

7.5 Adaptive Control Design

Following the design approach in [13], we employ a SHL NN to approximate the inversion error (7.6). The following theorem from [31], [32] enables us to map the unknown dynamics of the *observable* system (7.1) from available input/output history.

Theorem 7.1. Given $\varepsilon^* > 0$, there exists a set of bounded weights M, N, such that $\Delta(\boldsymbol{x},u)$ in (7.6) can be approximated over a compact set $\mathcal{D} \subset \Omega \times \mathbb{R}$ by a SHL NN

$$\Delta(\boldsymbol{x},u) = M^T \boldsymbol{\sigma}\left(N^T \boldsymbol{\eta}\right) + \varepsilon(d,\boldsymbol{\mu}), \qquad |\varepsilon| < \varepsilon^* \tag{7.29}$$

using the input vector

$$\begin{aligned} \boldsymbol{\eta}(t) &= \begin{bmatrix} 1 & \bar{\boldsymbol{v}}^T(t) & \bar{\boldsymbol{y}}^T(t) \end{bmatrix}^T, \qquad \|\boldsymbol{\eta}\| \le \eta^*, \qquad \eta^* > 0 \\ \bar{\boldsymbol{v}}^T(t) &= \begin{bmatrix} \bar{v}(t) & \bar{v}(t-d) & \cdots & \bar{v}\left(t-(k-r-1)d\right) \end{bmatrix}^T \quad , \\ \bar{\boldsymbol{y}}^T(t) &= \begin{bmatrix} y(t) & y(t-d) & \cdots & y\left(t-(k-1)d\right) \end{bmatrix}^T \end{aligned} \tag{7.30}$$

with $k \ge n$ and $d > 0$, $\boldsymbol{\sigma}$ being a vector of squashing functions $\boldsymbol{\sigma}(\cdot)$, its jth element being defined like $\left[\boldsymbol{\sigma}\left(N^T\boldsymbol{\eta}\right)\right]_j = \left[\boldsymbol{\sigma}\left(N^T\boldsymbol{\eta}\right)_j\right]$.

Design of the adaptive signal, adaptation laws, and the stability analysis follow from [13] with necessary modifications due to the use of the reduced order error observer in (7.23). The adaptive signal is chosen to be the output of a SHL NN:

$$v_{ad} \triangleq \hat{M}^T \boldsymbol{\sigma}\left(\hat{N}^T \boldsymbol{\eta}\right), \tag{7.31}$$

where $\hat{M}$, $\hat{N}$ are estimates of M, N that are updated according to the following adaptation laws:

$$\begin{aligned} \dot{\hat{M}} &= -\Gamma_M \left[2\left(\hat{\boldsymbol{\sigma}} - \hat{\sigma}'\hat{N}^T\boldsymbol{\eta}\right)\hat{\boldsymbol{E}}_r^T P\bar{\mathbf{b}} + k\left(\hat{M} - M_0\right)\right] \\ \dot{\hat{N}} &= -\Gamma_N \left[2\boldsymbol{\eta}\hat{\boldsymbol{E}}_r^T P\bar{\mathbf{b}}\hat{M}^T\hat{\sigma}' + k\left(\hat{N} - N_0\right)\right] \end{aligned} \tag{7.32}$$

in which M_0, N_0 are initial values (or guess) of the NN weights, $\hat{\boldsymbol{\sigma}} = \boldsymbol{\sigma}\left(\hat{N}^T \boldsymbol{\eta}\right)$, $\hat{\sigma}'$ denotes the Jacobian matrix, $k > 0$, and Γ_M, Γ_N are adaptation gain matrices.

Using (7.29) and (7.31), the error dynamics in (7.19) can be expressed as:

$$\begin{aligned} \dot{\boldsymbol{E}} &= \bar{A}\boldsymbol{E} + \bar{\mathbf{b}}\left[\hat{M}^T \boldsymbol{\sigma}\left(\hat{N}^T \boldsymbol{\eta}\right) - M^T \boldsymbol{\sigma}\left(N^T \boldsymbol{\eta}\right) - \varepsilon\right] + Gw \\ z &= \bar{C}\boldsymbol{E} + Hw. \end{aligned} \tag{7.33}$$

Define $\tilde{M} = \hat{M} - M$, $\tilde{N} = \hat{N} - N$, $\tilde{Z} = \begin{bmatrix} \tilde{M} & 0 \\ 0 & \tilde{N} \end{bmatrix}$, and note that $\|\hat{M}\| < \|\tilde{M}\| + M^*$, $\|\hat{N}\|_F < \|\tilde{N}\|_F + N^*$ where $\|\cdot\|$ represents the two norm and M^*, N^* are the upper bounds for the norms of the weight matrices in (7.29):

$$\|M\| < M^*, \quad \|N\|_F < N^*, \tag{7.34}$$

the subscript F denoting the Frobenius norm. With (7.34), the representation

$$\nu_{ad} - \Delta = \hat{M}^T \boldsymbol{\sigma}\left(\hat{N}^T \boldsymbol{\eta}\right) - M^T \boldsymbol{\sigma}\left(N^T \boldsymbol{\eta}\right) - \varepsilon \tag{7.35}$$

allows for the following upper bound:

$$\left|\nu_{ad} - \Delta\right| \le \alpha_1 \|\tilde{Z}\|_F + \alpha_2, \quad \alpha_1 > 0, \quad \alpha_2 > 0. \tag{7.36}$$

For the stability proof we will need the following representation:

$$\hat{M}^T \boldsymbol{\sigma}\left(\hat{N}^T \boldsymbol{\eta}\right) - M^T \boldsymbol{\sigma}\left(N^T \boldsymbol{\eta}\right) = \tilde{M}^T \left(\hat{\boldsymbol{\sigma}} - \hat{\sigma}' \hat{N}' \boldsymbol{\eta}\right) + \hat{M}^T \hat{\sigma}' \tilde{N}^T \boldsymbol{\eta} + \omega$$

where $\omega = \tilde{M}^T \hat{\sigma}' N^T \boldsymbol{\eta} - M^T \mathcal{O}\left(\tilde{N}^T \boldsymbol{\eta}\right)^2$. Such a representation is achieved via Taylor series expansion of $\boldsymbol{\sigma}\left(N^T \boldsymbol{\eta}\right)$ around the estimates $\hat{N}^T \boldsymbol{\eta}$ (refer to [58] for more details).

With the bound in (7.30), a bound for ($\omega - \varepsilon$) over a compact set can be presented as follows [58]:

$$|\omega - \varepsilon| \le \gamma_1 \|\tilde{Z}\|_F + \gamma_2, \quad \gamma_1 > 0, \quad \gamma_2 > 0, \tag{7.37}$$

where γ_1, γ_2 are computable constants, and γ_1 depends on the unknown constant η^*, γ_2 depends on ε^*. Thus the first forcing term in (7.19) can be written:

$$\nu_{ad} - \Delta = \tilde{M}^T \left(\hat{\boldsymbol{\sigma}} - \hat{\sigma}' \hat{N}^T \boldsymbol{\eta} \right) + \hat{M}^T \hat{\sigma}' \tilde{N}^T \boldsymbol{\eta} + \omega - \varepsilon \,. \tag{7.38}$$

7.6 Stability Analysis

In this section we show through Lyapunov's direct method that error vector $\boldsymbol{\zeta} = \begin{bmatrix} \boldsymbol{E}^T & \tilde{\mathbf{e}}^T & \operatorname{vec} \tilde{Z}^T \end{bmatrix}^T$ is ultimately bounded. Recall that Theorem 7.1 introduces the compact set $\mathcal{D}$ over which the NN approximation is valid. From (7.29) it follows that

$$\bar{\boldsymbol{x}} \triangleq \begin{bmatrix} \boldsymbol{x}^T & u \end{bmatrix}^T \in \mathcal{D} \quad \Leftrightarrow \quad \varpi \triangleq \begin{bmatrix} \boldsymbol{\xi}^T & \boldsymbol{\chi}^T & u \end{bmatrix}^T \in \Omega_{\mathcal{D}} \,, \tag{7.39}$$

where $\Omega_{\mathcal{D}}$ is the map of the compact set $\mathcal{D}$ on the domain of transformed variables. The set $\Omega_{\mathcal{D}}$ can be viewed as $\Omega_{\mathcal{D}} = \Omega_{\boldsymbol{\xi}} \times \Omega_{\boldsymbol{\chi}} \times \Omega_u$, where $\boldsymbol{\xi} \in \Omega_{\boldsymbol{\xi}}$, $\boldsymbol{\chi} \in \Omega_{\boldsymbol{\chi}}$, $u \in \Omega_u$ all three being compact sets. Notice that the static map in (7.3), (7.4) ensures that $\nu \in \Omega_\nu$, Ω_ν being a compact set. The relationship in (7.7) and the boundedness of ν_{dc}, as a stabilizer of (7.15) ensure that $\boldsymbol{x}_c \in \Omega_{\boldsymbol{x}_c}$, and $\tilde{Z} \in \Omega_{\tilde{Z}}$, these two sets being compact as well. Since the observer in (7.23) is driven by the measured output tracking error $\tilde{y}_m = y_c - y_m$, having $\boldsymbol{\xi} \in \Omega_{\boldsymbol{\xi}}$, $y_c \in \Omega_{y_c}$ implies that $\hat{\mathbf{e}} \in \Omega_{\hat{\mathbf{e}}}$, the latter being a compact set.

The vector $\boldsymbol{\zeta}$ can be viewed as a function of the constant matrix Z, the state variables $\boldsymbol{\xi}, \boldsymbol{x}_c, \tilde{\mathbf{e}}, \tilde{Z}$, and the command vector $\boldsymbol{y}_c \triangleq \begin{bmatrix} y_c & \dot{y}_c & \cdots & y_c^{(r)} \end{bmatrix}^T$:

$$\boldsymbol{\zeta} = \boldsymbol{F}\left(\boldsymbol{\xi}, \boldsymbol{y}_c, \boldsymbol{x}_c, \tilde{\mathbf{e}}, \hat{Z}, Z \right), \tag{7.40}$$

where $\hat{Z} = \begin{bmatrix} \hat{M} & 0 \\ 0 & \hat{N} \end{bmatrix}$, $Z = \begin{bmatrix} M & 0 \\ 0 & N \end{bmatrix}$. The relation in (7.40) represents a mapping from the original domains of the arguments to the space of error variables $\boldsymbol{F} : \Omega_{\boldsymbol{\xi}} \times \Omega_{\boldsymbol{y}_c} \times \Omega_{\boldsymbol{x}_c} \times$

$\Omega_{\tilde{\mathbf{e}}} \times \Omega_{\hat{Z}} \times \Omega_Z \to \Omega_{\boldsymbol{\zeta}}$. Thus, (7.39) and the implicit dependence in (7.40) ensure that $\Omega_{\boldsymbol{\zeta}}$ is a bounded set. Introduce the largest ball, which is included in $\Omega_{\boldsymbol{\zeta}}$ in the error space:

$$B_R \triangleq \left\{ \boldsymbol{\zeta} \middle| \|\boldsymbol{\zeta}\| \le R \right\}, \quad R > 0. \tag{7.41}$$

For every $\boldsymbol{\zeta} \in B_R$, we have $\bar{\boldsymbol{x}} \in \mathcal{D}$, where $\mathcal{D}$ is the set over which the NN approximation has been defined. Introduce the following level set:

$$\Omega_\alpha = \left\{ \boldsymbol{\zeta} \in B_R \middle| V = \alpha \right\}. \tag{7.42}$$

Assumption 7.4. Assume

$$R > \gamma \sqrt{\frac{T_M}{T_m}} \ge \gamma, \tag{7.43}$$

where T_M and T_m are the maximum and minimum eigenvalues of the following matrix:

$$T \triangleq \frac{1}{2} \begin{bmatrix} 2P & 0 & 0 & 0 \\ 0 & 2\tilde{P} & 0 & 0 \\ 0 & 0 & \Gamma_N^{-1} & 0 \\ 0 & 0 & 0 & \Gamma_M^{-1} \end{bmatrix}, \tag{7.44}$$

and γ is defined as $\gamma = \max\left(C_1, C_2, C_3\right)$ with

$$C_1 = \sqrt{\frac{\kappa_2^2 + \beta_2^2 + \bar{Z}}{\lambda_{\min}\left(Q\right) - 2 - \left\|\tilde{P}\mathbf{b}\boldsymbol{c}_c\right\|^2}}$$

$$C_2 = \sqrt{\frac{\kappa_2^2 + \beta_2^2 + \bar{Z}}{\lambda_{\min}\left(\tilde{Q}\right) - 3}}$$

$$C_3 = \sqrt{\frac{\kappa_2^2 + \beta_2^2 + \bar{Z}}{\frac{k}{2} - \kappa_1^2 - \beta_1^2}}$$

where $\bar{Z} = \frac{k}{2}\left[\left\|M - M_0\right\|^2 + \left\|N - N_0\right\|_F^2\right]$, $k > 2\left(\kappa_1^2 + \beta_1^2\right)$, $\kappa_1 = \alpha_1\left(\left\|P_{11}\mathbf{b}\right\| + \left\|\tilde{P}\mathbf{b}\right\|\right) + \gamma_1\left\|P\bar{\mathbf{b}}\right\|$, $\kappa_2 = \alpha_2\left(\left\|P_{11}\mathbf{b}\right\| + \left\|\tilde{P}\mathbf{b}\right\|\right) + \left\|\tilde{P}\tilde{G}\right\| w_0 + \gamma_2\left\|P\bar{\mathbf{b}}\right\|$, $\beta_1 = \gamma_1\left\|P\bar{\mathbf{b}}\right\|$, $\beta_2 = \gamma_2\left\|P\bar{\mathbf{b}}\right\| + \left\|PG\right\| w_0$, P_{11} is the

$(r \times r)$ matrix obtained by partitioning P as $P = \begin{bmatrix} P_{11} & P_{12} \\ P_{12}^T & P_{22} \end{bmatrix}$ and $\tilde{P}$ solves $\tilde{A}^T \tilde{P} + \tilde{P}\tilde{A} = -\tilde{Q}$, for some $\tilde{Q} > 0$ with minimum eigenvalue $\lambda_{\min}\left(\tilde{Q}\right) > 3$.

Theorem 7.2. Let the Assumptions 7.1-7.4 hold, and let $\lambda_{\min}\left(Q\right) > 2 + \left\|\tilde{P}\mathbf{b}\boldsymbol{c}_c\right\|^2$ for Q introduced in (7.26). Then, if the initial errors belong to the compact set Ω_α, defined in (7.42), the feedback control law given by (7.3), (7.7), along with (3.27), guarantees that the signals $\boldsymbol{E}, \tilde{\mathbf{e}}, \tilde{M}, \tilde{N}$ in the closed loop system are ultimately bounded.

Proof. See APPENDIX C.

7.7 Experimental Application

To demonstrate the effectiveness of the reduced order error observer in comparison with the full order observer, we designed both full order and reduced order observers needed to implement the adaptive output feedback controller architecture to the 3 DOF helicopter model depicted in Figure 1-4 [70]. The experimental results also demonstrate that the control architecture is adaptive to both parametric uncertainty and unmodeled dynamics.

The model helicopter consists of a rectangular frame with two propellers mounted at its two ends. The motors' axes are parallel and the thrust vector is normal to the frame. The helicopter frame is suspended from an instrumented joint mounted at the end of a long arm and is free to roll about its center. The arm is gimbaled on a 2 DOF joint and is free to rotate in pitch and yaw. Hence the system has a total of three degrees of freedom. For the experiment, control voltage is equally applied to both motors. Hence the helicopter remains nearly parallel to the table, and only its elevation is controlled. The arm that carries the helicopter is balanced such that it remains horizontal when the motors are not actuated. We use the angle between the arm and the horizon, the pitch angle of the arm, denoted as θ, as a measure of the elevation of the helicopter. The angle is

measured with a 12 bit optical angular position sensor. This means that angular resolution of the sensor is approximately 0.088 deg and hence the measurement error w introduced in (7.12) appears as a high frequency error that is bounded by this value.

There are significant nonlinearities in the system due to actuators and friction in the joints. Positive and negative elevation commands require that the propellers operate in both forward and reverse directions. Consequently there are significant nonlinearities and unmodeled dynamics due to a combination of the dc motor and unsteady aerodynamic effects associated with the actuation process.

Theoretical analysis of the 3 DOF model helicopter shows that pitch attitude has a relative degree of four [33]. Since one of the modes (due to the dc motor time constant) is quite fast, the practical relative degree within the bandwidth of the control design (6 rad/sec) is three. Thus the controller design was performed assuming $r = 3$. A third order dynamic compensator with

$$A_c = \begin{bmatrix} -16.56 & 1 & 0 \\ -137.16 & 0 & 1 \\ -600.36 & -26.28 & -8.40 \end{bmatrix}, \qquad \boldsymbol{b}_c = \begin{bmatrix} 16.56 \\ 137.16 \\ 567.96 \end{bmatrix}, \qquad (7.45)$$
$$\boldsymbol{c}_c = \begin{bmatrix} 32.40 & 26.28 & 8.40 \end{bmatrix}, \qquad d_c = 0$$

places the poles of the closed loop error dynamics in (7.18) at -3.6, -8.28, $-2.4 \pm 1.8j$, $-4.14 \pm 7.17j$. The full order observer dynamics in (7.21) were designed so that its poles are four times faster than those of the error dynamics. For the design of the reduced order error observer in (7.23), the poles were selected from the six poles of the full order design. These consisted of the slower complex conjugate pair and the slower real pole. Sensitivities of the full and reduced order observers to sensor noise for this particular design were presented in Figure 7-2. We implemented 10 hidden neurons and the following sigmoidal basis function $\sigma_i(x) = (1 + e^{-a_i x})^{-1}$ with $a_i, i = 1, \ldots, 10$ varying evenly between 0.1 and 1. The adaptation gains were set to $F = 100I$ and $G = 100I$, with

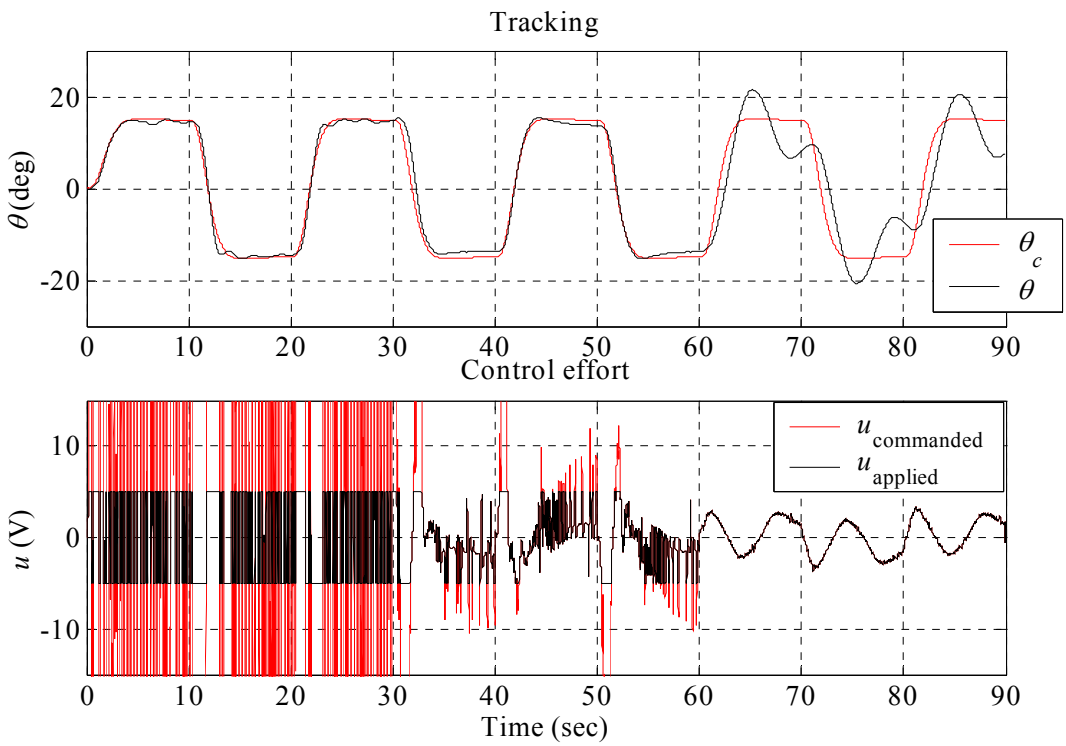

Figure 7-3. Output tracking and control histories with NN adaptation with full order observer (0 – 30 secs), reduced order observer (30 – 60 secs), and without adaptation (60 – 90 secs).

sigma modification gain $k = 0.1$. A third order command filter was implemented with a real pole at –1.8 and a pair of complex conjugate poles with $\omega_n = 1.5$ rad/sec and $\xi = 0.8$.

In Figure 7-3 we show the tracking performance in the upper plot and the control activity in the lower plot. The absolute value of the control voltage applied to the motors is limited to be less than 5 V. Both the commanded and applied voltages are shown in the lower plot. First the experiment starts with NN adaptation with the full order observer. At 30 seconds the controller switches to the reduced order observer and at 60 seconds the adaptation turns off. It is evident that the reduced order error observer reduces the noise in the control signal considerably, in agreement with the noise sensitivity plots in Figure 7-2. Another advantage of the reduced order observer is that reduction of noise and elimination of control saturations result in smoother response. In the last 30 seconds we see that the noise in control is mostly due to adaptation.

7.8 Summary

A reduced order error observer is designed to replace the full order error observer of the adaptive output feedback control architecture presented in [13]. The reduced order observer estimates the tracking error and its derivatives up to order $r - 1$, where r is the relative degree of the regulated output. It eliminates the redundancy in the full order design in estimating the already available compensator states. Both numerical and experimental evidence suggest that the proposed design significantly reduces the effect of sensor error on the control. A stability analysis is provided that guarantees the control architecture with the reduced order observer renders all error signals and the NN weights uniformly ultimately bounded. Experiments on a 3 DOF laboratory model helicopter illustrate the improvements provided by the reduced order observer design.

CHAPTER 8

CONCLUDING REMARKS

8.1 Conclusions

This thesis has investigated application of novel NN based adaptive output feedback controllers of [12]–[23] to a diverse range of problems. Whenever we encountered a problem the existing adaptive control theory failed to accommodate, we explored ways to extend the theory to encompass that problem with the ultimate goal of improving applicability of adaptive controllers to real world problems.

We observed that the model inversion based adaptive output feedback controllers of [12], [13] are sensitive to sensor noise. We proposed a modification to the linear observer design in [13] that estimates the augmented error vector that contains tracking error and its derivatives and the states of the linear compensator. The proposed observer eliminates the redundancy in estimating the already available compensator states and only estimates the unknown tracking error derivatives. Although we do not have a theoretical explanation as to how this *ad hoc* modification helps to reduce sensitivity to sensor noise, numerical and experimental results showed that it improved robustness of the controller to sensor noise for the cases we tested.

The best way to utilize adaptive control theory on problems for which well established controller designs exist, such as flight control problems, is to augment these controllers to further increase their capabilities. Adaptive augmenting controllers developed in [16]–[23] either implicitly or explicitly assume a linear existing controller. In this thesis we have proven that the open loop and arbitrary reference model-following augmenting controllers can be applied to augment nonlinear controllers and laid out the conditions under which this can be possible. Then we applied the open loop reference

model approach to augment the nonlinear guidance law of a spinning projectile. Six-DOF nonlinear simulations showed substantial improvements.

Due to its less restrictive requirements regarding the linear model of the system, the arbitrary reference model-following adaptive augmenting controller of Ref. [23] can be applied to a larger class of systems compared to the open and closed loop approaches. We further broadened the class of systems that the arbitrary reference model approach can be applied by formulating the command hedging implementation, which makes it applicable to systems with input nonlinearities. We also adopted a framework that makes it applicable to non-minimum phase systems for which non-minimum phase characteristics are modeled with sufficient accuracy and treated properly in the design of the existing controller. We have proven boundedness of the closed loop systems with the command hedging and non-minimum phase systems formulations separately and presented successful implementations on numerical simulations. Finally we extended its formulation to the MIMO case for distributed control of interconnected systems. We presented a stability analysis that proves boundedness of the large scale system in the distributed control framework that sets a tradeoff between the performance and simplicity of the centralized and decentralized setups. We showed on a wind tunnel experiment that the approach has a great potential for handling substantial unsteady uncertain coupling effects.

In this thesis, we also laid out a preliminary adaptive control design for closed loop hingeless flight control of a 2-DOF wind tunnel model using micro adaptive flow controllers. Hingeless flight control using MAFC actuators is an interesting problem and an active area of research. Behavior of MAFC actuators in closed loop control under dynamic flight conditions has still not been investigated fully. We tested the adaptive controller designed in simulation using a fictitious MAFC model that captures possible coupling effects between actuation, the dynamics of flow field, and the rigid body dynamics of the model.

8.2 Recommendations for Future Research

The research approach followed in this thesis can lead to more interesting developments in the field of adaptive control as more challenging problems are encountered. In particular we can provide the following directions for future research as a result of findings of this thesis.

In Chapter 7 we showed that the adaptive output feedback controllers of [12] and [13] are sensitive to sensor noise. We proposed an *ad hoc* modification that yielded promising improvements in practice. Our efforts to develop a theoretically justified approach to this problem have been fruitless. Further research in this area is recommended. A systematic method for controlling sensitivity of the adaptive controller to sensor noise while maintaining its performance would be a major development in adaptive output feedback control.

Hingeless flight control using active flow actuators is an interesting and active area of research. Characteristics of such actuators in dynamic flight conditions are yet to be investigated. Interdisciplinary research in this area is recommended to develop low order models for active flow control actuators and control methods to address the resulting systems. We are currently working towards this goal in an ongoing collaborative effort with research groups in the areas of experimental flow physics and flow control to develop reduced order models and control designs and to test them in wind tunnel experiments, and flight tests [71].

APPENDIX A

CHAPTER 3 PROOF

Proof of Theorem 3.2: Consider the following positive definite radially unbounded function as a candidate Lyapunov function for the dynamics in (3.17), (3.25), (3.27).

$$V\left(\boldsymbol{E},\tilde{\boldsymbol{E}},z_2,\tilde{Z}\right)=\boldsymbol{E}^T\bar{P}\boldsymbol{E}+\tilde{\boldsymbol{E}}^T\tilde{P}\tilde{\boldsymbol{E}}+\frac{1}{2}\operatorname{tr}\left(\tilde{M}^T\Gamma_M^{-1}\tilde{M}\right)+\frac{1}{2}\operatorname{tr}\left(\tilde{N}^T\Gamma_N^{-1}\tilde{N}\right)+V_z\left(z_2\right). \tag{A.1}$$

Its derivative along (3.17), (3.25) is

$$\begin{aligned}\dot{V}=&-\boldsymbol{E}^T\bar{Q}\boldsymbol{E}-\tilde{\boldsymbol{E}}^T\tilde{Q}\tilde{\boldsymbol{E}}+2\boldsymbol{E}^T\bar{P}\bar{B}y_c+2\boldsymbol{E}^T\bar{P}B_1\left(u_{ad}-\Delta_1\right)+2\boldsymbol{E}^T\bar{P}\bar{\Delta}_2\\&-2\tilde{\boldsymbol{E}}^T\tilde{P}B_1\left(u_{ad}-\Delta_1\right)-2\tilde{\boldsymbol{E}}^T\tilde{P}\bar{\Delta}_2+\operatorname{tr}\left(\tilde{M}^T\Gamma_M^{-1}\dot{\tilde{M}}\right)+\operatorname{tr}\left(\tilde{N}^T\Gamma_N^{-1}\dot{\tilde{N}}\right)+\dot{V}_z\left(z_2\right).\end{aligned} \tag{A.2}$$

Using $\tilde{\boldsymbol{E}}=\hat{\boldsymbol{E}}-\boldsymbol{E}$, (3.31), and (3.27) we can write

$$\begin{aligned}\dot{V}=&-\boldsymbol{E}^T\bar{Q}\boldsymbol{E}-\tilde{\boldsymbol{E}}^T\tilde{Q}\tilde{\boldsymbol{E}}+2\boldsymbol{E}^T\bar{P}\bar{B}y_c+2\hat{\boldsymbol{E}}^T\bar{P}B_1\left(\omega-\varepsilon\right)-2\tilde{\boldsymbol{E}}^T\left(\bar{P}+\tilde{P}\right)B_1\left(u_{ad}-\Delta_1\right)\\&+2\boldsymbol{E}^T\bar{P}\bar{\Delta}_2-2\tilde{\boldsymbol{E}}^T\tilde{P}\bar{\Delta}_2-k\operatorname{tr}\left(\tilde{M}^T\hat{M}\right)-k\operatorname{tr}\left(\tilde{N}^T\hat{N}\right)+\dot{V}_z\left(z_2\right)\end{aligned} \tag{A.3}$$

With the upper bounds (3.6), (3.30), (3.32), (3.33), (3.34), and the equalities

$$\begin{aligned}\operatorname{tr}\left(\tilde{N}^T\hat{N}\right)&=\frac{1}{2}\left\|\tilde{N}\right\|_F^2+\frac{1}{2}\left\|\hat{N}\right\|_F^2-\frac{1}{2}\left\|N\right\|_F^2\\\operatorname{tr}\left(\tilde{M}^T\hat{M}\right)&=\frac{1}{2}\left\|\tilde{M}\right\|_F^2+\frac{1}{2}\left\|\hat{M}\right\|_F^2-\frac{1}{2}\left\|M\right\|_F^2,\end{aligned}$$

(A.3) can be upper bounded as

$$\begin{aligned}\dot{V}\le&-\bar{Q}_m\left\|\boldsymbol{E}\right\|^2-\tilde{Q}_m\left\|\tilde{\boldsymbol{E}}\right\|^2+2\left\|\boldsymbol{E}\right\|\left\|\bar{P}\bar{B}\right\|y_c^*+2\left(\left\|\boldsymbol{E}\right\|+\left\|\tilde{\boldsymbol{E}}\right\|\right)\left\|\bar{P}B_1\right\|\left(\gamma_1\left\|\tilde{Z}\right\|_F+\gamma_2\right)\\&+2\left\|\tilde{\boldsymbol{E}}\right\|\Theta\left(\alpha_1\left\|\tilde{Z}\right\|_F+\alpha_2\right)+2\left\|\boldsymbol{E}\right\|\left\|\bar{P}\right\|\left(\delta_1\left\|\boldsymbol{E}\right\|+\beta_2\left\|z_2\right\|+\delta_2\right)\\&+2\left\|\tilde{\boldsymbol{E}}\right\|\left\|\tilde{P}\right\|\left(\delta_1\left\|\boldsymbol{E}\right\|+\beta_2\left\|z_2\right\|+\delta_2\right)+\frac{\left(c_4c_5\right)^2}{c_3}\left\|\boldsymbol{E}\right\|^2+\frac{\left(c_4c_5\right)^2}{c_3}\beta_4^2\\&-\frac{k}{2}\left\|\tilde{M}\right\|_F^2-\frac{k}{2}\left\|\hat{M}\right\|_F^2+\frac{k}{2}\left\|M\right\|_F^2-\frac{k}{2}\left\|\tilde{N}\right\|_F^2-\frac{k}{2}\left\|\hat{N}\right\|_F^2+\frac{k}{2}\left\|N\right\|_F^2-\frac{3c_3}{4}\left\|z_2\right\|^2\end{aligned} \tag{A.4}$$

We insert the following inequalities obtained using completion of squares

$$
\begin{aligned}
2\|\boldsymbol{E}\|\|\bar{P}\|\delta_2 &\le \|\boldsymbol{E}\|^2 + \left(\|\bar{P}\|\delta_2\right)^2 \\
2\|\tilde{\boldsymbol{E}}\|\|\tilde{P}\|\delta_2 &\le \|\tilde{\boldsymbol{E}}\|^2 + \left(\|\tilde{P}\|\delta_2\right)^2 \\
2\|\tilde{\boldsymbol{E}}\|\|\tilde{P}\|\beta_2\|\boldsymbol{z}_2\| &\le \frac{c_3}{4}\|\boldsymbol{z}_2\|^2 + \frac{\left(2\|\tilde{P}\|\beta_2\right)^2}{c_3}\|\tilde{\boldsymbol{E}}\|^2 \\
2\|\boldsymbol{E}\|\|\bar{P}\|\beta_2\|\boldsymbol{z}_2\| &\le \frac{c_3}{4}\|\boldsymbol{z}_2\|^2 + \frac{\left(2\|\bar{P}\|\beta_2\right)^2}{c_3}\|\boldsymbol{E}\|^2
\end{aligned}
\tag{A.5}
$$

into (A.4) to get

$$
\begin{aligned}
\dot{V} \le &-\left(\bar{Q}_m - 1 - 2\|\bar{P}\|\delta_1 - \frac{\left(c_4c_5\right)^2}{c_3} - \frac{\left(2\|\bar{P}\|\beta_2\right)^2}{c_3}\right)\|\boldsymbol{E}\|^2 + \left(\delta_2\|\bar{P}\|\right)^2 \\
&-\left(\tilde{Q}_m - 1 - 2\|\tilde{P}\|\delta_1 - \frac{\left(2\|\tilde{P}\|\beta_2\right)^2}{c_3}\right)\|\tilde{\boldsymbol{E}}\|^2 + \left(\delta_2\|\tilde{P}\|\right)^2 \\
&+2\|\boldsymbol{E}\|\|\bar{P}B_1\|\gamma_1\|\tilde{Z}\|_F + 2\|\boldsymbol{E}\|\|\bar{P}B_1\|\gamma_2 + 2\|\boldsymbol{E}\|\|\bar{P}\bar{B}\|y_c^* \\
&+2\|\tilde{\boldsymbol{E}}\|\left[\kappa_1\|\tilde{Z}\|_F + \kappa_2\right] - \frac{k}{2}\|\tilde{Z}\|_F^2 + \bar{Z} - \frac{c_3}{4}\|\boldsymbol{z}_2\|^2 + \frac{\left(c_4c_5\right)^2}{c_3}\beta_4^2
\end{aligned}
\tag{A.6}
$$

One more completion of squares on the remaining terms gives the inequalities

$$
\begin{aligned}
2\|\boldsymbol{E}\|\|\bar{P}B_1\|\gamma_1\|\tilde{Z}\|_F &\le \|\boldsymbol{E}\|^2 + \left(\|\bar{P}B_1\|\gamma_1\right)^2\|\tilde{Z}\|_F^2 \\
2\|\boldsymbol{E}\|\|\bar{P}B_1\|\gamma_2 &\le \|\boldsymbol{E}\|^2 + \left(\|\bar{P}B_1\|\gamma_2\right)^2 \\
2\|\boldsymbol{E}\|\|\bar{P}\bar{B}\|y_c^* &\le \|\boldsymbol{E}\|^2 + \left(\|\bar{P}B\|y_c^*\right)^2 \\
2\|\tilde{\boldsymbol{E}}\|\kappa_1\|\tilde{Z}\|_F &\le \|\tilde{\boldsymbol{E}}\|^2 + \kappa_1^2\|\tilde{Z}\|_F^2 \\
2\|\tilde{\boldsymbol{E}}\|\kappa_2 &\le \|\tilde{\boldsymbol{E}}\|^2 + \kappa_2^2
\end{aligned}
\tag{A.7}
$$

Inserting (A.7) into (A.6) gives

$$\dot{V} \le -\left(\bar{Q}_m - 4 - 2\left\|\bar{P}\right\|\delta_1 - \frac{\left(c_4 c_5\right)^2}{c_3} - \frac{\left(2\left\|\bar{P}\right\|\beta_2\right)^2}{c_3}\right)\left\|\boldsymbol{E}\right\|^2$$

$$-\left(\tilde{Q}_m - 3 - 2\left\|\tilde{P}\right\|\delta_1 - \frac{\left(2\left\|\tilde{P}\right\|\beta_2\right)^2}{c_3}\right)\left\|\tilde{\boldsymbol{E}}\right\|^2 - \left(\frac{k}{2} - \kappa_1^2 - \left(\left\|\bar{P}B_1\right\|\gamma_1\right)^2\right)\left\|\tilde{Z}\right\|_F^2 \tag{A.8}$$

$$-\frac{c_3}{4}\left\|z_2\right\|^2 + \left(\left\|\bar{P}B_1\right\|\gamma_2\right)^2 + \left(\left\|\bar{P}B\right\|y_c^*\right)^2 + \kappa_2^2 + \bar{Z} + \frac{\left(c_4 c_5\right)^2}{c_3}\beta_4^2 + \left(\delta_2\left\|\tilde{P}\right\|\right)^2 + \left(\delta_2\left\|\bar{P}\right\|\right)^2$$

Either of the following conditions

$$\left\|\boldsymbol{E}\right\| > \sqrt{\frac{\left\|\bar{P}B_1\right\|^2\gamma_2^2 + \kappa_2^2 + \bar{Z} + \delta_2^2\left(\left\|\tilde{P}\right\|^2 + \left\|\bar{P}\right\|^2\right) + \frac{\left(c_4 c_5\right)^2}{c_3}\beta_4^2 + \left(\left\|\bar{P}B\right\|y_c^*\right)^2}{\bar{Q}_m - 4 - 2\delta_1\left\|\bar{P}\right\| - \frac{\left(c_4 c_5\right)^2}{c_3} - \frac{\left(2\left\|\bar{P}\right\|\beta_2\right)^2}{c_3}}} \tag{A.9}$$

$$\left\|\tilde{\boldsymbol{E}}\right\| > \sqrt{\frac{\left\|\bar{P}B_1\right\|^2\gamma_2^2 + \kappa_2^2 + \bar{Z} + \delta_2^2\left(\left\|\tilde{P}\right\|^2 + \left\|\bar{P}\right\|^2\right) + \frac{\left(c_4 c_5\right)^2}{c_3}\beta_4^2 + \left(\left\|\bar{P}B\right\|y_c^*\right)^2}{\tilde{Q}_m - 3 - 2\delta_1\left\|\tilde{P}\right\| - \frac{\left(2\left\|\tilde{P}\right\|\beta_2\right)^2}{c_3}}} \tag{A.10}$$

$$\left\|\tilde{Z}\right\|_F > \sqrt{\frac{\left\|\bar{P}B_1\right\|^2\gamma_2^2 + \kappa_2^2 + \bar{Z} + \delta_2^2\left(\left\|\tilde{P}\right\|^2 + \left\|\bar{P}\right\|^2\right) + \frac{\left(c_4 c_5\right)^2}{c_3}\beta_4^2 + \left(\left\|\bar{P}B\right\|y_c^*\right)^2}{\frac{k}{2} - \kappa_1^2 - \left(\gamma_1\left\|\bar{P}B_1\right\|\right)^2}} \tag{A.11}$$

$$\left\|z_2\right\| > 2\sqrt{\frac{\left\|\bar{P}B_1\right\|^2\gamma_2^2 + \kappa_2^2 + \bar{Z} + \delta_2^2\left(\left\|\tilde{P}\right\|^2 + \left\|\bar{P}\right\|^2\right) + \frac{\left(c_4 c_5\right)^2}{c_3}\beta_4^2 + \left(\left\|\bar{P}B\right\|y_c^*\right)^2}{c_3}} \tag{A.12}$$

will render $\dot{V} < 0$ outside a compact set. To complete the proof, consider the following hypersphere

$$B_\gamma = \left\{\boldsymbol{\zeta} \in B_R \middle| \left\|\boldsymbol{\zeta}\right\| < \gamma\right\}$$

in the space of the error vector $\boldsymbol{\zeta}$ outside of which $\dot{V}(\boldsymbol{\zeta}) < 0$. Notice from (3.37) that $B_\gamma \subset B_R$. Let

$$\Gamma \triangleq \max_{\|\boldsymbol{\zeta}\|=\gamma} \boldsymbol{\zeta}^T T_2 \boldsymbol{\zeta} = \gamma^2 T_{2_M} .$$

Introduce the set

$$\Omega_\gamma = \left\{ \boldsymbol{\zeta} \middle| \boldsymbol{\zeta}^T T_2 \boldsymbol{\zeta} \le \Gamma \right\} .$$

The condition (3.37) ensures that $\Omega_\gamma \subset \Omega_\alpha$. Thus, if the initial error $\boldsymbol{\zeta}_0 = \boldsymbol{\zeta}(0)$ belongs to Ω_α, then there exists a time constant $t_\zeta(\boldsymbol{\zeta}_0)$ such that $\boldsymbol{\zeta}(t)$ will enter the set Ω_γ at t_ζ and remain inside it for all $t > t_\zeta$. This implies ultimate boundedness of $\boldsymbol{\zeta}$ and completes the proof. ■

APPENDIX B

CHAPTER 5 PROOF

Proof of Theorem 5.1: Consider the following Lyapunov function candidate for each of the subsystems

$$V_i = \boldsymbol{E}_i^T P_i \boldsymbol{E}_i + \tilde{\boldsymbol{E}}_i^T \tilde{P}_i \tilde{\boldsymbol{E}}_i + \frac{1}{2}\tilde{M}_i^T F_i^{-1} \tilde{M}_i + \frac{1}{2}\operatorname{tr}\left(\tilde{N}_i^T G_i^{-1} \tilde{N}_i\right). \tag{B.1}$$

The dynamics equations for $\boldsymbol{E}_i$, $\tilde{\boldsymbol{E}}_i$, $\tilde{\boldsymbol{M}}_i$, and $\tilde{\boldsymbol{N}}_i$ given in (5.13), (5.18), and (5.19) are exactly in the same form as the corresponding equations in [13]. Therefore, the stability analysis laid out in [13] can be followed to show that

$$\dot{V}_i \le -\left(\lambda_{\min}\left(Q_i\right) - 2\right)\left\|\boldsymbol{E}_i\right\|^2 - \left(\lambda_{\min}\left(\tilde{Q}_i\right) - 2\right)\left\|\tilde{\boldsymbol{E}}_i\right\|^2 - \alpha_i \left\|\tilde{Z}_i\right\|_F^2 + \omega_i \tag{B.2}$$

where

$$\tilde{Z}_i = \begin{bmatrix} \tilde{M}_i & 0 \\ 0 & \tilde{N}_i \end{bmatrix}$$

$$\omega_i = \frac{k_i}{2}\left(\left\|M_i\right\|^2 + \left\|N_i\right\|_F^2\right) + \left[\left(\left\|P_i \boldsymbol{b}_{m_i}\right\| + \left\|\tilde{P}_i \boldsymbol{b}_{m_i}\right\|\right)\alpha_{2,i} + \left\|P_i \boldsymbol{b}_{m_i}\right\|\gamma_{2,i}\right]^2 + \gamma_{2,i}^2 \left\|P_i \boldsymbol{b}_{m_i}\right\|^2$$

$$\alpha_i = \frac{k_i}{2} - \left[\left(\left\|P_i \boldsymbol{b}_{m_i}\right\| + \left\|\tilde{P}_i \boldsymbol{b}_{m_i}\right\|\right)\alpha_{1,i} + \left\|P_i \boldsymbol{b}_{m_i}\right\|\gamma_{1,i}\right]^2 - \gamma_{1,i}^2 \left\|P_i \boldsymbol{b}_{m_i}\right\|^2$$

in which $\alpha_{1,i}$, $\alpha_{2,i}$, $\gamma_{1,i}$, and $\gamma_{2,i}$ are computable constants that define the bounds on the NN approximation error detailed in [13]. Now following an argument similar to that in [20] introduce the following Lyapunov function for the whole system:

$$V = \sum_{i=1}^{m} V_i$$

Its derivative can be upper bounded as

$$\dot{V} = \sum_{i=1}^{m} \dot{V}_i \le \sum_{i=1}^{m} \left[-\left(\lambda_{\min}\left(Q_i\right)-2\right)\left\|\boldsymbol{E}_i\right\|^2 - \left(\lambda_{\min}\left(\tilde{Q}_i\right)-2\right)\left\|\tilde{\boldsymbol{E}}_i\right\|^2 - \alpha_i \left\|\tilde{Z}_i\right\|_F^2 + \omega_i \right]. \tag{B.3}$$

Defining the vectors $\boldsymbol{E} \triangleq \left[\left\|\boldsymbol{E}_1\right\| \ \cdots \ \left\|\boldsymbol{E}_m\right\|\right]^T$, $\tilde{\boldsymbol{E}} \triangleq \left[\left\|\tilde{\boldsymbol{E}}_1\right\| \ \cdots \ \left\|\tilde{\boldsymbol{E}}_m\right\|\right]^T$, $\tilde{Z} \triangleq \left[\left\|\tilde{Z}_1\right\|_F \ \cdots \ \left\|\tilde{Z}_m\right\|_F\right]^T$ and matrices $Q \triangleq \mathrm{diag}\left[\lambda_{\min}\left(Q_1\right)-2 \ \cdots \ \lambda_{\min}\left(Q_m\right)-2\right]$, $\Lambda \triangleq \mathrm{diag}\left[\alpha_1 \ \cdots \ \alpha_m\right]$, and $\tilde{Q} \triangleq \mathrm{diag}\left[\lambda_{\min}\left(\tilde{Q}_1\right)-2 \ \cdots \ \lambda_{\min}\left(\tilde{Q}_m\right)-2\right]$, we can rewrite the expression in (B.3) in the following form:

$$\dot{V} \le -\boldsymbol{E}^T Q \boldsymbol{E} - \tilde{\boldsymbol{E}}^T \tilde{Q} \tilde{\boldsymbol{E}} - \tilde{Z}^T \mathrm{A} \tilde{Z} + \Omega \tag{B.4}$$

where $\Omega = \sum_{i=1}^{m} \omega_i$. The following upper bound

$$\dot{V} \le -\lambda_{\min}\left(Q\right)\left\|\boldsymbol{E}\right\|^2 - \lambda_{\min}\left(\tilde{Q}\right)\left\|\tilde{\boldsymbol{E}}\right\|^2 - \lambda_{\min}\left(\mathrm{A}\right)\left\|\tilde{Z}\right\|^2 + \Omega \tag{B.5}$$

implies that either of the following conditions

$$\begin{aligned} \left\|\boldsymbol{E}\right\| &> \sqrt{\frac{\Omega}{\lambda_{\min}\left(Q\right)}}, \\ \left\|\tilde{\boldsymbol{E}}\right\| &> \sqrt{\frac{\Omega}{\lambda_{\min}\left(\tilde{Q}\right)}}, \\ \left\|\tilde{Z}\right\| &> \sqrt{\frac{\Omega}{\lambda_{\min}\left(\Lambda\right)}} \end{aligned} \tag{B.6}$$

will render $\dot{V} < 0$ outside the compact set $B_\gamma = \left\{\boldsymbol{\zeta} \in B_R \middle| \left\|\boldsymbol{\zeta}\right\| < \gamma\right\}$. Notice from (5.20) that $B_\gamma \subset B_R$. Let Γ be the maximum value of the function $V\left(\boldsymbol{\zeta}\right)$ on the boundary of B_γ

$$\Gamma \triangleq \max_{\|\boldsymbol{\zeta}\|=\gamma} \boldsymbol{\zeta}^T T \boldsymbol{\zeta} = \gamma^2 T_M .$$

Introduce the level set of $V\left(\boldsymbol{\zeta}\right)$ that touches the ball B_γ from outside

$$\Omega_\gamma = \left\{ \boldsymbol{\zeta} \middle| V\left(\boldsymbol{\zeta}\right) = \Gamma \right\}.$$

The condition in (5.20) ensures that $\Omega_\gamma \subset \Omega_\alpha$. Thus, if the initial error $\boldsymbol{\zeta}_0 = \boldsymbol{\zeta}\left(0\right)$ belongs to Ω_α, then there exists a time constant $t_\zeta\left(\boldsymbol{\zeta}_0\right)$ such that $\boldsymbol{\zeta}\left(t\right)$ will enter the set Ω_γ at t_ζ and remain inside it for all $t > t_\zeta$. This implies ultimate boundedness of $\boldsymbol{\zeta}$ and completes the proof. ■

APPENDIX C

CHAPTER 7 PROOF

Proof of Theorem 7.2: Consider the following positive definite radially unbounded function as a candidate Lyapunov function for the dynamics in (7.24), (7.33):

$$V = \boldsymbol{E}^T P \boldsymbol{E} + \tilde{\mathbf{e}}^T \tilde{P} \tilde{\mathbf{e}} + \frac{1}{2}\left[\operatorname{tr}\left(\tilde{M}^T \Gamma_M^{-1} \tilde{M} \right) + \operatorname{tr}\left(\tilde{N}^T \Gamma_N^{-1} \tilde{N} \right) \right]. \tag{C.1}$$

The derivative of V along (7.19), (7.24) will be

$$\begin{aligned} \dot{V} = & -\boldsymbol{E}^T Q \boldsymbol{E} - \tilde{\mathbf{e}}^T \tilde{Q} \tilde{\mathbf{e}} - 2\left(\tilde{\boldsymbol{E}}^T P \bar{\mathbf{b}} + \tilde{\mathbf{e}}^T \tilde{P} \mathbf{b} \right)\left[\nu_{ad} - \Delta \right] + \\ & 2\hat{\boldsymbol{E}}^T P \bar{\mathbf{b}} \left[\nu_{ad} - \Delta \right] + 2\tilde{\mathbf{e}}^T \tilde{P} \mathbf{b} \boldsymbol{c}_c \boldsymbol{x}_c + 2\boldsymbol{E}^T P G w + \\ & 2\tilde{\mathbf{e}}^T \tilde{P} \tilde{G} w + \operatorname{tr}\left(\tilde{M}^T \Gamma_M^{-1} \dot{\tilde{M}} \right) + \operatorname{tr}\left(\tilde{N}^T \Gamma_N^{-1} \dot{\tilde{N}} \right). \end{aligned} \tag{C.2}$$

where we have used $\tilde{\boldsymbol{E}}^T = \hat{\boldsymbol{E}}^T - \boldsymbol{E}^T$. Using (7.20) and (7.25) we can write

$$\begin{aligned} \tilde{\boldsymbol{E}}^T P \bar{\mathbf{b}} + \tilde{\mathbf{e}}^T \tilde{P} \mathbf{b} &= \begin{bmatrix} \tilde{\mathbf{e}}^T & 0 \end{bmatrix} \begin{bmatrix} P_{11} & P_{12} \\ P_{12}^T & P_{22} \end{bmatrix} \begin{bmatrix} \mathbf{b} \\ 0 \end{bmatrix} + \tilde{\mathbf{e}}^T \tilde{P} \mathbf{b} \\ &= \tilde{\mathbf{e}}^T \left(P_{11} + \tilde{P} \right) \mathbf{b}. \end{aligned} \tag{C.3}$$

Using (7.32) and (7.38), (C.2) can be rewritten:

$$\begin{aligned} \dot{V} = & -\boldsymbol{E}^T Q \boldsymbol{E} - \tilde{\mathbf{e}}^T \tilde{Q} \tilde{\mathbf{e}} - 2\tilde{\mathbf{e}}^T \left(P_{11} + \tilde{P} \right) \mathbf{b} \left[\nu_{ad} - \Delta \right] + \\ & 2\hat{\boldsymbol{E}}^T P \bar{\mathbf{b}} \left(\omega - \varepsilon \right) + 2\tilde{\mathbf{e}}^T \tilde{P} \mathbf{b} \boldsymbol{c}_c \boldsymbol{x}_c + 2\boldsymbol{E}^T P G w + 2\tilde{\mathbf{e}}^T \tilde{P} \tilde{G} w + \\ & -k \operatorname{tr}\left(\tilde{M}^T \left(\hat{M} - M_0 \right) \right) - k \operatorname{tr}\left(\tilde{N}^T \left(\hat{N} - N_0 \right) \right). \end{aligned} \tag{C.4}$$

Using the following property for matrices

$$\operatorname{tr}\left(\tilde{N}^T \left(\hat{N} - N_0 \right) \right) = \frac{k}{2} \left\| \tilde{N} \right\|_F^2 + \frac{k}{2} \left\| \hat{N} - N_0 \right\|_F^2 - \frac{k}{2} \left\| N - N_0 \right\|_F^2$$

and (7.13), (7.36), (7.37), we can upper bounded (C.4) as

$$\dot{V} \le -\lambda_{\min}(Q)\|\boldsymbol{E}\|^2 - \lambda_{\min}\left(\tilde{Q}\right)\|\tilde{\mathbf{e}}\|^2 + 2\|\tilde{\mathbf{e}}\|\left(\kappa_1\|\tilde{Z}\|_F + \kappa_2\right) + \\ 2\|\boldsymbol{E}\|\left(\beta_1\|\tilde{Z}\|_F + \beta_2\right) + 2\|\tilde{\mathbf{e}}\|\left\|\tilde{P}\mathbf{b}\boldsymbol{c}_c\right\|\|\boldsymbol{E}\| - \frac{k}{2}\left\|\tilde{Z}\right\|_F^2 + \bar{Z}. \tag{C.5}$$

Following inequalities obtained using completion of squares

$$2\kappa_1\|\tilde{\mathbf{e}}\|\|\tilde{Z}\|_F \le \|\tilde{\mathbf{e}}\|^2 + \kappa_1^2\|\tilde{Z}\|_F^2$$
$$2\kappa_2\|\tilde{\mathbf{e}}\| \le \|\tilde{\mathbf{e}}\|^2 + \kappa_2^2$$
$$2\beta_1\|\boldsymbol{E}\|\|\tilde{Z}\|_F \le \|\boldsymbol{E}\|^2 + \beta_1^2\|\tilde{Z}\|_F^2$$
$$2\beta_2\|\boldsymbol{E}\| \le \|\boldsymbol{E}\|^2 + \beta_2^2$$
$$2\|\tilde{\mathbf{e}}\|\left\|\tilde{P}\mathbf{b}\boldsymbol{c}_c\right\|\|\boldsymbol{E}\| \le \|\tilde{\mathbf{e}}\|^2 + \left\|\tilde{P}\mathbf{b}\boldsymbol{c}_c\right\|^2\|\boldsymbol{E}\|^2$$

can be used to further upper bound (C.5) as

$$\dot{V} \le -\left(\lambda_{\min}(Q) - 2 - \left\|\tilde{P}\mathbf{b}\boldsymbol{c}_c\right\|^2\right)\|\boldsymbol{E}\|^2 + \\ -\left(\lambda_{\min}\left(\tilde{Q}\right) - 3\right)\|\tilde{\mathbf{e}}\|^2 + \\ \kappa_2^2 + \beta_2^2 + \bar{Z} - \left(\frac{k}{2} - \kappa_1^2 - \beta_1^2\right)\|\tilde{Z}\|_F^2. \tag{C.6}$$

Either of the following conditions $\|\boldsymbol{E}\| > C_1$, $\|\tilde{\mathbf{e}}\| > C_2$, or $\|\tilde{Z}\|_F > C_3$ will render $\dot{V} < 0$ outside a compact set.

Define the compact set on the space of the error variables:

$$B_\gamma = \left\{\boldsymbol{\zeta} \in B_R \middle| \|\boldsymbol{\zeta}\| \le \gamma\right\}, \tag{C.7}$$

outside which $\dot{V} < 0$. Note from (7.43) that $B_\gamma \subset B_R$. Consider the Lyapunov function candidate in (C.1) and write it as $V = \boldsymbol{\zeta}^T T \boldsymbol{\zeta}$. Let Γ be the maximum value of the Lyapunov function V on the edge of B_γ: $\Gamma \triangleq \max_{\|\boldsymbol{\zeta}\|=\gamma} V = \gamma^2 T_M$. Introduce the level set: $\Omega_\gamma = \left\{\boldsymbol{\zeta} \middle| V = \Gamma\right\}$. Let α be the minimum value of the Lyapunov function V on the edge of B_R: $\alpha \triangleq \max_{\|\boldsymbol{\zeta}\|=R} V = R^2 T_m$. The condition in (7.43) ensures that $\Omega_\gamma \subset \Omega_\alpha$, and thus ultimate boundedness of $\boldsymbol{\zeta}$. ■

REFERENCES

[1] KUO, B., *Automatic control systems*. Prentice Hall, New Jersey, 5th ed., 1987.

[2] NISE, S. N., *Control systems engineering*. Benjamin/Cummings, California, 2nd ed., 1995.

[3] OGATA, K., *Modern control engineering*. Prentice Hall, New Jersey, 3rd ed., 1997.

[4] BROGAN, W. L., *Modern control theory*. Prentice Hall, New Jersey, 3rd ed., 1991.

[5] BRYSON, A. E., HO, Y. C., *Applied optimal control: optimization, estimation, and control*. Hemisphere Publishing Corporation, Washington, Revised printing, 1975.

[6] ZHOU, K., DOYLE, J. C., GLOVER, K., *Robust and optimal control*. Prentice Hall, New Jersey, 1996.

[7] KHALIL, H., *Nonlinear Systems*. Prentice Hall, New Jersey, 3rd ed., 2002.

[8] ISIDORI, A., *Nonlinear control systems*. Springer, Berlin, 1995.

[9] ASTROM, K. J., WITTENMARK, B., *Adaptive Control*. Addison Wesley, Massachusetts, 2nd ed., 1995.

[10] NARENDRA, K. S., ANNASWAMY, A. M., *Stable Adaptive Systems*. Prentice Hall, New Jersey, 2nd ed., 1989.

[11] LEWIS, F. L., *Nonlinear network structures for feedback control – survey paper*. Asian Journal of Control, vol. 1, no. 4, pp. 205–228, 1999.

[12] CALISE, A. J., HOVAKIMYAN, N., and IDAN, M., *Adaptive output feedback control of nonlinear systems using neural networks*. Automatica, vol. 37, no. 8, pp. 1201–1211, 2001.

[13] HOVAKIMYAN, N., NARDI, F., CALISE, A. J., and KIM, N., *Adaptive output feedback control of uncertain systems using single hidden layer neural networks*. IEEE Transactions on Neural Networks, vol.13, no. 6, pp.1420–1431, 2002.

[14] HOVAKIMYAN and CALISE, A. J., *Adaptive output feedback control of uncertain multi-input multi-output systems using single hidden layer neural networks*. In Proceedings of American Control Conference, Anchorage, AK, vol. 2, pp. 1555–1560, 2002.

[15] SHARMA, M., and CALISE, A. J., *Neural-Network Augmentation of Existing Linear Controllers*. AIAA Journal of Guidance, Control, and Dynamics, vol. 28, no. 1, pp. 12–19, 2005.

[16] CALISE, A. J., YANG, B. J., and CRAIG, J. I., *Augmentation of an existing linear controller with an adaptive element*. In Proceedings of the 2002 American Control Conference, 08–10 May 2002, Anchorage, Alaska.

[17] CALISE, A. J., YANG, B. J., and CRAIG, J. I., *An augmenting adaptive approach to control of flexible systems*. In Proceedings of AIAA Guidance, Navigation, and Control Conference, Monterey, California, 2002.

[18] YANG, B. J., CALISE, A. J., and CRAIG, J. I., *Adaptive output feedback control with input saturation*. In Proceedings of the 2003 American Control Conference, 2003, pp. 1572–1577, Denver, Colorado.

[19] HOVAKIMYAN, N., YANG, B. J., and CALISE, A. J., *An adaptive output feedback control methodology for non-minimum phase systems*. In Proceedings of Conference on Decision and Control, December 2002, Las Vegas, Nevada.

[20] HOVAKIMYAN, N., LAVRETSKY, E., YANG, B. J., and CALISE, A. J., *Coordinated decentralized adaptive output feedback control of interconnected systems*. IEEE Transactions on Neural Networks, vol. 16, no. 1, pp. 185–194, 2005.

[21] HOVAKIMYAN, YANG, B. J., and CALISE, A. J., Adaptive output feedback control methodology applicable to non-minimum phase nonlinear systems. Submitted to Automatica, 2005.

[22] YANG, B. J., *Adaptive output feedback control of flexible systems*. PhD thesis, Georgia Institute of Technology, School of Aerospace Engineering, April 2004.

[23] KIM, N., Improved methods in neural network-based adaptive output feedback control, with applications to flight control. PhD thesis, Georgia Institute of Technology, School of Aerospace Engineering, November 2003.

[24] IDAN, M., CALISE, A. J., KUTAY, A. T., and PAREKH, D. E., *Adaptive neural network based approach for active flow control*. In ASME Fluids Engineering Division Summer Meeting, number FEDSM2001-18281, New Orleans, Louisiana, May 2001.

[25] CALISE, A. J., EL-SHIRBINY, H., KIM, N., and KUTAY, A. T., *An adaptive guidance approach for spinning projectiles*. In Proceedings of AIAA Guidance, Navigation, and Control Conference, Providence, Rhode Island, 2004.

[26] JOHNSON, E. N., *Limited authority adaptive flight control*. PhD thesis, Georgia Institute of Technology, School of Aerospace Engineering, December 2000.

[27] JOHNSON, E. N. AND CALISE, A. J., *Limited authority adaptive flight control for reusable launch vehicles*. AIAA Journal of Guidance, Control and Dynamics, vol. 26. no. 6, pp. 906–913, 2003.

[28] JOHNSON, E. N. AND CALISE, A. J., *Neural network adaptive control of systems with input saturation*. In Proceedings of the 2001 American Control Conference, Jun 2001, Arlington, Virginia.

[29] HORNIK, K., STINCHCOMBE M., AND WHITE H., *Multilayer feedforward networks are universal approximators*. IEEE Transactions on Neural Networks, vol.2, pp.359–366, 1989.

[30] FUNAHASHI, K., *On the approximate realization of continuous mappings by neural networks*. IEEE Transactions on Neural Networks, vol.2, pp. 183–192, 1989.

[31] HOVAKIMYAN, N., LEE, H. and CALISE, A. J., *On approximate NN realization of an unknown dynamic system from its input-output history*. In Proceedings of the American Control Conference, 2000.

[32] LAVRETSKY, E., HOVAKIMYAN, N., and CALISE, A., *Upper Bounds for Approximation of Continuous-Time Dynamics Using Delayed Outputs and Feedforward Neural Networks*. IEEE Transactions on Automatic Control, vol. 48, no. 9, 2003, pp. 1606–1610.

[33] KUTAY, A. T., CALISE, A. J., IDAN, M., and HOVAKIMYAN, N., *Experimental results on adaptive output feedback control using a laboratory model helicopter*. In Proceedings of AIAA Guidance, Navigation, and Control Conference, Monterey, California, 2002.

[34] KUTAY, A. T., CALISE, A. J., IDAN, M., and HOVAKIMYAN, N., *Experimental results on adaptive output feedback control using a laboratory model helicopter*. IEEE Transactions on Control Systems Technology, vol. 13, no. 2, pp. 196–202, 2005.

[35] M'SAAD, M., LANDAU, I. D., and SAMAAN, M., *Further evaluation of partial state model reference adaptive design*. International Journal of Adaptive Control and Signal Processing, vol. 4, no. 2, pp. 133–148, 1990.

[36] NARENDRA, K. S. and BOSKOVIC, J. D., *Robust adaptive control using a combined approach*. International Journal of Adaptive Control and Signal Processing, vol. 4, no. 2, pp. 111–131, 1990.

[37] KELLY, M. J., and TONCICH, D. J., *Overcoming encoder quantization noise in an adaptive position controller*. International Journal of Machine Tools and Manufacture, vol. 40, no 14., pp. 2031–2046, 2000.

[38] KUTAY, A. T., CALISE, A. J., and HOVAKIMYAN, N., *Adaptive output feedback control with reduced sensitivity to sensor noise*. In Proceedings of the 2003 American Control Conference, vol. 6, pp. 5141-5146, 4–6 June 2003, Denver, Colorado.

[39] RAZA H. and IOANNOU, P., *Vehicle following control design for automated highway systems*. IEEE Control Systems, vol. 16, pp. 43–60, June 1996.

[40] PACHTER, M., D'AZZO, J. J., and PROUD, A. W., *Tight formation flight control*. Journal of Guidance, Control and Dynamics, vol. 24, no. 2, pp. 246–254, 2001.

[41] SINGH, S. N., CHANDLER, P., BANDA, S., SCHUMACHER, C., and M. PACHTER, *Nonlinear adaptive close formation control of unmanned aerial vehicles*. Dynamics and Control, vol. 10, no. 2, pp. 179–194, 2000.

[42] BELANGER, G., SPEYER, J., ANANYEV, S., CHICHKA, D., AND CARPENTER, R., *Decentralized Control of Satellite Clusters Under Limited Communication*. In Proceedings of AIAA Guidance, Navigation, and Control Conference and Exhibit, Providence, Rhode Island, 2004.

[43] Lee, K. H., Cortelezzi, L., Kim, J., and Speyer, J., *Application of reduced-order controller to turbulent flows for drag reduction*. Physics of Fluids, vol. 13, no. 5, pp. 1321–1330, 2001.

[44] Jiang, Z. P., Decentralized disturbance attenuating output feedback trackers for large-scale nonlinear systems. Automatica, vol. 38, no. 8, pp. 1407–1415, 2002.

[45] D'ANDREA, R. and DULLERUD, G. E., *Distributed control of spatially interconnected systems*. IEEE Transactions on Automatic Control, vol.48, no. 9, pp. 1478–1495, 2003.

[46] LANGBORT, C., CHANDRA, R. S., and D'ANDREA, R., *Distributed control design for systems interconnected over an arbitrary graph*. IEEE Transactions on Automatic Control, vol. 49, no. 9, pp. 1502–1519, 2004.

[47] AMITAY, M. and GLEZER, A., *Aerodynamic flow control using synthetic jet actuators*. In Proc. of the 3rd ASME/JSME Joint Fluids Engineering Conference, San Francisco, CA, 1999.

[48] AMITAY, M. and GLEZER, A., *Controlled transient of flow reattachment over stalled airfoils*. International Journal of Heat and Fluid Flow, vol. 22, pp. 690–699, 2002.

[49] Traub, L., Miller, A., Singla, P., Tandale, M., Junkins, J., Rediniotis, O., and Zeiger, M., *Distributed hingeless flow control and rotary synthetic jet actuation*. AIAA Paper, 42nd AIAA Aerospace Sciences Meeting and Exhibit, 2004, pp. 2284–2313.

[50] CALISE, A. J., EL-SHIRBINY, H., *An analysis of aerodynamic control for direct spinning projectiles*. In Proceedings of AIAA Guidance, Navigation, and Control Conference, Montreal, Canada, 2001.

[51] MCCOY, R. L., Modern exterior ballistics: The Launch and Flight Dynamics of Symmetric Projectiles. Schiffer Publishing, Ltd., 1999.

[52] JITPRAPHAI, T. AND COSTELLO, M., *Dispersion reduction of a direct fire rocket using lateral pulse jets*. 39th Aerospace Sciences Meeting and Exhibit. Reno, Nevada, 2001

[53] ISIDORI, A., A Tool for Semiglobal Stabilization of Uncertain Non-Minimum-Phase Nonlinear Systems via Output Feedback. IEEE Transactions on Automatic Control, vol. 45, no. 10, 2000, pp. 1817–1827.

[54] ISIDORI, A. and BYRNES, C., *Output Regulation of Nonlinear Systems*. IEEE Transactions on Automatic Control, Vol. 35, No. 2, 1990, pp. 131–140.

[55] DEVASIA, S., CHEN, D., and PADEN, B., *Nonlinear Inversion-Based Output Tracking*. IEEE Transactions on Automatic Control, vol. 41, no. 7, 1996, pp. 930–942.

[56] TOMLIN, C. and SASTRY, S., *Bounded Tracking for Non-Minimum Phase Systems with Fast Zero Dynamics*. International Journal of Control, vol. 68, no. 7, 1998, pp. 819–847.

[57] CHEN, Y., *Design of Robust Controllers for Uncertain Dynamical Systems*. IEEE Transactions on Automatic Control , vol. 33, no. 5, 1988, pp. 487–491.

[58] LEWIS, F. L., YESILDIREK, A., and LIU, K., *Multilayer neural-net robot controller with guaranteed tracking performance*, IEEE Transactions on Neural Networks, vol. 7, no. 2, 1996, pp. 1–12.

[59] KUTAY, A. T., FOWLER, J. M., CALISE, A. J., and D'ANDREA, R., *Distributed adaptive output feedback control design and application to a formation flight experiment*. Accepted to be presented at the 2005 AIAA Guidance, Navigation, and Control Conference, 15-18 August 2005, San Francisco, CA.

[60] WITTMER, K. S., DEVENPORT, W. J., RIFE, M. C., and GLEGG, S. A. L., *Perpendicular bladevortex interactions*, AIAA Journal, vol. 33, no. 9, pp. 1667–1674, 1995.

[61] SHEVELL, R. S., *Fundamentals of Flight*. Englewood Cliffs, NJ: Prentice Hall, 1989.

[62] FOWLER, J. M. and D'ANDREA, R., A formation flight experiment: Constructing a test-bed for research in control of interconnected systems. Control Systems Magazine, vol. 23, no. 5, pp. 35–43, 2003.

[63] FOWLER, J. M. and D'ANDREA, R., *Distributed control of close formation flight*. In Proceedings of Conference on Decision and Control, Las Vegas, NV, pp. 2972–2977, 2002.

[64] WOLFE, J. D., CHICHKA, D. F., and SPEYER, J. L., *Decentralized controller for unmanned aerial vehicle formation flight*. In Proceedings of AIAA Guidance, Navigation, and Control Conference, San Diego, CA, 1996, AIAA paper 96-3833.

[65] CHICHKA, D. F. and SPEYER, J. L., *Solar-powered, formation-enhanced aerial vehicle system for sustained endurance*. In Proceedings of American Control Conference, Philadelphia, PA, 1998, pp. 684–688.

[66] LISSAMAN and SHOLLENBERGER, *Formation Flight of Birds*. Science, vol. 68, pp. 1003–1005, 1970.

[67] MILEY, S. J., *A Catalog of Low Reynolds Number Airfoil Data for Wind Turbine Applications*. College Station, TX: Department of Aerospace Engineering, 1982.

[68] ANDERSON, J. D., *Fundamentals of Aerodynamics*. New York, NY: McGraw Hill, 1991.

[69] ETKIN, B. and REID, L. D., *Dynamics of flight stability and control*. John Wiley and Sons, Inc., 1996.

[70] 3-DOF helicopter apparatus, Quanser. http://www.quanser.com.

[71] AFOSR Multidisciplinary Research Program of the University Research Initiative (MURI) Project, *Adaptive Vorticity Control Enabled Flight (AVOCET)*. http://www.fcbt.gatech.edu/avocet/index.htm

VITA

Ali Türker Kutay was born in Kirikkale, Turkey, on December 3, 1974. He was awarded Bachelor of Science and Master of Science degrees in Aerospace Engineering from Middle East Technical University, Ankara, Turkey, in 1996 and 1999, respectively. He worked as a design engineer in Turkish Aerospace Industries from 1999 to 2000. He joined Georgia Institute of Technology, School of Aerospace Engineering in 2000 to pursue a Doctor of Philosophy degree. His research interests include neural network based adaptive control, simulation, and experimental applications.